Reorganization of functional hubs in sleep and in epilepsy

Yimeng Wang

A Thesis

In the Department of

Physics

Presented in Partial Fulfillment of the Requirements

For the Degree of

Master of Science, Physics

at Concordia University

Montréal, Québec, Canada

September 2022

Concordia University

School of Graduate Studies

This is to certify that this thesis prepared

By: Yimeng Wang

Entitled: Reorganization of functional hubs in sleep and in epilepsy

And submitted in partial fulfillment of the requirements of the degree of

Master of Science (Physics)

Complies with the regulations of the University and meets the accepted standards with respect to originality and quality.

Signed by the final Examining Committee:

Claudine Gauthier Examiner

Boris Bernhardt Examiner

Christophe Grova Thesis Supervisor

Approved by

Pablo Bianucci Graduate Program Director

Pascale Sicotte Dean of Faculty

Date of examination: September 12th, 2022

Abstract

Reorganization of functional hubs in sleep and in epilepsy

Yimeng Wang

Resting-state functional Magnetic Resonance Imaging (rs-fMRI) is a non-invasive brain imaging technique that measures brain activity non-invasively. Functional connectivity (FC) quantifies how Blood-Oxygen-Level-Dependent (BOLD) signal of remote brain regions correlates with each other temporally. Using variety of methodologies such as Independent Component Analysis (ICA) or sparse dictionary learning, Resting-State Networks (RSNs) are consistently found in human brain connectome. Functional hubs denote the brain regions that exhibit connections denser than others, whereas connector hubs especially participate in inter-network communication. My Master thesis is based on a previously published methodology called Sparsity-based analysis of reliable k-hubness (SPARK), which estimates the functional hubs by counting the number of RSNs connected to each brain voxels. By acquiring simultaneous electroencephalogram (EEG)-fMRI, functional connectivity (FC) during sleep can also be investigated. In addition, functional connectivity has been commonly applied to find potential biomarkers for neurological disease, such as epilepsy. Therefore, in the first study of this thesis, we investigated functional segregation during a recovery nap after total sleep deprivation and its association with cognitive performance. We applied an algorithm called Hierarchical Segregation Index (HSI) based on the hubness estimated by SPARK. As a result, we found significant correlation between functional segregation during sleep and working memory performance after sleep. In the second study of this thesis, we investigated the different patterns of functional hub reorganization in temporal lobe epilepsy (TLE) and frontal lobe epilepsy (FLE). By applying similar methods used in the first study, we found significant and exclusive functional hub alteration both in TLE and FLE. To conclude, in sleep, functional segregation during a whole night sleep and its association between cognitive performance can be further investigated. In TLE and FLE, further research of the hub alterations in subcortical structures will be of interest, and might serve as potential biomarkers for post-surgical outcomes.

Acknowledgement

I would like to express my deepest gratitude to my supervisor Dr. Christophe Grova, for introducing and guiding me through my academic journey, providing me variety of research resources, offering me detailed assistance with his wisdom and extreme patience, as well as offering me supports and guidance in life, especially his supports and consideration during the pandemic.

I would like to also express my great appreciation to our research collaborates including but not limited to Dr. Boris Bernhardt, Dr. Thanh Dang-Vu, Dr. Jean Gotman, Dr. Nathan Cross, Dr. Jessica Royer and Dr. Raúl Rodríguez Cruces, who have offered me resources, supports and suggestions to my projects. I would like to extend my sincere thanks to my committee member, Dr. Claudine Gauthier and Dr. Boris Bernhardt for their time, dedication, and supports to my academic development. I could not have undertaken this journey without my close collaborates Dr. Kangjoo Lee, who have consistently offered me supports and suggestions.

I am also grateful to my colleagues and friends who have helped my academic route and made me feel like home: Jawata Afnan, Édouard Delaire, Dr. Makoto Uji, Fatemeh Razavipour, Tamir Avigdor, Arielle Eden Dascal, Dr. Zhengchen Cai, Amanda Spilkin, Obaï Bin Ka'b Ali, Dr. Hassan Khajehpour, Dr. Chifaou Abdallah, Dr. Tanguy Hedrick, Ines Djelkhir, Hugo Keraudran, Christian Palmer, Dr. Ümit Aydin, Shahla Bakian-Dogaheh and Aura Ramire.

I am grateful to my parents and grandparents for being supportive. Special thanks to my friend Hanjia Zhang for her encouragement and company. Finally, thank you to my life partner and soulmate, Boheng Li, who is always by my side and supports me in every possible way.

Contribution of Authors

All works presented in this thesis were completed in collaboration with my supervisor Dr. **Christophe Grova** and our collaborator Dr. **Boris Bernhardt** from McGill university They have supported literature review, analysis development, discussion of results, and manuscript writing. The contribution of all co-authors other than my supervisor and myself are summarized below:

Study 1: Hierarchical segregation of functional brain networks during NREM sleep and impacts of the attention function.

Title: ***Hierarchical segregation of functional brain networks at NREM sleep and attention function*** **(Publication in preparation)**

Authors: Kangjoo Lee[1]+, Yimeng Wang[1,2,3]+, Nathan Cross[4,5,6], Aude Jegou[1], Fatemeh Razavipour[1], Florence B. Pomares[4,5,6], Aurore A. Perrault[4,5,6], Alex Nguyen[1,4,6], Ümit Aydin[1,7], Jean Gotman[3], Thien Thanh Dang-Vu[4,5,6], Christophe Grova[1,3,4]

(+: co-first authors)

- Dr. Lee designed the original Sparsity-based Analysis of Reliable k-hubness (SPARK) and Hierarchical Segregation Index (HSI) algorithms, assisted me in writing the manuscript. (The detailed work distribution between Dr. Kangjoo Lee and myself is further described in the section *Preface* of Chapter 3.)
- Dr. Nathan Cross supported the original code and the analysis of Functional Clustering Ratio (FCR) and assisted in the analysis of cognitive performance.
- Aude Jegou acquired the data during her MSc degree in Physics at Concordia University in 2018, performed the identification of sleep stages.
- Dr. Fatemeh Razavipour assisted in running SPARK algorithm and fMRI preprocessing.
- Dr. Ümit Aydin supported EEG/fMRI equipment setup for data acquisition.
- Dr. Florence Pomares assisted in the data acquisition and the analysis of cognitive performance.
- Dr. Jean Gotman, as the co-supervisor of Dr. Kangjoo Lee, contributed to the study design, analysis development, and result interpretation.
- Dr. Thien Thanh Dang-Vu designed the study of EEG/fMRI acquisition during recovery nap after sleep deprivation with Dr. Christophe Grova, supported data acquisition, and supported the interpretation of the results of this thesis.

Study 2: A preliminary study: connector hub reorganization in frontal lobe epilepsy and temporal lobe epilepsy

Title: ***Disruption of functional networks in frontal lobe epilepsy and temporal lobe epilepsy***

Authors: Yimeng Wang[1], Kangjoo Lee[1,2,3], Jessica Royer[3], Raúl Rodríguez Cruces[3], Birgit Frauscher[3], Boris Bernhardt[3], Christophe Grova[1,3,4] (In preparation)

- Dr. Kangjoo Lee supported the algorithms called hub disruption index and hub emergence index based on SPARK.
- Dr. Jessica Royer acquired the data and performed fMRI preprocessing with MICApipe toolbox, which is developed in the lab of Dr. Boris Bernhardt. Dr. Royer also assisted in running SPARK.
- Dr. Raúl Rodríguez Cruces performed fMRI preprocessing with MICApipe as well. Dr. Cruces also assisted in running SPARK.
- Dr. Birgit Frauscher designed the study with Dr. Boris Bernhardt and led patient screening and recruitment.

[1]Multimodal Functional Imaging Lab, Dept of Physics, Concordia University, Montreal, Canada
[2]Dept of Psychiatry, Yale University School of Medicine, New Haven, United States
[3]Montreal Neurological Institute, McGill University, Montreal, Canada
[4]PERFORM Centre, Concordia University, Montreal, Canada
[5]Centre de Recherche de l'Institut Universitaire de Gériatrie de Montréal, Montreal, Canada
[6]Center for Studies in Behavioral Neurobiology, Dept of Health, Kinesiology and Applied Physiology, Concordia University, Montreal, Canada
[7]Social, Genetic and Developmental Psychiatry Centre, Institute of Psychiatry, Psychology and Neuroscience, King's College London, London, United Kingdom

Funding: Natural Sciences and Engineering Research Council (NSERC) of Canada Discovery grants to Dr. Christophe Grova. Canadian Institutes of Health Research (CIHR) (PJT-159948and MOP-133619) to Dr. Christophe Grova. Fonds de Recherche du Quebec, Nature et Technology (to the research team of *Study 1)*. Especially, the data acquisition of *Study 1* is also supported by an internal grant from PERFORM center and the Faculty of Arts and Science of Concordia University to Dr. Christophe Grova. CIHR (FDN-154298), SickKids Foundation (NI17-039), NSERC (Discovery-1304413), Azrieli Center for Autism Research of the Montreal Neurological Institute (ACAR), Brain Canada, FRQ-S, and the Canada Research Chairs Program to Dr. Boris Bernhardt. PERFORM Graduate Scholarship, Concordia Merit Scholarship, Concordia Steven Goldberg Entrance Bursary, and Research Bursary from the Faculty of Arts and Science of Concordia University to Yimeng Wang.

Table of Contents

List of Figures

Chapter 1 Introduction

As the most intricate organ, the human brain accounts for about 20% of the energy consumption of the body, although it only composes 2% of total body weight. Surprisingly, neuronal activity caused by external stimulations explains less than 5% of brain energy consumption, while the rest is contributed by the intrinsic brain activity disclosed by background neuronal activations (Raichle & Mintun, 2006; Zhang & Raichle, 2010), which inspired more research to examine the brain at rest. Functional Magnetic Resonance Imaging (fMRI) has a higher spatial resolution compared to other functional imaging techniques and offers a unique opportunity to investigate neuronal activity from deep brain structure without an invasive procedure. fMRI indirectly measures brain activity by measuring the slow hemodynamic fluctuations evoked by bioelectrical neuronal activity. Resting-state fMRI (rs-fMRI) serves as a powerful modality to explore intrinsic brain activity, whereas the participant is instructed to lie still and stay awake inside the scanner, in the meantime Blood-Oxygen-Level-Dependent (BOLD) signal are acquired without requiring any external task. By calculating the Pearson correlation coefficient between time courses of voxels from the grey matter, functional connectivity can be assessed that represents the temporal similarity between two regions. A variety of methodologies have been proposed to investigate functional connectivity includes seed-based connectivity maps, principal component analysis (PCA), independent component analysis (ICA), as well as clustering, sparse coding method and graph theory. Although using different methods, resting-state Networks (RSNs) that could be associated with specific functions were consistently found, such as for instance the default mode network (DMN), the visual network, or the attention network. However, some of those aforementioned methodologies contain shortcomings such as requiring a priori definition of region of interest (ROI), requiring the assumption of a threshold to generate a sparse matrix, issues of multi-collinearity, or assumption of non-overlap between RSNs. An innovative data-driven method called Sparsity-based Analysis of Reliable k-hubness (SPARK) based on sparse dictionary learning was recently developed, which identifies connector hubs regions responsible for internetwork coordination, by counting the number of RSNs involved in each voxel, while in the meantime, carefully handles some of the previous issues (Lee et al., 2018).

Functional connectivity summarizes the macro-organization of the human brain as a “small-world” structure, which consists of local communities with short-range connections and long-range bridges between them (Watts & Strogatz, 1998). Such organization is not only efficient and reactive for lower-level tasks requiring a specific local brain region such as preliminary sensory functions, but

also highly efficient for higher-level tasks requiring synchronization of different neuronal regions such as complex motor coordination or making decisions. Accordingly, the basis of the "small-world" structure is functional segregation (defined by the differences in functions of the brain regions with distinct anatomy and physiology) and functional integration (defined by the synchronization between those brain regions) (Tononi et al., 1994). Functional segregation and integration appear at different levels of brain network structure, forming the hierarchical organization of the brain functional connectome. The extent of segregation and integration altering across different arousal states has been quantified by a method called functional clustering ratio (FCR) (Boly et al., 2012; N. E. Cross et al., 2021), suggesting increased functional segregation during non-rapid-eye-movement (NREM) sleep when compared to wakefulness (N. Cross et al., 2021a). However, different segregation patterns are yet to be explored between different NREM stages.

Although the "small-world" brain structure provides high efficiency for complex information processing in the healthy brain, alteration of such a structure may indicate potential problems in neurological disease, whereas if certain brain regions are pathologically altered, different severity of brain network disruption can occur. For example, abnormal hub disruption and new hub emergence have been found by our group when studying resting state fMRI from patients with mesial temporal lobe epilepsy (TLE) using SPARK (Lee et al., 2018). However, while emerging literature has explored altered functional connectivity and its clinical relevance for TLE, more investigation is required for different types of epilepsy (Royer et al., 2022).

Therefore, in the context of this Master Thesis, we extended the application of SPARK in two contexts: (a) the network segregation across different vigilance states and sleep stages in the healthy brain and (b) the network disruption in epileptic brains with different type of focal drug resistant epilepsy. In (a), we quantified the functional network segregation at the voxel-level by comparing wakefulness, NREM2, and NREM3 sleep stages, while assessing the interaction between network segregation during sleep and cognitive performances. Only NREM2 and NREM3 stages were compared because they are the most commonly identified NREM stages across subjects in our study. In (b), we studied the group level comparison of connector hubs reorganization using resting state fMRI data from patients with in temporal lobe epilepsy (TLE) and frontal lobe epilepsy (FLE). We are providing preliminary results for this second study.

In this thesis, Chapter 2 introduces the specificity and problems of rs-fMRI studies, while presenting a state-of-the-art of the methodologies considered to analyze functional connectivity using fMRI. Chapter 3 is a manuscript in preparation for publication, currently under review with

co-authors and expected to be submitted shortly, which describes *study 1: Hierarchical segregation of functional brain networks during NREM sleep and impacts of the attention function.* Notably, Dr. Kangjoo Lee and I shared co-first authorship on this study. It also includes an introduction, methodology, presentation of results, discussion, and preface describing the work distribution between Dr. Lee and myself. Chapter 4 is a preliminary manuscript on *Study 2: Connector hub reorganization in frontal lobe epilepsy and temporal lobe epilepsy*, including an introduction to epilepsy, methodology, presentation of preliminary results, and discussion closely focusing on the results. Chapter 5 includes the overall conclusion of this thesis, the limitation of our methodology, and possible directions for future research in the area.

Chapter 2 State of art of functional connectivity

2.1 Resting-state fMRI

2.1.1 Blood Oxygen Level Dependent signal detected by fMRI

FMRI measures brain activity with the BOLD signals, which was invented in the early 1990s by Dr. Seiji Ogawa and Dr. Ken Kwong (Huettel, 2004; Ogawa et al., 1990). As a non-invasive imaging method, fMRI indirectly measures neuronal activity by measuring the hemodynamic response of the human brain. While two different kinds of hemoglobin exist in capillaries, the oxygenated hemoglobin (Hb) is diamagnetic and the deoxygenated hemoglobin (dHb) is paramagnetic. The magnetic field distortion caused by dHb can therefore be detected as the BOLD signal. Whenever there is neural activity in one part of the brain, the demand for O_2 consumption in the neurons will increase. The nearby capillary will introduce more cerebral blood flow and blood volume. Consequently, the ratio of dHb / Hb will decrease in the nearby capillary, leading to a change in the BOLD signal.

A typical fMRI acquisition scans the human brain slice by slice from one direction to another. A parameter named Repetition Time (TR) is the time difference between successive MRI pulse sequences applied to the same slice of the brain and indicates the time resolution of fMRI acquisition. A conventional fMRI acquisition has a time resolution of TR=2000~3000ms (i.e., the sampling frequency is around 0.5Hz), while a multiband-accelerated fMRI that starts scanning multiple slices simultaneously, achieves a time resolution of around TR=600~900ms (~1.6 Hz), (Smitha et al., 2018). Although still having temporal resolutions lower than those of electrophysiology, fMRI has a higher spatial resolution (up to 2~4 mm^3 presently) than electrophysiology or other functional imaging and is especially suited to detect functional activity even from deep brain structure non-invasively.

A task-fMRI applies a series of external stimuli (e.g., visual or auditory stimulus) to the participants, and uses general linear models (GLM) and statistical parametric maps to locate the brain regions that show significant activations during tasks compared to rest. Interestingly, using seed regions in the contralateral motor regions that show activation during task-fMRI (finger tapping), Biswal et al discovered that even without any motor behavior, the spontaneous slow oscillation of BOLD time-series (0.01~0.1Hz) (Cordes et al., 2001) of those seed voxels still exhibits high correlations with each other suggesting regulated neuronal activity in remote brain regions during rest (B. Biswal et al., 1995; B. B. Biswal et al., 1997). Since then, the “resting-state” fMRI (rs-fMRI) has been introduced, where the participants are instructed to lie still inside the MRI scanner with eyes

opened and fixed on a cross (or eyes closed in some studies), stay awake, and try to avoid any specific thought, without applying any external task. A BOLD time series will then be acquired. Technically, the "resting-state" fMRI is generally acquired in a wakeful, relaxed, and task-free condition. Nonetheless, similar rs-fMRI acquisitions have also been applied to explore the intrinsic neuronal activity during other brain states, such as sleep or anesthesia (Fox & Raichle, 2007)

2.1.2 Origin of spontaneous slow oscillations of rs-fMRI

The origin of the spontaneous slow-oscillation detected during rs-fMRI has been questioned during the past two decades: whether the resting-state BOLD signal is originated mainly by fluctuations of the underlying neuronal (bioelectrical) activity? Or is it mainly generated by physiological processes such as respiratory and cardiac rhythm at higher frequencies? Although studies proved the contamination of physiological process (>0.3Hz) to rs-fMRI time-series (Birn et al., 2006, 2008; Cordes et al., 2001), other studies found that the brain regions that exhibit high correlation in rs-fMRI are also highly related in brain anatomy (B. Biswal et al., 1995; Salvador et al., 2005). It has been demonstrated that the temporally correlated regions found in rs-fMRI are supported by actual anatomical white matter pathways (Honey et al., 2009). Additionally, in the sensory cortex, some have found correlations between rs-fMRI and gamma-power local field potential (LFP), which is an electrophysiological technique that records brain activity with micro-electrodes placed in extracellular space near neurons (Nir et al., 2008), offering more evidence of the neural origin of rs-fMRI signals.

Using rs-fMRI acquisition with high temporal resolution (TR=400ms), Cordes et al have found that the frequency components of the seed regions in the auditory, visual, and motor cortex are indeed different from those of the artery, vein, and cerebrospinal fluid (Cordes et al., 2001). The cortical seed regions virtually contribute to the rs-fMRI signals within 0~0.1 Hz, while the rs-fMRI signals of the artery, vein, and cerebrospinal fluid contributed to wider frequency ranges (0~0.1Hz, 0.1~0.5Hz, and 0.6~1.1 Hz). Accordingly, with appropriate fMRI preprocessing techniques, the influence of physiological processes in rs-fMRI can be reduced.

2.1.3 fMRI preprocessing

To minimize the aforementioned influence of the physiological components on the fMRI time series, a variety of strategies have been introduced that identify the spatiotemporal characteristics of the targeted effect (e.g., cerebrospinal fluid, white matter, or vascular noise), and then remove their fluctuation from the fMRI data of interest. A typical example of package for fMRI preprocessing is the Neuroimaging Analysis Kit (NIAK) (Bellec et al., 2010a). NIAK is the fMRI preprocessing toolbox we considered for the study presented in *Chapter 3*. It includes a

physiological noise removal algorithm named CORSICA (CORrection of Structured noise using spatial Independent Component Analysis) (Perlbarg et al., 2007). CORSICA is an automated process that utilizes spatial Independent Component Analysis (ICA) to extract and remove the components from physiological origins or body movements, assisted by the spatial location priors of the dominant physiological process (cerebrospinal fluid and white matter), the variance of the fMRI map, and external monitoring of cardio-respiratory rhythm (if available). Similar to NIAK, another recently developed fMRI preprocessing pipeline named "**MICApipe**" (developed in Dr. Bernhardt's lab) was considered for the sudy presented in *Chapter 4.* **MICApipe** uses the ICA-FIX algorithm from FSL to remove physiological noise and motion components (Cruces et al., 2022; Griffanti et al., 2014; Salimi-Khorshidi et al., 2014). Some literatures model and then remove the average of global BOLD signal with the linear regression model, which can be correlated with vascular nuisance signal as well (Fox et al., 2005; Fransson, 2005).

Aside from physiological denoising, a typical fMRI preprocessing pipeline also includes slice timing correction to compensate for the acquiring time differences between each slice of the brain, motion correction by spatially co-registering all volumes to a reference volume with rigid-body transformation, temporal high-pass/band-pass filtering to detrend and remove high-frequency disturbance if any, co-registration between fMRI and individual anatomical MRI, normalization to a template space for group-level analysis with non-linear transformation, and spatial smoothing to increase the signal-to-noise (SNR) ratio. Gradient distortion correction can also be applied if field maps are available (Jovicich et al., 2006).

2.2 Analysis of Functional connectivity and connector hub

Functional connectivity is defined as the statistical correlation between two voxels (or regions) of the brain, mostly calculated with Pearson correlation coefficients between two averaged fMRI time series (Aertsen et al., 1989; K. J. Friston et al., 1993), but other unconventional parametric or nonparametric methods have been considered as well (Damoiseaux et al., 2006a; K. Friston et al., 2006; Salvador et al., 2005), as summarized by (Zhang & Raichle, 2010). Most commonly, functional connectivity is calculated using rs-fMRI, but FC can be analyzed for a variety of studies as well, such as during tasks or sleep. Nonetheless, functional connectivity calculated with task-free fMRI is rather versatile and can be easily applied to a wide category of healthy or diseased participants, with its easy-to-achieve acquisition condition (B. B. Biswal et al., 2010; Zuo & Xing, 2014). The whole brain functional connectivity patterns of a person are mostly consistent even across different brain states (e.g., sleep), suggesting the functional connectivity patterns are the intrinsic "fingerprint" of the brain (Finn et al., 2015; Fox & Raichle, 2007). In general, methodologies used to investigate functional connectivity can be divided into two main categories:

hypothesis-driven such as seed-based connectivity map, and hypothesis-free (data-driven) methods including but not limited to independent component analysis (ICA), hierarchical clustering, principal component analysis (PCA) (Viviani et al., 2005), sparse coding such as singular value decomposition (SVD) and functional gradient (Bethlehem et al., 2020; N. Cross et al., 2021a). When looking at the connectivity matrix of the whole brain, i.e., the connectome (Leergaard et al., 2012), graph theory is also a powerful tool to quantify the local and global efficiency of the network structure (He et al., 2015; Rubinov & Sporns, 2010; Watts & Strogatz, 1998).

2.2.1 Seed-based functional connectivity studies

Seed-based functional connectivity mapping is one of the most popular approaches since researchers first started revealing intrinsic neuronal coactivations from rs-fMRI (B. B. Biswal et al., 1997; Cordes et al., 2000; Pittau et al., 2012). The relatively simple implementation and the straightforward interpretation of results are the two strongest advantages of seed-based study (Buckner & Vincent, 2007). Initially, a rather small area of the region of interest (ROI) is required, which is named the "seed" region. The seed region can either be determined by a priori hypothesis (e.g., a study aiming at finding an association between functional connectivity and mTLE anatomical abnormalities might use the hippocampus and amygdala as the "seeds") (Pittau et al., 2012), or can be chosen as the activated regions in related task-fMRI analysis, which requires another study design of the task. After a seed is chosen, the Pearson correlation coefficient will then be calculated between the averaged fMRI time-course of this seed region and every other voxel (or region) of the whole brain. An example of a seed-based functional connectivity map can be found in **Figure 2-1B**. Nonetheless, an obvious disadvantage of seed-based method is that it requires an a priori choice of seed region, which can bias the results and also complicate the comparison of results across different studies.

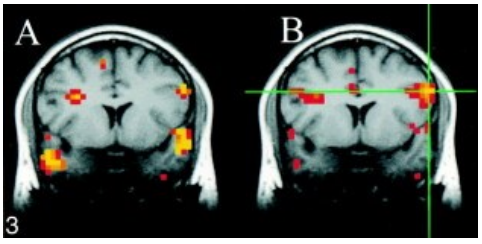

Figure 2-1 An example of a seed-based functional connectivity map. (Cordes et al., 2000). Adapted from Figure 3 of Cordes et al 2000. A is the brain regions that show significant activations in fMRI during a text-listening task. B shows the areas that exhibit significant correlation with the seed voxel (located at the green crosshairs) in the resting-state fMRI of the same subject.

2.2.2 ICA and RSNs

Independent component analysis (ICA) is a more revolutionary, model-free method in functional connectivity studies (Beckmann et al., 2005; Calhoun et al., 2001; Damoiseaux et al., 2006b; de Luca et al., 2006), allow a data-driven summary of general connectivity without any assumption (van den Heuvel & Hulshoff Pol, 2010). ICA decomposes the fMRI time series of the whole brain into several spatial components that exhibit maximum spatial independence from each other (Buckner & Vincent, 2007), and interprets the whole functional activity as the contribution of several spatially independent components. High consistency of results findings has been reported across different ICA studies (Damoiseaux et al., 2006b). Another advantage of ICA is that it can also be applied to further identify and remove any "noisy" components that are contributed by non-neuronal sources. However, a possible disadvantage includes that ICA-based or similar methods must require an a priori definition of the number of components, and a standard estimation algorithm to define the number of components is yet to be developed (Beckmann et al., 2005). In addition, the naming of the independent components is usually required at the later stages of analysis, whereas current techniques are mostly manual or semi-manual algorithms that compare components maps to existing templates (Zhang & Raichle, 2010), which is time-consuming and might be biased by subjective judgment. Most importantly, ICA aims to generate a series of non-overlapping spatial networks that have maximum independence from each other's, therefore, ICA is not, "in theory", able to handle the overlaps between each network, although some degree of spatial overlap does exist and has been investigated.

Several resting-state networks (RSNs) with distinct spatial maps have been consistently found across different ICA decomposition of rs-fMRI, including (a) Primary sensory networks like sensorimotor network, primary visual network, and auditory network; (b) Higher-order secondary networks that integrate information and participate in the decision making processes, such as Default Mode Network (DMN), executive controls networks, dorsal attention network, ventral attention networks, salience network, and language network; (c) as well as cortical-subcortical connections including thalamus subcortical network, basal ganglia network, limbic network and cerebellum (Fox & Raichle, 2007; Zhang & Raichle, 2010). An example illustration of 10 commonly found RSNs with ICA is shown in **Figure 2-2** (Smith et al., 2009). Smith et al applied 20-components ICA on the BrainMap dataset, which is a dataset that consists of 29671 brain activation maps collected from a variety of task-based fMRI studies, in the meantime applying ICA on resting-state fMRI acquired from 36 healthy individuals. Then, the association between the components from BrainMap and the components from 36 rs-fMRI were assessed with Pearson spatial correlation. Eventually, 10 components from 36 rs-fMRI were found with significant correlation with BrainMap ($r>0.25$) (Smith et al., 2009). Notably, RSNs can also be identified by

seed-based method, e.g., Zhou et al extracted the posterior DMN using the posterior cingulate cortex (PCC) region as seeds and extracted anterior DMN using medial prefrontal cortex (MPFC) as seeds (Zhou et al., 2012). Interestingly, those aforementioned resting-state networks are found with high reproducibility, even with different methodologies used (ICA, seed, or hierarchical clustering) (van den Heuvel & Hulshoff Pol, 2010b), as well as similar RSNs identified from graph theory (Moussa et al., 2012). RSNs indicate the extended brain regions that work closely together and show synchrony in intrinsic functional connectivity within each RSN. Nonetheless, the synchrony between RSNs, such as existing communication between DMN and attention network (Fox et al., 2005; Fransson, 2005). Additionally, diverse functions have been found within an RSN (Vincent et al., 2006), despite being less characterized (Zhang & Raichle, 2010), which brings attention to the possible hierarchy organization of brain functional networks.

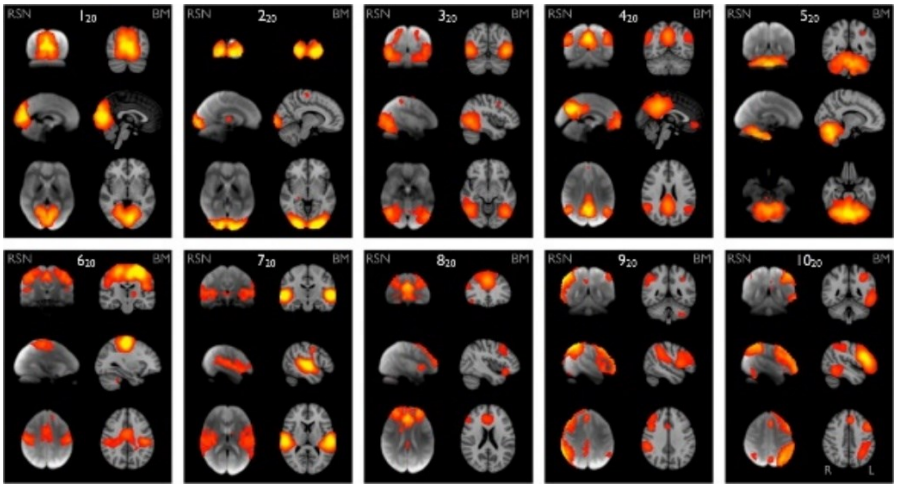

Figure 2-2 An example of RSNs found using ICA-based method. It shows 10 consistently found RSNs by applying a 20-component ICA analysis on a database with 29671 brain activation maps and 36 resting-state fMRI time series. Adapted from Figure 1 of Smith et al., PNAS 2009 (Smith et al., 2009).

However, a fundamental limitation of ICA is the assumption of independence between networks. The brain is a complex organ with multiple interacting networks and potential dynamic reconfigurations of their spatial extent. It is potentially challenging to assume fully independence between RSNs in ICA. SPARK, on the other hand, decompose the whole brain networks while modelling the dependency between networks. SPARK will be further illustrated in section 2.2.4 and Chapter 3.

2.2.3 hierarchical clustering

The aforementioned hierarchical organizations of functional networks can be investigated by ICA, by adjusting the assumed number of components. Another effective method is hierarchical

clustering. Hierarchical clustering can be fully data-driven and requires no a priori information, which usually starts from basic parcellation of the whole brain to reduce dimension, and then repeatedly clustering parcels with temporal similarity together (Salvador et al., 2005). At the end, this method generates a hierarchical tree of different levels of spatial networks, being another hypothesis-free methodology to identify RSNs and explore multi-level functional connectivity organizations (Bellec et al., 2010a).

Some other studies, despite not being hypothesis-free, instead quantify the functional integration and segregation among a known hierarchical tree, serving as a powerful tool to explore how known sub-networks of RSNs coordinate with each other (Boly et al., 2012; N. E. Cross et al., 2021). However, hierarchical clustering also usually only generates spatially non-overlapping networks, making the statistical assumption that functional networks are spatially independent, while the existence of multiple networks in one brain region has been proven (Thomas Yeo et al., 2011a).

2.2.4 Sparse coding algorithms

Nonetheless, a series of sparse coding algorithms based on various dictionary learning techniques have been developed and used in functional connectivity studies recently, which handle overlapping of networks because of the sparsity property. Some studies use SVD to reduce the dimensionality of fMRI time-series and summarize the intrinsic correlation, either applying SVD in PCA to summarize whole-brain connectivity patterns (Worsley et al., 2005) or applying SVD to extract a series of hierarchical networks (Sahoo et al., 2019). L1 regularization learning was also applied to extract different RSNs (Campos et al., 2015; Xie et al., 2017). Other studies applied K-SVD to extract RSNs (Le et al., 2018; Lee et al., 2011, 2016; Nguyen et al., 2022; Seghouane & Iqbal, 2017; Xie et al., 2017), which is a generalized form of k-mean clustering that tries to estimate spatially overlapping atoms that explain the fMRI data using nearest neighbor estimation. Xie et al particularly found sparse coding algorithm outperformed ICA in predicting fMRI activations in machine learning analysis (Xie et al., 2017).

Significantly, the sparsity-based analysis of reliable k-hubness and overlapping network structure in brain functional connectivity (SPARK), developed by our colleague Dr. Kangjoo Lee extracts overlapping RSNs using K-SVD as well (Lee et al., 2016). It applies K-SVD to solve a generalized linear model which decomposes the fMRI time series into several sparse spatial networks. The specificity of SPARK is that it counts the number of sparse RSNs involved in each brain voxels, while in the meantime offering the spatial maps of each RSN involved in each voxel (hub), providing easy-to-interpret results. Certainly, SPARK is a data-driven method that requires no assumption of connectivity. Extra advantages of SPARK include that it requires no thresholding

assumption as in Graph Theory that might bias the results, and it handles the multi-collinearity issues that can occur in other correlation-based methods. The multi-collinearity is defined as follows: if A and B have high correlations as well as B and C, A and C may be identified as correlated even if they come from different RSNs. Therefore, a standard functional connectome based on pairwise correlation will then be sensitive to the problem of multi-collinearity. Another way to handle this issue is by partial correlation, which was originally proposed by Marrelec et al (Marrelec et al., 2006a, 2007, 2008a).

SPARK is used in both ***Chapter 3*** and ***Chapter 4*** and will be elaborated on in ***Chapter 3***.

However, most sparse coding algorithms are mathematically-complicated, which might limit their application by researchers from other backgrounds.

2.2.5 Graph theory

Graph theory is a strong tool for characterizing and quantifying the connectivity organization on the whole brain level (He et al., 2015; Rubinov & Sporns, 2010; Watts & Strogatz, 1998), which also focus on identifying overlapping connectivity. Graph theory represents brain parcels (or voxels) as **nodes** and functional connectivity (usually, the Pearson correlation coefficient) between two nodes as **connections or edges**. To do so, after calculating the Pearson correlation coefficient between any possible combination of any two nodes of the whole brain (voxel, region, parcel), a predefined threshold will be applied to the connectivity matrix, to binarize the whole brain functional connectivity (or called "connectome"), then represented as a topological map.

Graph theory studies have also proposed several connectivity models of the whole brain structure – "small-world", which is a type of network organization that has several local and dense communities connected by a few long-range connections between local communities (Watts & Strogatz, 1998). The "small-world" models align with the aforementioned findings of functional synchrony between large RSNs (Fox et al., 2005). As opposed to "small-world" network, in graph theory, regular networks denote a regular lattice-like network where each node has the same number of connections. A regular network is characterized by both high clustering-coefficients and high path length, whose local efficiency is high but global efficiency is low. In addition, a random network is generated by randomly disturbing the regular network, resulting in a randomizing organization which contains a lot of long-range connections between remote nodes. Random network is characterized by both low clustering-coefficients and low path length, whose global efficiency is high but local efficiency is low. The "small-world" network, instead, combines the

advantages of two aforementioned network, is characterized by high clustering ratio and low path length, therefore highly efficient both locally and globally.

In graph theory, hubs are defined as the regions (nodes) exhibiting dense or essential connections. Among them, a provincial hub refers to a hub in local communities whereas a connector hub refers to brain regions that participate in internetwork communication. In graph theory analysis, hubs can be identified by **high degree centrality**, **high betweenness centrality,** or **high eigenvector centrality** (Royer et al., 2022). Degree centrality simply implies the number of connections to a node. Betweenness centrality quantifies how many times a given node sits on the shortest paths between any two remote nodes of the overall network (Perez & Germon, 2016). Eigenvector centrality quantifies the importance of the nodes that are connected to the given node. Instead of quantifying how many nodes or regions are "connected" to a specific node (or voxel), SPARK methodology mentioned in section **2.2.4** quantifies the number of RSNs connected to each voxel. Since the decomposition of the signal in each voxel is sparse it will only involve contribution from the time course of a small/sparse number of RSNs defined as "k-hubness" ($k<10$ networks). Therefore, voxels exhibiting higher k-hubness values, tends to be connectors hubs involving in long-distance communication between RSNs (Lee et al., 2016).

Participation coefficients is another measure of hubness in graph theory proposed by Power et al. (Power et al., 2013), which is also similar to the method of k-hubness. Participation coefficients quantify the contribution of a node's edges to all communities of the whole brain. If a node (voxels or brain regions) has low participation coefficients, it denotes that this node has minimum contribution to the communities. If a node has high participation coefficients, it denotes that this node has maximum contribution to different clusters over the brain. Therefore, a low participation coefficient indicates this node tends to be a provincial hub, and a high participation coefficient indicates a connector hub.

Despite offering a global perspective of the functional connectome, the shortcomings of graph theory are also obvious. Other than the multi-collinearity issue mentioned in section **2.2.4**, graph theory methods also depend on the assumption of the threshold applied to the connectivity matrix, although a variety of data-driven methods to estimate the optimal threshold based on data variability have been proposed (Bordier et al., 2017). SPARK, on the other hand, requires no a priori definition of threshold and offers a straightforward representation of RSNs, because of its sparse dictionary learning algorithm.

2.3 Functional connectivity during sleep

Sleep allows restoring physical capability and cognition. It is generally characterized by low arousal states, low reaction to external stimuli, and reduced muscle activity, which can be monitored by Electromyography (EMG) (Ferri et al., 2008). Monitoring brain bioelectrical activity using Electroencephalogram (EEG), several sleep specific patterns, such as slow rhythms involving low frequency bands of neural activity and specific featured neuronal events such as sleep spindles and k-complex can be recorded and are used to characterize sleep (Caporro et al., 2012). A systematic judgment and scoring of sleep are usually conducted following the American Academy of Sleep Medicine (AASM) Manual for the Scoring of Sleep and Associated Events, according to which sleep can be categorized into rapid-eye-movement (REM) sleep and non-rapid-eye-movement (NREM) sleep (AASM, 2007). NREM sleep as a deeper state of sleep can be further categorized into NREM1, NREM2, NREM3 and NREM4 based on different characteristics of electrophysiology, with NREM4 being the deepest NREM sleep stage. Emerging evidence in EEG studies suggested the association between NREM sleep and cognition, reflected both in brain maturation of children (Knoop et al., 2021) and brain aging (Taillard et al., 2019). Functional imaging using functional Near-infrared spectroscopy (fNIRS) (Le et al., 2018) or fMRI can be utilized in sleep studies to understand the intrinsic link between neuronal activity and cognitive function. However, functional imaging studies of sleep must be companied by electrophysiological recording to monitor sleep stages, thus requiring EEG-fNIRS or EEG-fMRI simultaneous acquisition and additional preprocessing techniques.

The EEG recording will then need to be manually scored by professionals according to the AASM scoring manual (AASM, 2007). As described in Acharya et al (Acharya et al., 2015), EEG shows different characteristics at different NREM stages: in NREM1, Alpha band of EEG (8-12Hz) disappears and Theta band of EEG (4-7Hz) appears; in NREM2, the characteristic sleep spindles (11-15Hz) and K-complexes waves will appear with Theta waves; in NREM3, sleep spindles and K-complexes still exist but Delta band of EEG starts appearing (1-3Hz); in NREM4, Delta waves of frequency <2Hz will be dominant and have high EEG amplitude. An illustration of EEG characteristics in NREM sleep can be found in **Figure 2-3**. However, EEG obtained from simultaneous EEG-fMRI acquisition is largely contaminated by magnetic resonance related noise, including gradient artefacts and ballistocardiogram noise (Uji et al., 2021). Gradient artefacts are due to the large voltage amplitude induced by varying magnetic field gradients (Allen et al., 2000). Although because its high reproducibility, it can be removed by the average artefact subtraction approach. On the other hand, ballistocardiogram noise caused by head motion from the cardiac process, is less unreproducible and require more advanced denoising techniques to remove. A

recently published paper from our group proposed a data-driven beamforming technique to remove ballistocardiogram, tested on the same dataset in *Study 1* of the present thesis (Uji et al., 2021).

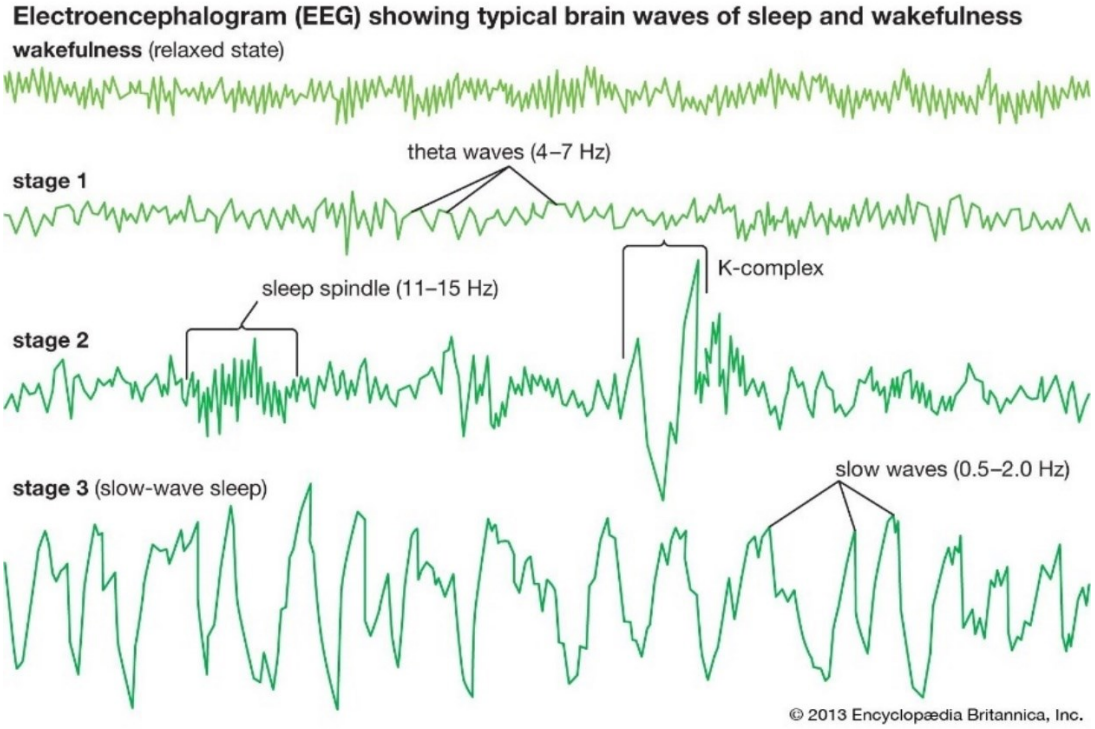

Figure 2-3 Illustration of EEG characteristic waves in wakefulness, NREM1, NREM2 and NREM3 stages. Adapted from a webpage article authored by Dang-Vu et al (Dang-Vu et al., 2022). https://www.britannica.com/science/sleep#ref38758.

Simultaneous EEG-fMRI acquisition made it possible to assess functional connectivity during sleep. Cross et al recently found significantly increased functional network segregation during a recovery nap quantified by functional clustering ratio (FCR) (N. E. Cross et al., 2021). Using the same metric FCR, Boly et al found significantly increased network segregation in NREM sleep comparing to wakeful rest, especially in Visual network and salience network (Boly et al., 2012). The topic of investigating the association between functional connectivity and sleep will be further discussed in **Chapter 3**, where we applied SPARK to investigate brain network segregation during sleep.

2.4 Functional connectivity in epilepsy

As mentioned in graph theory studies, the "small-world" structure of the human brain is highly efficient both globally and locally. However, the disadvantage of "small-world" is that the connector hub brain regions are even sensitive to neuronal disease, then leading to significant functional network alteration. In epilepsy, anatomical abnormalities can appear in connector hub regions, such as the hippocampus, leading to overall network disruption. A growing literature has reported altered functional connectivity in epilepsy (Bettus et al., 2009; Lee et al., 2018; W. Liu et al., 2021; Royer et al., 2022; Waites et al., 2006; Zhang & Raichle, 2010). Royer et al reviewed and summarized recent discoveries regarding functional and structural hub reorganization in common epilepsy types, based on fMRI, structural MRI, and electrophysiological imaging findings (Royer et al., 2022). As suggested by Royer et al., not only do the atypical hub maps help understand the underlying seizure-generating network, but hub maps may also serve as potential biomarkers for epilepsy-related cognitive disruption and predicting postsurgical seizure outcomes (Royer et al., 2022). The association between functional connector hub and epilepsy will be further discussed in the introduction in **Chapter 4**, where we apply SPARK as a novel method to quantify the hub reorganization in TLE and FLE.

Evidence of long-term post-surgical failures raises concerns about whether patients are receiving the most effective care. Rs-fMRI reveals highly organized spatial functional networks across subjects (Fox & Raichle, 2007), which are often reorganized in epilepsy (Constable et al., 2013; Lee et al., 2018). Whereas the reorganizations depend on the etiology of the disease, specific functional network properties are likely to predict postsurgical outcomes (He et al., 2015). In addition, structural connectivity analyzed using Diffusion Weighted Imaging (DWI) reveals white matter pathways, which suggests alteration of structural connectivity in epilepsy, as another candidate biomarker for the postsurgical outcome (Alizadeh et al., 2019). In this next study, we will focus our investigation on the analysis of functional connector hubs of brain networks, whereas hubs are defined as brain regions exhibiting denser connections with distant brain regions than others (Bullmore & Sporns, 2009). Connector hubs are the key regions participating in inter-network connectivity through long-range connections and ensuring overall network integrity (Heuvel & Sporns, 2011). Temporal Lobe Epilepsy (TLE) and Frontal Lobe Epilepsy (FLE) are two typical categories of focal epilepsy (Culhane-Shelburne et al., 2002). Using SPARK (Lee et al., 2016), a new methodology proposed by our group to estimate connector hubs in rs-fMRI, alterations of functional connector hubs have been previously reported in TLE (Lee et al., 2018). When comparing TLE and FLE, other groups reported different functional networks, involving notably specific subcortical connectivity patterns (Výtvarová et al., 2017), together with the

specific reorganization of structural pathways detected using DWI (Campos et al., 2015).

In conclusion, in **Chapter 2**, we introduced the concept of functional connectivity studies. We introduced the state-of-the-art methodologies used to investigate functional connectivity. Functional connectivity can also be a powerful tool to investigate brain functions in sleep and discovering brain alterations in disease.

Chapter 3 – *Study 1: Hierarchical segregation of functional brain networks at NREM sleep and attention function*

Title: ***Hierarchical segregation of functional brain networks at NREM sleep and attention function*** **(Publication in preparation)**

Authors: Kangjoo Lee+, Yimeng Wang+, Nathan Cross, Aude Jegou, Fatemeh Razavipour, Florence B. Pomares, Aurore A. Perrault, Alex Nguyen, Umit Aydin, Jean Gotman, Thien Thanh Dang-Vu, Christophe Grova

(+: co-first authors)

3.1 Preface

This study is based on a dataset of 20 healthy participants who underwent total sleep deprivation then took a one-hour recovery nap while being scanned for fMRI time-series. This dataset was acquired by Aude Jegou during her Master's degree at Concordia. This dataset was supported by Dr. Christophe Grova and Dr. Thien Thanh Dang-Vu. Three papers have been published based on this study focusing on research interests by our colleagues (N. Cross et al., 2021a; N. E. Cross et al., 2021; Uji et al., 2021). The present study specially focusing on functional segregation during NREM sleep and its association with cognitive performance after nap. The present study is under close collaboration between Dr. Kangjoo Lee and I. The present study is adapted from one of the projects in Dr. Kangjoo Lee's PhD dissertation. A detailed description of the work distribution between us can be found in **section 3.7.** Notably, section 3.7 will not be included in the publishing paper, but only included in the thesis for clarity of my work.

3.2 Abstract

Decline in cognitive performance is usually observed after sleep deprivation in healthy adults, where non-rapid eye movement (NREM) sleep may play a role. Neuroimaging can be used to decipher complex patterns of interconnection between brain regions the awake condition but also during sleep. We hypothesize that patterns of integration within hierarchical network organizations alter at NREM sleep compared to wakefulness.

Using a sparse dictionary learning based analysis of resting state fMRI, we identify individual hub regions located at the intersection of spatiotemporally overlapping networks by measuring k-hubness, which is the number of overlapping networks in each voxel. To quantify systematic changes in hub-associated network organizations, we propose a new metric, the hierarchical segregation index (HSI), using the ratio of k-hubness estimated at the voxel level and at the regional level.

We found increased network segregation occurring during NREM2 sleep, when compared to awake resting state, mainly within the visual, default mode and association cortex areas. In the visual network, we also found further segregation increase in NREM3 when compared to NREM2. Such patterns were associated with the amount of working memory performance decline associated with sleep deprivation. The observed state-dependent changes in HSI provided complementary information to those estimated using the functional clustering ratio which is an algorithm quantifying network segregation based on a Bayesian framework. The correspondence between the two measures is inhomogeneous over the cortex, exhibiting the strongest correspondence in the dorsal attention network. This study provides multi-faceted evidence of functional brain network segregation during NREM sleep and a role of network segregation in the association areas during sleep and attention function.

Keywords: non-rapid eye movement sleep, fMRI, sleep deprivation, hub, attention

3.3 Introduction

The role of sleep in human cognition can be studied using neuroimaging techniques able to track variations in brain activity across different sleep stages. Non-rapid eye-movement (NREM) sleep stages are usually defined using spontaneous brain waves detected on scalp electroencephalography (EEG) in the absence of rapid eye movements (Berry et al., 2015). Spindles are transient oscillations that mostly occur during NREM sleep stage 2 (NREM2)(de Gennaro & Ferrara, 2003; Steriade et al., 1993) and are suggested to play an important role in memory consolidation and sleep quality (Dang-Vu et al., 2008). The deepest NREM stage, NREM3, is related to sleep homeostasis (Marshall et al., 2006; Ngo et al., 2013), characterized by the occurrence of slow waves on scalp EEG. Using simultaneous recordings of scalp EEG with functional magnetic resonance imaging (fMRI), one can monitor hemodynamic processes through the measurement of the blood-oxygen-level-dependent (BOLD) signal, during different sleep stages or conditions (few review). Such studies have notably reported fMRI signals consistently synchronized to slow waves activity (< 1 Hz) on scale EEG (Dang-Vu et al., 2008). Considering potential roles of sleep in cognitive functions, experiments involving cognitive tasks following sleep deprivation (SD) can be useful to study the relationship between sleep, cognition and functional organizations of the brain (N. E. Cross et al., 2021).

Mapping brain functions to the brain can be facilitated by further understanding the brain organizations as patterns of large-scale networks. Large-scale networks can be identified by measuring functional connectivity between brain regions from resting state fMRI data. Several resting state networks patterns have been consistently found during wakeful resting state (Smith et al., 2009), whereas during NREM sleep, resting state network architecture was associated with reorganization, especially in the visual and salience network (Boly et al., 2012). Indeed, EEG/fMRI sleep studies have reported functional connectivity decreases during sleep within the default mode network (Horovitz et al., 2009) and between the default mode and its anti-correlated networks (de Havas et al., 2012; Sämann et al., 2011). Using high-density scalp EEG and source imaging, activation of the premotor region evoked by non-invasive transcranial magnetic stimulation was associated with propagations of neuronal activity to neighboring regions, whereas during NREM sleep, such an evoked response disappeared more rapidly with no propagations (Massimini et al., 2005). Decrease in thalamo-cortical connectivity during NREM1 was followed by disruption of cortical-cortical connectivity during deep NREM sleep (Spoormaker et al., 2010), suggesting a systematic reorganization of brain networks associated with different sleep stages.

Integration within and between brain networks plays a key role in information processing and cognition, whereas decreases in network integration has been reported in low vigilance states (Lee et al., 2022; T. T. Liu & Falahpour, 2020; Tagliazucchi et al., 2013). Decrease of corticocortical functional connectivity have been found in slow-wave sleep (NREM3 and 4) (Spoormaker et al., 2010). Brain regions exhibiting several connections to other regions are identified as hubs using graph theory, whereas some have found increased number of hubs in NREM1 and 2 sleep stages when comparing to wakefulness, and following by decreased number of hubs in NREM3 and 4 (Spoormaker et al., 2011). Using a metric derived from information theory, Boly et al quantified hierarchical segregation of brain networks into their respective sub-networks during sleep (Boly et al., 2012), by measuring the so-called functional clustering ratio (FCR) (Marrelec et al., 2006b, 2008b). FCR was estimated as the ratio between the integration within sub-networks when compared with the integration between these subnetworks, therefore reflecting the balance of between-network integration and within-network integration. They reported increased FCR in motor, visual, default mode, dorsal attention, executive control and salience networks during NREM sleep when compared to wakefulness, suggesting more segregation between networks during NREM sleep (Boly et al., 2012). Recently, by measuring FCR during task-based fMRI after normal sleep and after a night of total SD, our group reported reduced network integrations following SD which is associated with attention and executive cognitive performance (N. E. Cross et al., 2021). These studies, however, did not study potential variations of network integration during different NREM sleep stages (e.g., NREM2 and 3).

We aim at quantifying and assessing brain network integration up to the voxel resolution from resting state fMRI, while aiming at evaluating hubs during NREM sleep which was lack of attention before. We hypothesize that hub regions that participate in between-network integration play a role in state-dependent changes in functional brain integration, and such changes are associated with maintenance or loss of cognitive performances elicited by sleep deprivation.

Analyzing hubs of brain network from connectome matrices, reporting correlation between brain regions, is actually biased by multicollinearity, since the time-courses of networks decomposed from the whole brain are themselves related (Lee et al., 2022; Yeo et al., 2014). To detect such complex structures reliably at the single subject level, we recently developed a method called a sparsity-based analysis of reliable *k*-hubness (SPARK) based on sparse dictionary learning. *k*-hubness is the number of overlapping networks in each voxel or region, and has been applied to identify reorganization of hubs in epilepsy (Lee et al., 2018) and in healthy adults across different levels of arousal (Lee et al., 2022).

In the present study, we propose to investigate resting state network segregation during NREM2 and NREM3 sleep stages, measured during a one-hour nap following a whole-night SD, in comparison to wakeful resting state after normal sleep. We used the SPARK method to estimate overlapping network structures and hubs from individual resting state fMRI. An important contribution of this work is to propose and validate the usefulness of a new metric, the hierarchical segregation index (HSI), to quantify network segregation using the ratio of *k*-hubness estimated across two spatial resolutions. The HSI utilizes the unique ability of SPARK to provide the hubness in the voxel-to-region hierarchy at the same time. In comparison to FCR (Boly et al., 2012; N. E. Cross et al., 2021), our proposed HSI is computed at the lower-level system (i.e., voxel) of this hierarchy, i.e., at the voxel level, thus providing a finer-scale evaluation of network segregation, when compared to other approaches such as FCR assessing segregation at higher levels of the hierarchy of brain networks (Boly et al., 2012; N. E. Cross et al., 2021).

3.4 Results

We recruited 20 volunteers according to our inclusion criteria, which is the same as Cross et al (N. E. Cross et al., 2021): participants were aged between 18 to 30 years, healthy and good sleepers. For each subject, we obtained and analyzed simultaneous high-density EEG/fMRI data from the 5-minute resting state fMRI scan following normal sleep night and the 60-minute resting state fMRI scan during the 1-hour nap inside the scanner, after a whole night of SD (highlighted in orange boxes in **Figure 3-1A**). During the night of SD, to ensure the subject does not fall asleep, an investigator accompanied the subject and offered to talk, watch movies and play games. Sleep stages during the recovery nap were marked by expert for the 60-minute EEG data acquired during the nap after SD. Subsequently, fMRI segments being in NREM2 or NREM3 stages for >5 min was selected and trimmed to 5 min. We considered the following datasets for further network analysis: resting state fMRI data obtained from 14 subjects after normal sleep, 18 subjects during NREM2 after whole-night SD, and 12 subjects during NREM3 after whole-night SD. We obtained a total duration of 36 ± 13.4 minutes (mean and standard deviation across subjects) for NREM2 and 10.8 ± 8.8 minutes for NREM3 (**Figure 3-1B**). The total number of time windows (segments) exhibiting 5 minutes or more of sequential time frames during a specific sleep stage was 2.4 ± 1.1 segments for NREM2 and 0.9 ± 0.8 segments for NREM3 (**Figure 3-1C**). Finally, one continuous 5-minute fMRI run was selected for each state per subject based on our inclusion criteria (See **Methods**). SPARK method was applied on those selected datasets to estimate the functional hub organizations in each 5-minute run within a specific sleep stage.

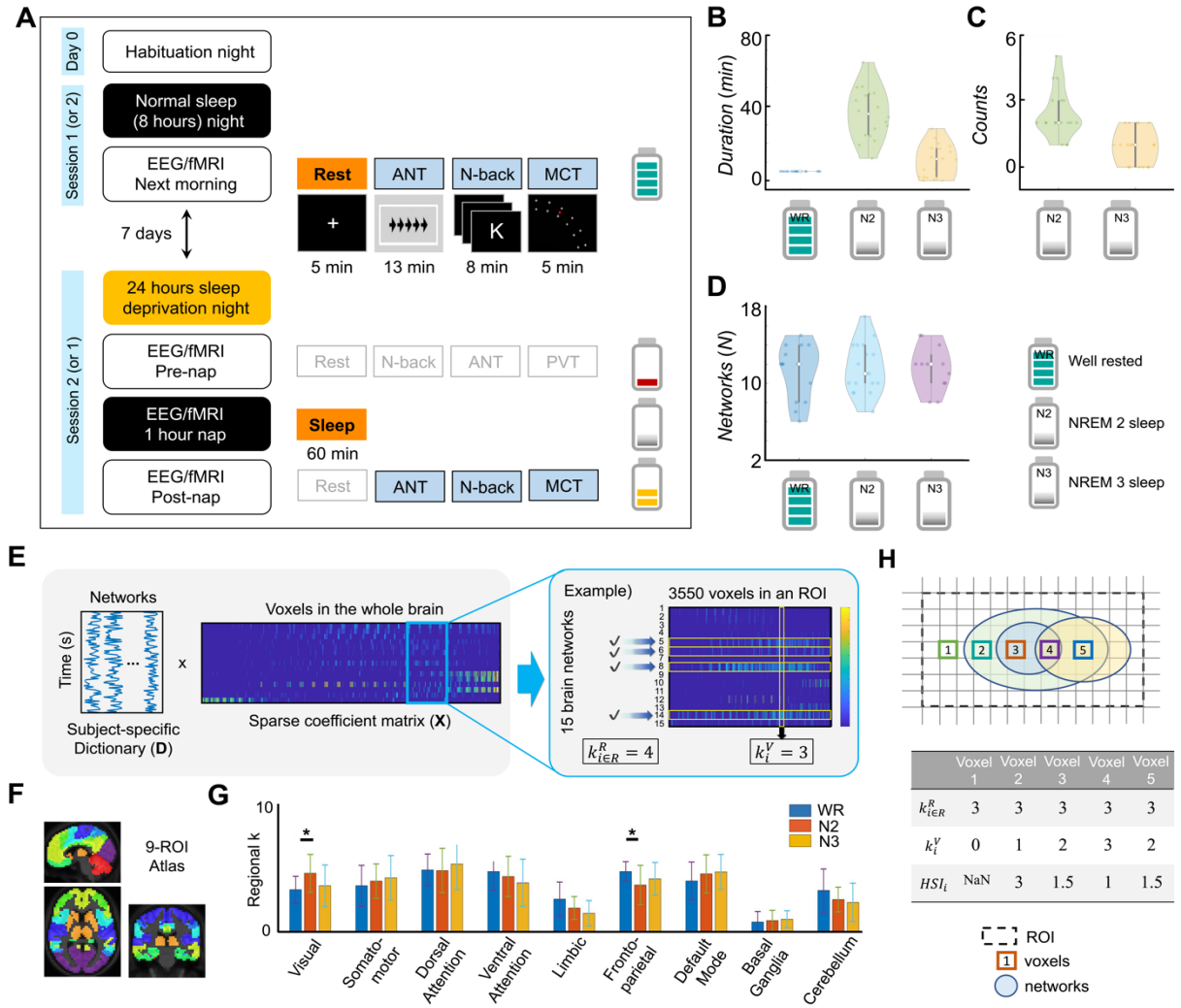

Figure 3-1 Simultaneous EEG/fMRI data across vigilance states. (A) Overview of study design, which is the same study design as Cross et al (N. E. Cross et al., 2021). Participants visited to the lab three times: a habituation night to evaluate their eligibility (good sleepers), followed by a counterbalanced design of two experimental nights, starting with either session 1 or 2. In the morning following a normal sleep (at least 8 hours), high-density EEG/fMRI scans are acquired while the subjects either perform three cognitive tasks (ANT: Attention network task, N-back and MCT: Mackworth clock test) or rest while watching a fixation cross. In the morning following a whole-night SD (0-hour sleep), subjects underwent high-density EEG/fMRI acquisition while first performing the same three cognitive tasks and rest for 5 minutes. Next, subjects were provided an opportunity to sleep inside the scanner for one hour, before performing again the same three tasks and rest for 5 minutes after this recovery nap. Data analyzed in this study are highlighted in orange (imaging data) and blue (behavioral data) boxes. **(B)** Total duration of NREM2 sleep (N2) and NREM3 sleep (N3) during the one-hour nap inside the MRI scanner after a whole-night SD of each individual. **(C)** Total number of time windows (segments) equal or longer than 5 min that N2 or N3 sleep stages. **(D)** Distribution of the global network scale, i.e., the total number of networks N estimated by SPARK at the individual level. The total number of functional networks, estimated for each 5-minute individual fMRI run using SPARK, was preserved across

brain states. (**E**) Estimation of the voxel-level (k^V) and region-level (k^R) *k*-hubness from the individual sparse coefficient matrix (N networks by voxels) using SPARK. (**F**) The 9-region atlas used to estimate *k*-hubness at the region level. (**G**) The mean and standard deviation of region-level *k*-hubness within the nine pre-defined networks. (**H**) The hierarchical segregation index (HSI) is computed for each voxel as the ratio between *k*-hubness values estimated at the region-level and at the voxel-level. In this toy example, voxel 5 that has the highest number of network overlaps exhibits the lowest HSI value (i.e., more integration or less segregation within that region).

Functional network hubs reconfigure during NREM sleep

We first assessed using SPARK if the global network scale N, i.e., the total number of networks estimated for each analyzed fMRI segment, was preserved across brain states within individuals (Achard et al., 2012; T. T. Liu & Falahpour, 2020). To do so we applied the methodology developed in (Lee et al NIMG clin), to estimate N from the data. We found that the estimated total number of networks in the whole brain in individuals was preserved across brain states: 10.7 ± 3.4 (mean ± standard deviation) for resting state after a normal night, 11.6 ± 2.6 during NREM2 sleep and 11.6 ± 2.4 during NREM3 sleep (**Figure 3-1D**). In the subsequent analyses, we tested our hypothesis that topological patterns of network integration alter from wakeful resting state to NREM sleep, even if the global network scale N was preserved within individuals across different states. For each state per subject, in addition to the estimation voxel level *k*-hubness estimated using SPARK (k^V: the number of networks overlapping in this voxel), we proposed a new method to estimate *k*-hubness at the region level (k^R: the number of networks overlapping in a region of interest) from SPARK decomposition (**Figure 3-1D**).

To estimate the region level *k*-hubness, we considered nine larger networks, defined using a modified version of Yeo-7 functional atlas (Thomas Yeo et al., 2011b) combined with two additional networks defined using automated anatomical labeling (AAL) template (Rolls et al., 2020), the subcortical network (basal ganglia) and the cerebellum network-based subcortical regions (basal ganglia and cerebellum) (**Figure 3-1F**) (Thomas Yeo et al., 2011b; Tzourio-Mazoyer et al., 2002). The original Yeo-7 functional limbic network was modified to add the hippocampi and amygdalae from the AAL atlas. Estimating hubness at the regional level over those nine networks, we found that k^R increased in the visual regions and decreased in the frontoparietal regions during NREM2 sleep when compared to wakeful resting state (**Figure 3-1G**, Bonferroni corrected $p<.05$). Our results are in agreement with our previous work showing arousal level-dependent changes in region-level *k*-hubness during wakeful resting state (Lee et al., 2022).

We then assessed how patterns of hubness values estimated at the voxel level (k_V), would vary across vigilance states, as a measure of integration between networks. During wakeful resting state

(WR), the group average k_V over subjects was found high in the default mode, frontoparietal association, somatomotor, and visual areas (**Figure 3-2A**), in agreement with our previous work estimating voxel-level *k*-hubness (Lee et al., 2016, 2018). Such patterns were found to alter when subjects slept in scanner after whole-night SD (permutation test, FDR corrected $p<.05$, **Figure 3-2B**). When comparing NREM2 relative to wakeful resting state, we found decreases in *k*-hubness in parts orbitofrontal cortex. Specifically, we found sleep-associated hubs in the hippocampus, right posterior cingulate cortex, right cerebellum, right inferior temporal gyrus, fusiform gyrus, posterior orbitofrontal cortex, insula, olfactory cortex, and subcortical structures including the putamen, caudate and ventral striatum (two-sample permutation test, $p_{FDR} < 0.05$, corrected for false discovery rate, **Figure 3-2B**). Surprisingly, we found that *k*-hubness then increased within these regions during NREM3 sleep when compared to WR ($p_{FDR} < 0.05$; N3 > WR > N2), suggesting that sleep stage specific changes in overlaps between brain networks and therefore hubness distribution. Note that between-network integration measured from overlapping networks using the SPARK framework should be interpreted differently from conventional measure of between-network integration of non-overlapping networks. It is because network overlap using SPARK can be observed at one of the core regions of large-scale network, rather than at its anatomical boundaries. See our discussion for details.

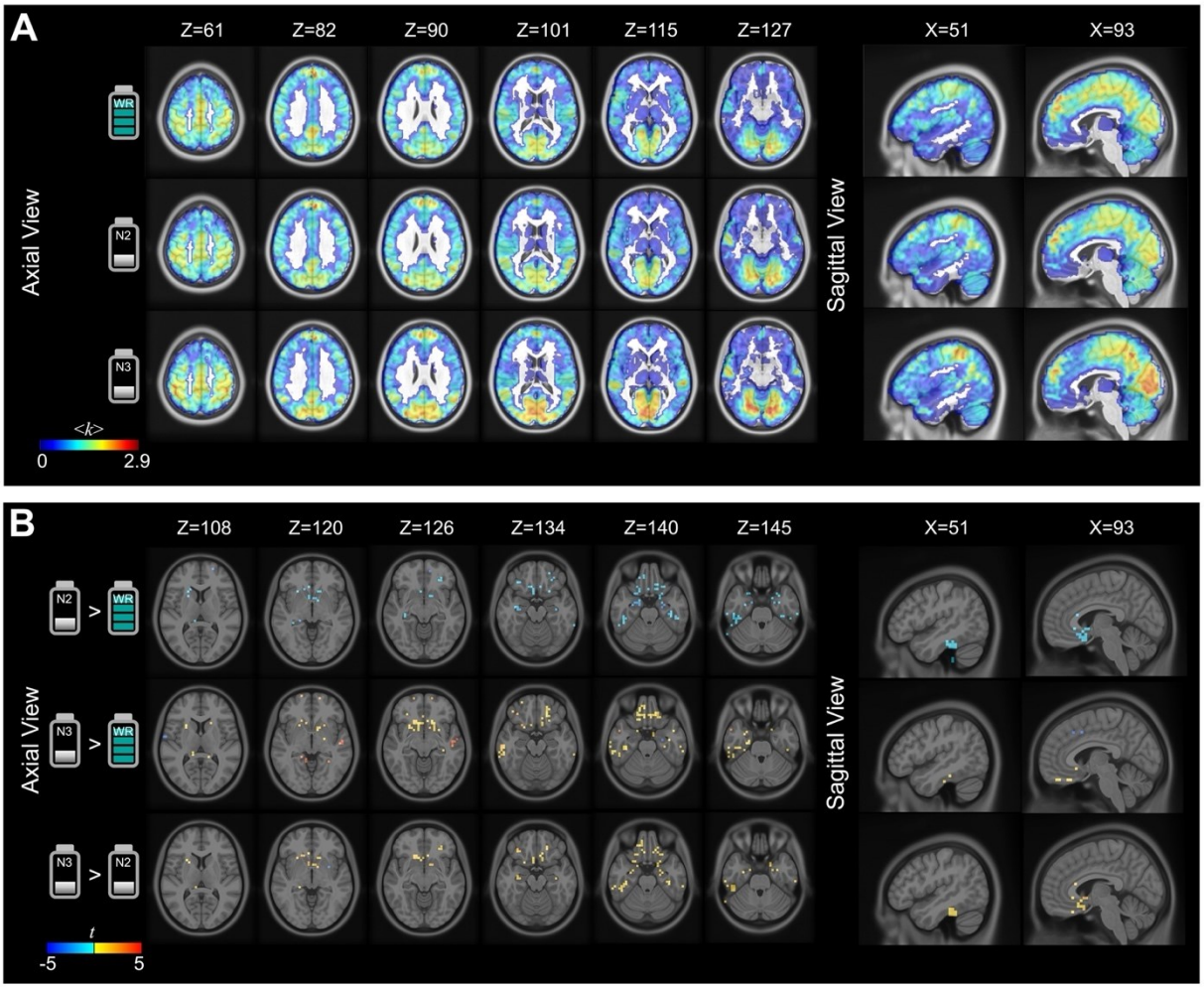

Figure 3-2 Altered patterns of functional network overlap across different vigilance states. (**A**) Group average voxel level *k*-hubness maps (k^V) estimated from wakeful resting (WR), NREM2 (N2) and NREM3 (N3) sleep states. (**B**) *t*-statistics map comparing k^V between states: N2 > WR (top), N3 > WR (middle), N3 > N2 (bottom). $p_{FDR} < 0.05$ using two-sample permutation tests with 10,000 permutations.

Hierarchical segregation of brain networks during NREM sleep

Our extension of SPARK was used to estimate *k*-hubness at two hierarchical levels, at the voxel level and at a regional level, within nine networks. We used this ability to define a new measure of network segregation. To assess if a region was functionally segregated into several sub-networks, we defined the HSI_i for each voxel i using the ratio of region-level *k*-hubness for a region R to which the voxel i belongs ($k^R_{i\in R}$), to voxel-level *k*-hubness (k^V_i) (**Figure 3-1H**).

$$HSI_i = k^R_{i\in R}/k^V_i$$

Therefore, a high HSI value reflects that the number of networks involved in a region *R*, to which the voxel *i* belongs to, is larger than the number of networks involved in this particular voxel. This also reflects that this voxel may be involved in several networks (k_i^V), but it belongs to a larger system (the pre-defined region *R*) that involves more subnetworks, whereas functional integration between those sub-networks is low, suggesting more segregation between subnetworks involved in the region/network *R*. A high HSI value suggests within-region inhomogeneity of the region R. On the other hand, a low HSI value reflects that this voxel *i* belongs to a system (the pre-defined region *R*) that involves a similar number of networks than the value k_i^V. Therefore, a low HSI suggests within -region homogeneity, reflecting large integration between subnetworks involved in region/network *R*. HSI is equal or larger than 1, because the network, in which a voxel belongs to, should involve an equal or larger number of networks than the number of networks involved in this particular voxel. The particular feature of this new proposed metric of network segregation, HSI, is that it can be estimated at the voxel level, for a specific level of the network hierarchy, i.e., the total number of R regions considered (here nine regions). For each state (WR, NREM2, NREM3), we estimated group average maps of *k*-hubness and HSI values by averaging the values across subjects in each voxel.

In **Figure 3-3A**, we are presenting group average HSI maps estimated using SPARK during wakeful resting state, NREM2 sleep and NREM3 sleep. During NREM2, when compared to WR, we found increased network segregation in regions of the visual and default mode networks (permutation test, FDR corrected $p<.05$, **Figure 3-3B**). Specifically, regions involving more network segregation during NREM2 sleep include parts of the visual association cortex, lingual occipital superior, left fusiform gyri, superior parietal, postcentral, paracentral lobule, precuneus, posterior cingulate, and medial superior frontal cortex. Among them, regions of the default mode and somatomotor network did not show any changes in HSI when comparing NREM2 and NREM3 sleep stages (N3 ≈ N2 > WR). On the other hand, regions involving the visual network showing decreases in HSI values (N2 > N3 ≈ WR). On the other hand, during NREM2 relative to wakeful resting state, we found decreased network segregation in regions of the orbitofrontal cortex, ventral striatum, rectus, medial orbitofrontal cortex, caudate, putamen, right fusiform, inferior temporal cortex, parahippocampal gyrus and hippocampus. These regions, however, then showed increases in HSI values during NREM3 sleep (N3 > WR > N2).

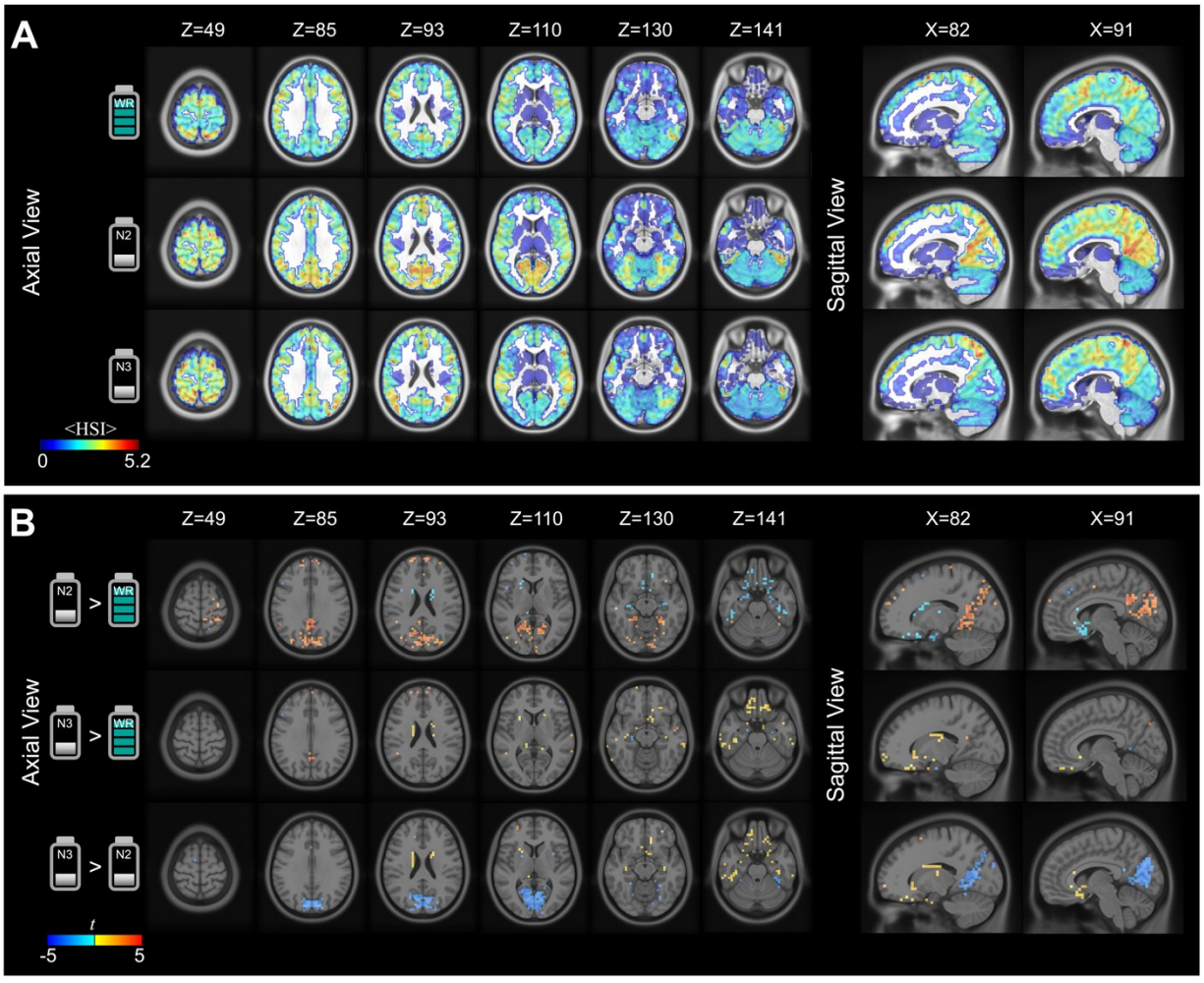

Figure 3-3 Altered patterns of functional network segregation across different vigilance states. (**A**) Group average HSI maps estimated from wakeful resting state (WR), NREM2 sleep (N2) and NREM3 sleep (N3). (**B**) *t*-statistics map comparing HSI between states: N2 > WR (top), N3 > WR (middle), N3 > N2 (bottom). Two-sample permutation tests, 10,000 permutations, $p_{FDR} < 0.05$.

More network segregation during NREM sleep was associated with decreases in task performance after SD.

We next investigated whether the observed functional network segregation during NREM sleep were associated with the level of cognitive performances after recovery nap. As reported by Cross et al., the cognitive performance after total sleep deprivation was significantly dropped comparing to the cognitive performance after a normal night of sleep (N. E. Cross et al., 2021). After a one-hour recovery nap, the cognitive performance was significantly increased comparing to SD, but still the level of performance remains low comparing to normal night (N. E. Cross et al., 2021).

Therefore, we want to specifically compare if the segregation during the recovery nap comparing to the segregation during WR will be associated with the performances after the recovery nap comparing to the performance after a normal night of sleep, i.e., using the wakefulness after a normal night as a baseline for each subject.

To assess cognitive performance during N-back, MCT and ANT tasks realized either during the WR period or following the recovery nap after SD, we measured reaction time (RT) in milliseconds and the accuracy as the percentage of correct responses. To assess if these behavioral scores were associated with network segregation during sleep, voxel-wise HSI measures were averaged within each region R for each subject ($< HSI >_R$). We considered 9 regions R, consisting in the modified Yeo-7 functional networks in addition to basal ganglia and cerebellum regions as mentioned before. We therefore obtained nine region-average $< HSI >_R$ values per subject in each state. Between-state difference in region-average $< HSI >_R$ values were then computed for each subject ($\Delta< HSI >_R$).

Our goal was to study if there was any association between state-dependent changes in $< HSI >_R$values and the scores assessing individual task performances: reaction time (ms) and accuracy (%). To quantify state-dependent changes in network segregation, we assessed the difference in HSI values ($\Delta< HSI >_R$) between NREM sleep (N2 or N3) and wakeful resting state after normal sleep (WR) together with the average change in task performance (RT or accuracy) between task completed during the recovery nap and the normal night. Pulling together results from all 9 regions R and all subjects, we found a weak correlation (p<0.05) between $\Delta< HSI >_R$ and the difference in N-back task performances between post-nap and normal night conditions. More precisely, increase network segregation associated with NREM 2 sleep (when compared to WR), was negatively correlated with task accuracy ($r = -0.2, p < 0.05$; **Figure 3-4A**) and positively correlated with latency ($r = 0.23, p < 0.05$; **Figure 3-4B**). More specifically, decrease in the task performances was correlated with increase $\Delta< HSI >_R$ during NREM2, in the regions belonging to the dorsal attention network, as defined using the Yeo-7 atlas (**Figure 3-4C, D**). Similarly, increases in network segregation during NREM 3 sleep was also negatively correlated with task accuracy ($r = -0.24, p < 0.05$; **Figure 3-4**) and positively correlated with latency ($r = -0.28, p < 0.01$; **Figure 3-4F**). We found a similar association of $\Delta< HSI >_R$ in the dorsal attention areas during NREM3 when compared to WR with changes in task performances (**Figure 3-4**G-H). Other than dorsal attention network region, we did not find any significant association between HSI and task performances for N-back task performance.

Given the fact that the whole-brain level results, pulling together average $\Delta< HSI >_R$ values for

all 9 regions and all subjects, showed an association with the N-back task scores, we also performed an *ad-hoc* analysis to obtain a more robust statistical evaluation. Instead of directly correlating difference $\Delta< HSI >_R$ of average HSI values within each region to the N-back task performance scores, we performed a bootstrap resampling approach, to obtain 1,000 bootstrap replications of average $< HSI >_R$ values for each region R by selecting parcels with replacement (See Methods). We then correlated each resampled $\Delta< HSI >_R$ values with corresponding task performance, therefore ensuring that averaging HIS values within each region R was robust. and computed the corresponding 1,000 correlation coefficients (see Methods). When re-analyzing the association for the $\Delta< HSI >_R$ (N2-WR) in **Figure 3-4A** and **Figure 3-4B** using the proposed bootstrap approach, the median correlation (r_{median}) computed between the $\Delta< HSI >_R$ values from the whole cerebral cortex with the N-back task performance accuracy was -0.65 (median of p-values, $p_{median} = 0.013$), whereas the median correlation r_{median} computed between these values with the latency was 0.64 ($p_{median} = 0.014$). When re-analyzing the same association using the bootstrap approach for the $\Delta< HSI >_R$ from each region separately, the $\Delta< HSI >_R$ (N2-WR) from the dorsal attention network was associated with the N-back task performance accuracy at $r_{median} = -0.553$ ($p_{median} = 0.04$) and with the latency at r_{median} =0.57 ($p_{median} = 0.033$). We did not find any effect when re-analyzing the association of the N3 sleep associated changes in $< HSI >$ and task performances using this bootstrap approach.

Other than the task performance of N-back task, we have also applied the aforementioned analysis for ANT task and MCT task. In ANT task, using the bootstrap resampling technique, the $\Delta< HSI >_R$ (N2-WR) from the dorsal attention network was associated with the accuracy at $r_{median} = -0.545$ ($p_{median} = 0.044$), but its latency showed no significant effect. Additionally, the $\Delta< HSI >_R$ (N2-WR) from the frontoparietal network was associated with latency at $r_{median} = -0.551$ ($p_{median} = 0.041$), but the accuracy showed no significant effect. However, in MCT task, we did not find significant association between HSI and MCT task performance.

Overall, our results suggest that more network segregation during NREM sleep following SD was as associated with further reduced post-nap task performance, when compared to the normal night. The dorsal attention network seems to play a particular role in this neural-behavioral relationship.

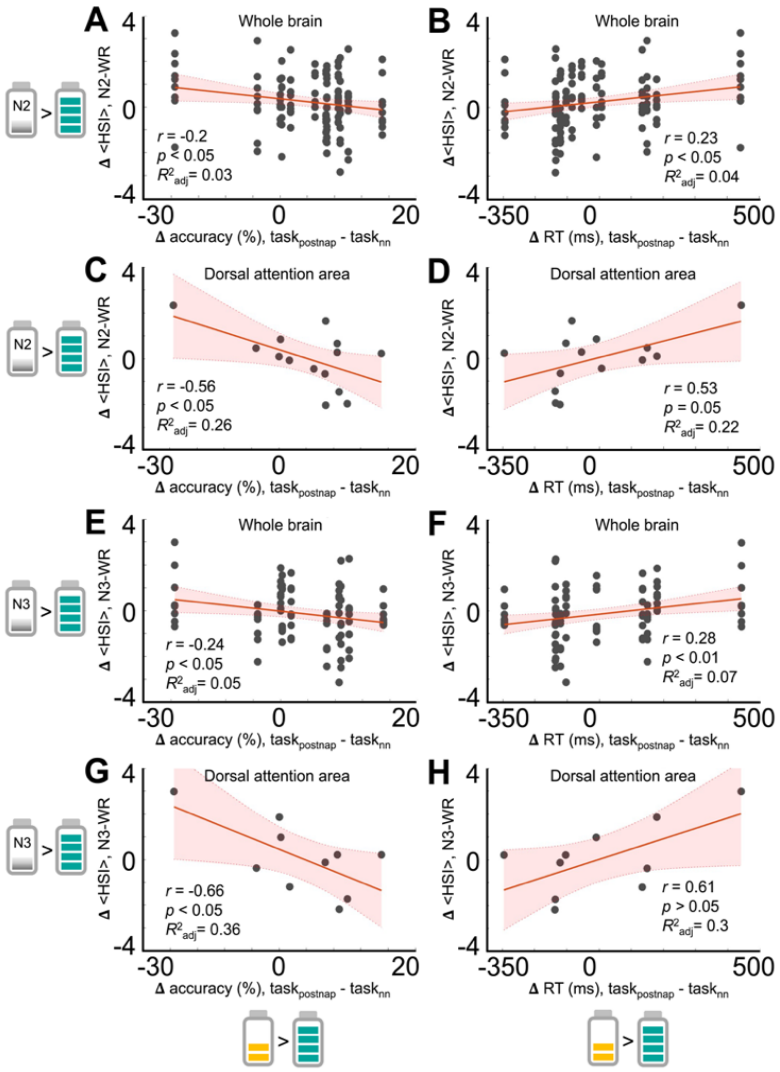

Figure 3-4 Network segregation during NREM sleep after a whole-night SD is associated with worse retrieval of N-Back task performance after the recovery nap following whole night SD. A region-average $< HSI >_R$ was computed averaging the voxel-level HSI values across the voxels belonging to a region R. Nine regions were pre-defined using the modified Yeo-7 functional network atlas, basal ganglia and cerebellum. $\Delta< HSI >_R$ was estimated as the difference in $< HSI >_R$ values between NREM sleep stage (N2 or N3) and well-rested state (WR). The correlated with the difference in task performance measured during task fMRI after normal night sleep (subscript: nn) and after the recovery nap after whole-night SD (subscript: postnap). In graph **A, B, E, F**, we pulled together results from all regions and all subject, and each dark grey dot represents one of the nine regions from an individual. The total number triangles are therefore 9 times the number of subjects at each state. In graph **C, D, G, H,** each dark grey dot represents the dorsal attention region only from an individual. Red solid line and shaded area represent a linear fit and 95% confidence interval, estimated between the $\Delta< HSI >_R$ and behavioral scores. r is the Pearson's linear correlation coefficient. p-value was calculated for the F-test on the model. R^2_{adj} is the adjusted coefficient of determination.

Relationship between the HSI and FCR

Functional Clustering Ratio (FCR) is defined as the ratio of the integration within subsystems and the integration between subsystems, originally proposed by Marrelec et al. (Marrelec et al., 2006b, 2008b), adapted in Boly et al (Boly et al., 2012) and Cross et al (N. E. Cross et al., 2021). An increase in FCR indicates that subsystems become functionally more independent of each other, indicating more segregation within the given system (Boly et al., 2012). Cross et al. found the task performances during WR, SD and after the recovery nap were associated with the network integration/segregation of the task fMRI during those stages, measured by FCR (N. E. Cross et al., 2021). Our objective instead was to investigate if the network segregation during NREM sleep of the recovery naps measured with HSI associates with the task performances after the recovery nap. HSI and FCR have different assumptions about network organizations and hierarchy. In addition, HSI generates a whole brain segregation quantification map as shown in **Figure 3-3**, while FCR generates a single value for a network of interest. However, both HSI and FCR showed association with cognitive performance. Therefore, we wanted to explore to which degree the two measures overlap and how they differ to each other. More specifically, in the present work, we computed FCR separately for each sleep stage (N2 and N3) during the recovery nap, and for the resting state after a normal night (WR) using our present fMRI data. For all brain stages, we evaluated FCR at two different level: (i) how functional connectivity of the whole cortex segregates into Yeo7 networks (FCR_W), and (ii) how brain functions on the scale of Yeo7 networks segregates into Yeo17 networks (FCR_R). More detail of the computation of FCR can be found in **Methods**. We then compared the resulting FCR values to the HSI maps. The whole-cortex level FCR_W was compared to the mean FCR of the whole cortex. The regional level (FCR_R) was compared to the mean FCR within each Yeo7 regions.

For each individual subject, we averaged the HSI values over the voxels belonging to the whole brain ($< HSI >_W$). For comparison purposes, subcortical and mesial temporal structures that were not part of the Schaefer100 parcellation considered for FCR estimation were therefore not considered. As a result, whole-brain average $< HSI >_W$ was 2.08 ± 0.47 during resting state following normal sleep, 2.36 ± 0.52 during NREM2 sleep, 2.23 ± 0.67 during NREM3 sleep, and 2.31 ± 0.58 when combining NREM2 and NREM3 sleep states (**Figure 3-5A**). The FCR_W was 0.66 ± 0.12 at resting state after normal sleep and increased to 0.74 ± 0.09 at N2 (Wilcoxon rank sum test, p<0.05), 0.73 ± 0.1 at N3 sleep, and 0.73 ± 0.1 when combined N2 and N3 sleep stages (p<0.01; **Figure 3-5B**). On the whole cortex level, we have found that the segregation measured by HSI and FCR were on a similar trend when comparing across stages, but only FCR (**Figure 3-5B**) showed significant differences between stages.

For the other analyses, we pooled together data from the three states (WR, N2, N3, in order to compare the FCR estimated for seven large networks (FCR_R) to the $< HSI >_R$ estimated for each of those 7 regions R. We first averaged the HSI values within each of the Schaefer100 parcels. We compared the FCR and HSI values collected from all brain states, opting out effects of vigilance state and focusing on the methodological comparison between the two metrics. A bootstrap approach was employed to obtain robust statistics for the association between the region-average HSI and the region-level FCR, to prevent a potential bias induced by within-region inhomogeneity when averaging HSI values over large regions. The bootstrap strategy was the same as the previous session of evaluating association between HSI and task performance. For each region R, 1,000 replications of $< HSI >_R$ were generated. The correlation coefficient (r) between the FCR_R and each bootstrap surrogate $< HSI >'_R$ was then calculated (see Methods). The distribution of r revealed the presence of three groups of regions, suggesting different HSI-FCR associations over the cerebral cortex (**Figure 3-5C**). Group ① mainly exhibiting significant correlation between HSI and FCR (r=0.38 ± 0.04, p<0.05) mainly included the regions of the somatomotor, dorsal attention network, and default mode network from the Yeo-7 atlas. Group ② reporting no significant correlation (r=0.11 ± 0.04, p>0.05) included the ventral attention network, limbic and frontoparietal network. Group ③ included reporting no significant correlation (r=-0.03 ± 0.02) with a tendency to show negative correlation pattern included the visual network. Since group ① was exhibiting the largest correlations, we then studied more specifically the HSI-FCR association for the three networks: somatomotor, dorsal attention and default mode network **(Figure 3-5D-F)**. Among those three, the dorsal attention network exhibited the largest correlation between the two measures, suggesting similar patterns of segregations assessed with those complementary metrics. Note that we observed that network segregation estimated using HSI in the dorsal attention network was also largely associated with changes in N-back attention task performances (**Figure 3-4**).

Together, our results demonstrate that the relationship between the two measures is inhomogeneous over the cerebral cortex, while the most relevance emerging from the dorsal attention network, supporting an association of functional brain network segregation and cognitive functions.

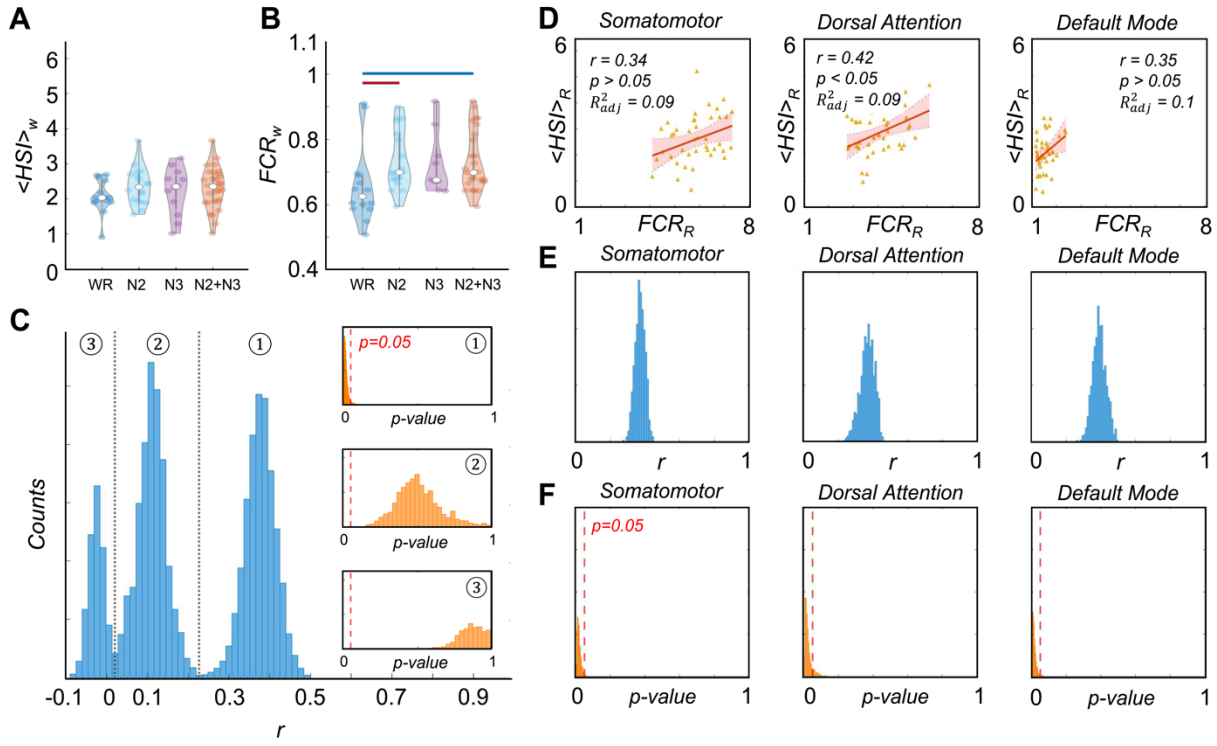

Figure 3-5 Comparison between two measure of network segregation: the hierarchical segregation index (HSI) and the functional clustering ratio (FCR), pooling together results from the three states (WR, N2, N3). (**A**) Network segregation estimated using HSI, as the ratio between *k*-hubness measured at the region- and voxel-levels. $< HSI >_W$ is the average of voxel-level HSI values estimated over the whole cerebral cortex. For comparison purposes, subcortical and mesial temporal structures that are not part of the Schaefer100 parcellation were not considered. Wilcoxon rank sum test applied, p<0.05. (**B**) Network segregation of whole cerebral cortex into seven large networks estimated using FCR_w. Each data point in (**A**) and (**B**) indicates a subject. (**C**) Distribution of the correlation coefficients between $< HSI >_R$ and FCR_R obtained using a bootstrap approach. Results from all seven cortical regions defined using the Yeo-7 network atlas were concatenated (resulting in a total of 7,000 data points). We identified three groups of data from this histogram (dotted gray lines at local minima r=0.02 and 0.23). Group ① mainly included regions of the somatomotor, dorsal attention and default mode networks, representing 42.94% of total data points in the histogram and suggesting significant correlation between HSI and FCR metrics. Group ② exhibiting weak or no correlation between HIS and FCR mainly included the ventral attention network, limbic and frontoparietal networks (42.26%). Group ③ mainly includes the visual network (15.41%) and suggested non-significant negative correlations. The distribution of p-values computed for each correlation coefficient is presented for each group in the boxes. Red vertical dotted lines indicate $p = 0.05$. (**D**) The correlations between $< HSI >_R$ and FCR_R for the somatomotor, dorsal attention and default mode networks are further illustrated. Yellow triangles in (**D**) indicate $< HSI >_R$, the average of HSI values of each region R (y-axis) and the FCR_R values obtained from the region (x-axis), while each yellow triangle corresponds to one state (WR, N2, N3) of one subject. The red line and shadow area indicates the linear regression models fitted to these data. The corresponding correlation coefficients (r), p-value and 95% confidence intervals are then presented shown. The distribution of correlation coefficients and p-values obtained from the

ad-hoc bootstrap analysis are presented in **(E)** and (**F**).

Reorganization of network overlap patterns within the dorsal attention network during NREM sleep

Taking advantage of SPARK unique ability to identify what are the actual networks associated in each hub, we finally investigated the actual patterns of network overlaps associated with the dorsal attention network and how such patterns were reorganized during NREM sleep when compared to wakeful resting state (WR). We applied such detailed analysis for the dorsal attention area only, since this network exhibited the most relevance association between HSI, FCR and changes in cognitive task performances (**Figure 3-4, 3-5**). To do so, we collected the maps of all networks involved in dorsal attention estimated at the individual level. Notably, network maps that involve less than 10% of volume overlap with the dorsal attention regions defined using Yeo-7 atlas were excluded and not collected to reduce artifactual voxel signals. Each network map was first converted to absolute values to avoid any ambiguity of signs in sparse dictionary learning and normalized to exhibit values between 0 and 1. Therefore, this analysis was limited to the spatial distribution of network overlap, without taking into account strengths of network involvement or information about antagonistic network relationships. Next, starting from all normalized networks estimating by SPARK and featuring sufficient spatial overlap with the dorsal attention are, we clustered the collection of resulted maps using the K-means clustering algorithm, where the number of clusters was determined by the median of individual region-level *k*-hubness (k^R) in this region across subjects. Network maps belonging to each cluster were finally averaged in each voxel.

Figure 3-6 shows the main clusters of functional networks involved in dorsal attention area, whereas the clusters 1/2/3/4 were manually named and organized according to their spatial similarity across states. During wakeful resting state, we found 4 clusters of networks that consistently overlap with the dorsal attention area (**Figure 3-6A**). The well-known dorsal-attention network and its anti-correlated default-mode network were found merged within in cluster 2. In addition, we also found three sensory networks functionally connected to parts of the dorsal attention area: the visual (cluster 1), somatomotor I (clusters 3), and somatomotor II (cluster 4) networks. During NREM sleep, we found three clusters involving the dorsal attention area during NREM2 sleep and three other clusters during NREM3 sleep (**Figure 3-6A**). As shown in **Figure 3-6B**, spatial patterns of clusters 1 and 2 were the least similar when comparing N2 to WR stages (cluster 1: $r_{(WR,N2)} = 0.62$; cluster 2: $r_{(WR,N2)} = 0.78$), while there is more spatial similarity of networks involved in dorsal attention region between N3 and WR (cluster 1: $r_{(WR,N3)} = 0.82$; cluster 2: $r_{(WR,N3)} = 0.84$). The spatial patterns of clusters 1 and 2 are the most similar when

comparing N2 to N3 (cluster 3: $r_{(WR,N2)} = 0.96$ and $r_{(WR,N3)} = 0.95$). In cluster 2 showing overlap between the default mode and dorsal attention networks, we observed decreased functional connectivity in the posterior cingulate cortex during NREM2 sleep, which was then partially recovered during NREM3 sleep. These results indicate that a larger network reorganization occurs during N2 comparing to WR, while less network reorganization occurs when between N3 and WR and between N2 and N3. On the other hand, we estimated cluster 4 exhibiting a strong functional connectivity in the motor and auditory areas overlap with dorsal attention region only during well-rested state after normal sleep but not during NREM sleep, suggesting a loss or decrease in functional processes in the dorsal attention area involving the motor and auditory functional connectivity during sleep. Indeed, our results provide converging evidence of different network reorganization during NREM2 and NREM3 sleep stages.

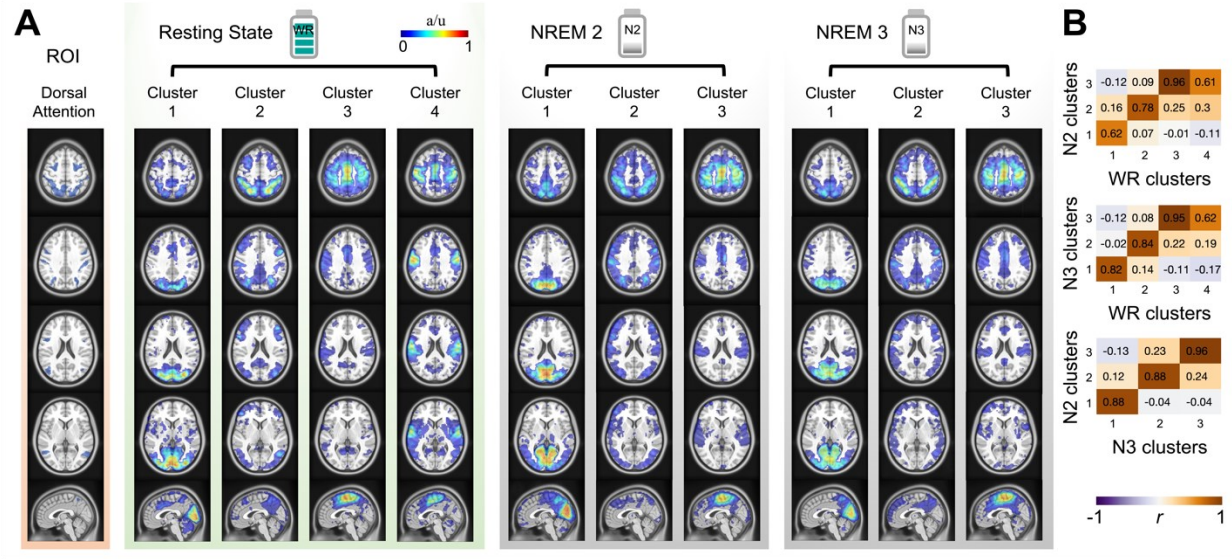

Figure 3-6 Reorganized patterns of network overlaps within the dorsal attention area during NREM sleep when compared to wakeful resting state. (**A**) The dorsal attention area was defined using the Yeo-7 functional network atlas. Individual functional networks were estimated using SPARK. Networks estimated using SPARK and overlapping with the dorsal attention region were collected from all subjects, spatially clustered and finally averaged within each cluster in order to identify the group-level network maps overlapping in this region. (**B**) Spatial correlation between the group-level network clusters overlapping with the dorsal attention area during wakeful resting state (WR) and to those estimated during NREM2 (N2) or NREM3 (N3) sleep states. Correlation heat maps are shown for the four clusters estimated for WR state and three clusters estimated for N2 (top) or N3 (bottom) states.

3.5 Discussion and Conclusions

In this study, we investigated whether and how patterns of integrations/segregation between and withing brain networks integration would reorganize during NREM2 and NREM3 sleep within a one-hour recovery nap following a whole-night SD, in comparison to wakeful resting state after normal sleep.

We hypothesized that hub regions that participate in between-network integration/segregation play a role in state-dependent changes in functional brain integration. To investigate these important questions, we applied our proposed and validated methodology entitled SPARK to estimate overlapping network structures and hubs from individual resting state fMRI, an original sparse decomposition approach which is not requiring conventional pairwise connectivity matrix and Graph Theory to characterize brain resting state networks (Lee et al., 2016, 2018).

To quantify systematic network integration and segregation, at the voxel resolution, we are proposing a new metric in this study, the Hierarchical Segregation Index HSI. HSI is computed as the ratio of *k*-hubness assessed at the region-level and at the voxel-level, taking advantage of the unique ability of SPARK to estimate hubs at these two levels of brain network architecture at the same time (**Figure 3-1**). First, in this study we are reporting resting state connector hubs found across the unimodal and multimodal cortices, in agreement with previous work (Lee et al., 2016, 2018, 2022), suggesting reliability of SPARK methodology. Moreover, we are reporting state-specific reorganization of connector hubs occurring during NREM sleep, where the global network scale, i.e., the total number of networks estimated in each state for each subject, was preserved (**Figure 3-2**).

Our analysis using our newly proposed HIS metric allowed us to demonstrate that NREM2 sleep was associated with more network segregation into-subnetworks within the visual, default mode and association cortex areas, when comparing to wakeful resting state, whereas the visual area also showed increased integration from NREM2 to NREM3 (**Figure 3-3**). Network segregation during NREM sleep, notably within the dorsal attention regions, was associated with larger decrease N-back working memory task performances obtained after a recovery nap following whole night SD, when compared to normal night (**Figure 3-4**). Our observed vigilance level-dependent changes in HSI were overall in agreement with finding using FCR, a complementary metric of network segregation proposed within the Bayesian framework (Boly et al., 2012; N. E. Cross et al., 2021). This correspondence between the two measures was inhomogeneous when assessing correlation within specific cortical regions, whilst the strongest correspondence was found within the dorsal

attention network (**Figure 3-5**). A more comprehensive analysis of what were actually the group-level networks that were overlapping with the dorsal attention network and visual hubs confirmed these findings (**Figure 3-6)**. Our results provide evidence that functional brain network segregation occurs during NREM sleep and impacts cognitive performance during task involving attention. The association to attention function suggests that our methodology using SPARK and HSI is a promising metric to quantify hierarchical network segregation at the voxel level.

We found preservation of global network scale, i.e., the total number of across brain states within individuals using SPARK. It is worth mentioning that as opposed to other approaches where the total number of decomposition networks is defined a priori, SPARK is actually estimating this global network scale from the data, using minimum description length criteria as described in Lee et al (Lee et al., 2018). Our global network scales were similar within the three explored states (WR, N2 and N3) and were also in agreement with previous findings from comatose patients in the absence of consciousness using Graph Theory (Achard et al., 2012). Similar preservation of global network scale was also found within healthy young adults across different pupil-size linked arousal levels even within wakeful resting state using SPARK (Lee et al., 2022). In this study, SPARK was actually applied to resting state fMRI data using two functional parcellation schemes involving 268 or 368 cortical and subcortical parcels. Together, these results demonstrate the preservation of global network scale across different vigilance levels using both region- and voxel-level analyses estimated using SPARK methodology.

In subsequent analyses, we then demonstrated that topological patterns of network overlap reorganized from wakeful resting state to NREM sleep, even if the global network scale was preserved for each individual. The region level *k*-hubness k^R increased within visual regions and decreased in the frontoparietal regions during NREM2 sleep when compared to wakeful resting state (**Figure 3-1G**). Then, k^R values decreased in these regions during NREM3 sleep, suggesting a pattern of increased segregation in N2 followed by increase integration in N3. When studying voxel level hubness using group average k_V, we first found resting state connector hubs mainly within the default mode, frontoparietal association and visual areas (**Figure 3-2A**), therefore reproducing our previous findings in healthy conditions using SPARK (Lee et al., 2016, 2018). During NREM2, when compare to wakeful resting state, *k*-hubness decreased in parts of the visual, default mode areas (**Figure 3-2B**), whereas *k*-hubness increased in the visual and association cortices during NREM3. Together, the results suggest differential changes in network overlaps across different NREM sleep stages.

However, the *k*-hubness map, the number of overlapping networks or comparison of *k*-hubness with conventional hubness measures in Graph theory should be interpreted with caution (Lee et al., 2022). Indeed, networks estimated using SPARK framework can have overlap at the core regions of well-known canonical resting state networks, not only at their anatomical boundaries (**Figure 3-1H**). Because SPARK offers the unique feature of estimating what are the network involved in each hub, as opposed to standard Graph Theory metric, we were able to carefully analyze those subject specific networks. Our newly proposed metric HSI is indeed assessing the level of correspondence between those subject specific networks estimated from the data using SPARK to a higher hierarchical representation of brain networks at the group level, using here a parcellation in 9 regions/networks. For example, in (Lee et al., 2016), using SPARK and voxel-level k-hubness, we showed that the posterior cingulate cortex (PCC) has been shown to be a hub where two sub-networks of default mode network were overlapping; one involving the midline components (the PCC and medial prefrontal cortex) and another one involving the midline, lateral, and mesial components (Lee et al., 2018). In another scenario, a network involving voxels in the V1 and V2 area in the visual cortex and a larger network involving voxels covering from the V1 to V4 areas overlap in the V1 area, resulting have *k*-hubness of 2. Similar patterns of networks reorganization have been also observed from the detailed network analysis associated with the dorsal attention region presented in this work (**Figure 3-6**). Similar findings have been suggested using an innovative co-activation pattern analysis. Indeed, patterns of network overlaps estimated using SPARK may involve information about intrinsic hierarchy among these networks

An important contribution of this work is the development of an HSI metric to assess integration/segregation between and within subnetworks, while offering the unique feature of providing voxel level mapping of these properties. To do so, we exploited the ability of SPARK to provide the region- and voxel-level measures of hubness at the same time for a pre-defined region, allowing to define HSI as the ratio of region-level *k*-hubness to voxel-level *k*-hubness associated with an underlying voxel-region hierarchy. We demonstrated the use of HSI for quantifying network segregation for each voxel and for detecting state-dependent changes in network segregation. During NREM2 relative to resting state, we found increases in the HSI, therefore more segregation, in the visual, somatomotor and default mode regions (**Figure 3-3**). On the other hand, HSI in regions of the default mode and somatomotor network did not exhibit any significant change when comparing data during NREM2 and NREM3 sleep (N3 ≈ N2 > WR). However, in the visual area, we found a significant decrease in segregation (decrease in HIS) during N3 when compared to N2 , (N2 > N3 ≈ WR). On the other hand, during NREM2 relative to resting state, we found decreased network segregation in regions of the orbitofrontal and temporal cortices, mesial

temporal, and subcortical structures. These regions, however, then showed increases in HSI values during NREM3 sleep (N3 > WR > N2).

Importantly, we found an association between the HSI values measured across the whole brain with individual variability in N-back working memory task performances. Overall, we found that increased segregation during sleep, during a recovery nap following whole night SD, was associated with worse cognitive performance in N-Back task when comparing post-recovery map and normal night conditions. Those finding were found to be mainly relevant with the dorsal attention network (**Figure 3-4**) Our findings are in agreement with previous findings using FCR for the same dataset (Boly et al., 2012; N. E. Cross et al., 2021), suggesting the HSI as a promising tool for studying the neural basis of cognitive functions and the role of sleep for cognition. In Cross et al., changes in FCR (ΔFCR) between sleep-deprived task states and post-recovery nap task states was positively related to changes in task performances, suggesting a role of network segregation in the improvement in task performances after taking a nap.

Although we found overall similar network segregation during sleep when compared to wakeful resting state, using the same dataset using the two different measures (HSI and FCR), the correspondence between the two measures was inhomogeneous across the cerebral cortex (**Figure 3-5**). These findings are not surprising since there are also differences in underlying methodological approaches considered for HSI and FCR. First, given a network hierarchy including an upper-level system and its lower-level systems, HSI is a measure estimating segregation for each lower-level system, whereas the FCR is a measure estimating segregation for the upper-level system. Therefore, to compare the two measures, it was necessary to have a representative metric summarizing all HSI values within the upper-level system. Indeed, whereas FCR was able to estimate levels of network integrations/segregation when comparing Yeo 17 and Yeo 7 parcellations, providing results at the spatial scale of Yeo 7, we add to integrate/average HSI voxel value over each Yeo-7 network to obtain a metric derived at the same spatial scale. Therefore, to avoid any bias induced by inhomogeneous HSI distribution when averaging HSI value along Yeo-7 regions, we proposed a bootstrap resampling strategy to achieve a robust estimation of regional average HSI values. Second, we did not include the subcortical areas including the basal ganglia, cerebellum, hippocampi, and amygdalae in our FCR estimation, due to the mathematical constraint in the computation of FCR that requires the number of fundamental parcels less than the number of time-points (Boly et al., 2012).

The HSI values were estimated using SPARK from the whole brain voxels including these subcortical areas, however, only the HSI values from the cerebral cortex that are part of

Schaefer100-atlas were considered and averaged within each region, to compare with the FCR values estimated for the same region.

There are also differences between the present study and our previous work in Cross et al (N. E. Cross et al., 2021). First, the assumed spatial hierarchy in this work (whole brain - Yeo7 - Yeo17; with the baseline resolution of Schaefer100 parcels) is not identical to the assumed hierarchy used in Cross et al (whole brain - Yeo7 - Yeo17 - 57 assemblies; with the baseline resolution of 400 parcels). Second, in Cross et al., FCR was measured for 20 individuals using task fMRI data and the whole period of concatenated timeframes of NREM sleep within one-hour nap, including both NREM2 and NREM3 (N. E. Cross et al., 2021). Here, we analyzed only a continuous 5-minute segment of NREM2 and NREM3 sleep datasets respectively to match with the total duration (5 minutes) of resting state data, to avoid any bias in sparse dictionary learning and network estimation procedures induced by the length or amount of data. When compared to Cross et al, a smaller number of subjects was included in our present study, due to our conservative data screening criteria for motion parameters, which is a limitation of this study.

We also found other sleep-associated changes in functional connectivity in the visual (cluster 1), somatomotor I (cluster 2), and somatomotor II (cluster 3) networks in relation to the dorsal attention area. While changes in spatial patterns of clusters 1 and 2 were larger at NREM2 from well-rested state than at NREM3 from well-rested state, the somatomotor I cluster 3 remained similar. () Cluster 4 involved a strong functional connectivity in the motor and auditory areas with dorsal attention region only at well-rested state after normal sleep but not at NREM sleep, suggesting a loss or decrease in functional processes in the dorsal attention area involving the motor and auditory functional connectivity. The results indicate that a larger reorganization of between-network integration occur during NREM2 sleep from wakefulness, and such changes partially recover its spatial pattern at NREM 3 similar to the patterns found at resting state.
In conclusion, our results provide converging evidence of different network reorganization during NREM2 and NREM3 sleep stages.

3.6 Materials and Methods

This study has been approved by le Comité central d'éthique de la recherche du ministre de la Santé et des Services sociaux (CCER) at Montreal, Quebec, Canada. The data acquisition was performed and completed in the Sleep Laboratory and in the Neuroimaging Unit of PERFORM Centre in Concordia University, Montreal, Quebec, Canada.

Participants

We recruited 53 volunteers according to the following inclusion criteria: participants aged between 18 to 30 years, healthy and good sleepers. Among them, 34 volunteers were selected as eligible after self-report assessment of sleep quality and ruling out the following exclusion criteria: volunteers without MRI compatibility (pregnancy, claustrophobia, metallic objects such as vascular clip, prosthetic valve, metal prosthesis, metal fragment or pacemaker into the body); with sleep disorders such as obstructive sleep apnea, narcolepsy, insomnia; with neurological disorders such as epilepsy, migraine and stroke; with medical conditions such as chronic pain and chronic respiratory disease, with psychiatric condition such as major depression, anxiety or psychotic disorder; and individuals taking psychotropic medications such as hypnotics and antidepressants. Selected participants were then involved in a three nights protocol, in the sleep laboratory of PERFORM Centre. After the first night assessment (control night), involving standard polysomnography monitoring to assess sleep quality, three participants were excluded; two had periodic leg movements during sleep and one had sleep apnea. Five participants were later excluded because of several unexpected equipment issues during data acquisition. Finally, six participants withdrew before the end of the experiment. This resulted in 20 eligible participants (age: 21.2 ± 2.5 years, 12 females) who completed the whole protocol.

Study design

The acquisition protocol for each participant included three visits with an interval of one week, as illustrated in **Figure 3-1A**. The first night acquisition was a control night using polysomnography monitoring to assess sleep quality and if participants were presented any sleep disorders. Once a participant was considered eligible after the first control night, a two-night experiment was planned with an interval of seven days between the two nights: one night with normal sleep and another with total whole-night SD. For each participant, the order between the normal and SD nights was randomly assigned to avoid potential bias induced by a specific order. In the next morning after each experimental night, a series of data acquisition was performed.

The experimental protocol for the night with normal sleep opportunity was the following. During seven days before the normal night acquisition, actigraphy data were acquired to record the movements and light sensitivity to ensure that the participants had regular sleep and followed their daily activities. During the normal sleep experimental night, we assessed the quality of sleep by acquiring a whole-night EEG. We used 18 electrodes for the EEG following the 10-20 system. The participant was asked to sleep before midnight and wake up around 6 and 7 AM the next morning, to sleep a minimum of 6 hours during the normal night in the Sleep Laboratory. The next morning around 8:30 AM after offering breakfast to the participant, we acquired four runs of high-density EEG/fMRI data during three cognitive tasks and resting states. The participants performed the N-back task with three levels (N = 0, 1 and 2; duration: 8 minutes) assessing working memory, attention network task (ANT, 13 minutes) and Mackworth clock test (MCT, 5 minutes) which both assessed attention ability. The duration of resting state scans was 5 minutes, during which the participant was asked not to fall asleep and to rest, while maintaining fixation on a cross presented on the screen inside the MRI scanner. Finally, an T1-weighted anatomical MRI was obtained.

The experimental protocol for the whole-night SD was the following. To ensure that the participant did not fall asleep during the whole night with SD, an investigator stayed overnight with the participant and offered to talk, watch movies or play games. The next morning around 8:30 AM after offering breakfast to the participant, we acquired high density EEG/fMRI data, while the participant performed the same three cognitive tasks: N-back, ANT and MCT followed by a 5-minute resting state fMRI was acquired with a fixation cross. Around 9:15 AM, the participant was then asked to take a nap inside the MRI scanner for a maximum of one hour, during which we continued acquiring high density EEG/fMRI data. After one hour of nap, we woke up the participant and acquired 5-minute resting state EEG/fMRI data, while the participant was staring at fixation cross. Next, participants were asked to perform the same three cognitive tasks again, while continuing acquiring EEG/fMRI data. Finally, a T1-weighted anatomical MRI was obtained.

Cognitive tasks

First, we considered N-back tasks, including three difficulty levels (N=0,1 and 2) to assess working-memory function (Chee & Choo, 2004). A series of English letters (e.g., R, K, K, F, and so on) was presented sequentially on the screen and the participants were asked to press the button if the letter presented on the current screen was the same as the letter presented N times before (make sure not to use the same letter N for N-back and for total number of networks for SPARK). The N-back task lasted 8 minutes and consisted in a block design, each block lasting 38 seconds followed

by 10 seconds between each trial (12 blocks, 4 of 0-back, 4 of 1-back, 4 of 2-back). Before the start of the block, a cross was presented for 500ms then 15 letters were presented during one block for a duration of 2.5 seconds.

Second, the ANT task was considered to assess different types of attention: alerting, orienting, validity, and executive control (Fan et al., 2005). This task consisting in a visual stimulus presenting two presentation boxes on the screen next to each other, either of which may include an array of five arrows (stimulus). The stimuli can have three forms: *uncued* (no arrows appear), *congruent cued* (all five arrows will point to the same direction), and *incongruent cued* (the middle arrow may point to the opposite direction than the other four). The task for participants was then to respond to the direction presented by the middle arrow by pressing the corresponding button (left or right) as quickly as possible. Prior to the appearance of arrows, cues (flashing box) will appear to allow the participants to predict on which presentation box the arrows will appear. To disturb the participants, different cues are presented: valid, invalid or double (i.e., both boxes are flashing).

Finally, to assess psychomotor vigilance function, we considered the Mackworth Clock test (Lichstein et al., 2000), to evaluate ability to watch the environment intensively and carefully with sustained attention. To do so, a clock that consisted of two-layer circles of white vertices (24 vertices for each of the inner- and outer-layer circles) was presented on the black screen. The visual stimuli were presented by the sequential movement of clock-ticking of a red vertex between each pair of two vertices in the inner and outer layers, while several random jumps skipping ticks on the clock were generated. Participants were instructed to press a button as quickly as possible in response to every random jump of the red vertex.

Data acquisition

The simultaneous high-density EEG/fMRI data was acquired using a 3T MRI scanner with 8 channels head coil (General Electric, GE) and an MRI-compatible high-density EEG with a cap of 256 electrodes (Magstim EGI, Eugene, OR, USA). High density EEG data were transmitted from the amplifier (1000 Hz sampling rate) to the EEG monitor outside the scanner room via optic fiber. Electrocardiography was also collected via 2 MR compatible electrodes through a bipolar amplifier (Physiobox, Magtism EGI). A T1-weighted anatomical image was obtained using the 3-dimensional inversion recovery-prepared fast spoiled gradient echo acquisition sequence (BRAVO), with inversion time (TI) = 450 ms, flip angle = 12°, 256 × 256 matrix, 196 slices, and voxel resolution = 1 × 1 × 1 mm. The functional images were acquired using a T2*-weighted gradient echo-planar imaging (EPI) sequence with echo time (TE) = 26 ms, repetition time

(TR)=2500 ms, flip angle = 77°, 64 × 64 matrix, 41 slices, and voxel resolution = 4 × 4 × 4 mm.

EEG preprocessing and analysis

We used BrainVision Analyzer 2 software (Brain Products, Munich, Germany) for EEG preprocessing. The MRI gradient artifacts and ballistocardiographic pulse-related artefacts were detected and corrected using an average artifact subtraction-based method, by BrainvisionAnalyzer (BrainProducts, Gilching, Germany). The MR-denoised EEG signal was then band-pass filtered (1-20 Hz) and down-sampled to 250 Hz, followed by re-referencing to the linked mastoids. Eye blinks in wake EEG recordings were removed with independent component analysis (ICA) using the MNE Python package (https://mne.tools/stable/index.html) (Gramfort et al., 2013). Any ICs that matched to the signals from electrooculogram electrodes were automatically detected and excluded from the original signal. This de-noised EEG signal was then used for all subsequent analysis. After preprocessing of EEG data acquired during nap inside the MRI scanner, we conducted the scoring of sleep-stages by visual inspection using Wonambi software, a Python-based toolbox for EEG visualization and analysis (https://github.com/wonambi-python/wonambi). Two experts segmented EEG data into several segments, providing an identification of sleep stages for each segment following to the American Academy of Sleep Medicine (AASM) manual for the scoring of sleep and associated events. A detailed presentation of EEG data preprocessing for this study was reported in (N. Cross et al., 2021b; Uji et al., 2021).

fMRI preprocessing

The first resting state fMRI scan was acquired with a duration of 5 minutes in the morning following a night of normal sleep. The second fMRI scan was obtained during a one-hour recovery nap following whole night SD. Sleep-stage scoring on EEG segments from data simultaneously acquired during the nap was used to identify fMRI runs corresponding to every sleep stage for each subject. Only the EEG segments corresponding to a continuous stage of 5 minutes or more were considered for further fMRI analysis. The duration of available data during NREM2 and NREM3 ranged between 5-40 minutes. To ensure that we analyzed and compared the same number of frames per state, we trimmed each continuous segment in sleep data, such that only the first 120 timeframes were selected from the runs if the length of time-course was longer than 120 timeframes (5 min). Therefore, we were not able to select fMRI data recorded during NREM1 sleep due to the short duration of the segments.

fMRI data were them preprocessed used the Neuroimaging Analysis Toolkit (NIAK) version 0.13.0,

with the MINC Tool Kit (Bellec et al., 2010b). The EPI volumes were first corrected for inter-slice timing differences. Six rigid-body motion parameters (3 translations and 3 rotations) were estimated within and between sessions using the median volume of the first session as a target. This coregistration procedure was obtained by maximization of correlation coefficient between volumes, using Minctracc software (Collingnon et al., 1995; Minoshima et al., 1992; Woods et al., 1993). T1 anatomical MRI images were preprocessed using CIVET pipeline (Ad-Dab'bagh et al., 1998; Zijdenbos et al., 2002). Linear coregistration of a T1 image in native space to the non-linear MNI ICBM 152 template stereotaxic space (Grabner et al., 2006) was performed accounting for a nine-parameter transformation (3 translations, 3 rotations and 3 scales), estimated by maximization of correlation coefficient using Minctracc software. Non-linear coregistration from T1 native to the MNI template (Grabner et al., 2006) was then performed by maximization of correlation coefficient with a multiresolution iterative strategy. Non-uniformity correction was then applied (Orżanowski, 2016). Individual coregistration between an averaged EPI volume (mean volume of the first session, after motion correction) to the anatomical T1-weighted volume in native space was done by maximization of the mutual information, considering a rigid transformation (3 translations and 3 rotations) by Minctracc. Then, the EPI volumes were resampled at a voxel resolution of $4 \times 4 \times 4$ mm in the MNI space, by combining a linear transformation from EPI to T1 and a non-linear transformation from T1 to the MNI template. Once coregistration step was completed, time frames exhibiting excessive motion, i.e., showing a frame displacement > 0.5 mm, we discarded by scrubbing (Power et al., 2014). The remaining motion artefacts were further estimated and removed using SPARK (see below). Slow time drifts were removed by applying a high pass filter using discrete cosine basis functions to ensure a cutoff of 0.01 Hz. Confounds consisting in motion parameters, the average signals from the white matter and the lateral ventricles were regressed out from data. To do so, we considered the six rigid-body motion parameters (3 translations and 3 rotations) and their square, before applying a principal component analysis to retain 95% of the variance of these twelve parameters, to extract regressors for motion correction in fMRI time series (Lund et al., 2006). Each fMRI run in the MNI space was spatially smoothed using an isotropic Gaussian blurring kernel with 6 mm full-width half maximum. Several runs were excluded when there was too much motion, notably when more than 35% of the total time frames were removed by scrubbing. Finally, we selected a set of consecutive NREM2 and NREM3 runs (one fMRI data per state) for each subject.

As a result, we considered the following datasets for network/hubness analysis: resting state fMRI data obtained from 14 subjects wakeful rested (WR) after normal sleep, fMRI data obtained from 18 subjects during NREM2 and from 12 subjects during NREM3 after whole-night SD. In 9 subjects, we were able to select data from the three states (WR, NREM2, NREM3).

Brain masking and network atlases

From these preprocessed fMRI data, gray matter voxels were selected using a modified version of the AAL template (Tzourio-Mazoyer et al., 2002). This modified AAL template was generated by NIAK using non-linear coregistration to the MNI ICBM 152 template, using the same coregistration strategy applied for our fMRI preprocessing. We resampled the modified AAL template at a voxel resolution of $4 \times 4 \times 4$ mm^3 (the resolution used for resampling of our EPI images) and then selected gray matter voxels from each participant data actually belonging to the AAL mask. This gray matter mask was considered when applying our method SPARK for the estimation of hubs. For our proposed region-level analyses, we considered the two proposed scales of the Yeo atlas of consistent brain networks, the Yeo-7 and Yeo-17 templates (Thomas Yeo et al., 2011b). The Yeo functional atlases provide parcellations of the cerebral cortex into 7 or 17 functional networks estimated from the analysis of 1,000 young healthy adults. The Yeo-7 atlas included visual, somatomotor, dorsal attention, ventral attention, limbic, frontoparietal, default mode networks, while Yeo-17 atlas included definition of their sub-networks at the finer scale. The Yeo templates were resampled at a voxel resolution of $4 \times 4 \times 4$ mm^3 within the non-linear MNI 152 space. In addition, to take subcortical brain regions into account for our proposed analysis, we also defined 3 extra regions: (i) basal ganglia region including the thalamus, caudate nucleus, putamen and globus pallidus, (ii) the cerebellum and (iii) the hippocampus and amygdala, which were then merged with the limbic network in Yeo-7 template. Therefore, we finally considered obtained 9 regions of interest (ROIs) or networks including the modified Yeo-7 networks, the AAL-defined basal ganglia and cerebellum. Caudate, putamen, thalamus and pallidum defined by AAL were grouped as the "basal ganglia" ROI. 26 parcels defined by AAL with their name started with "cerebellum" or "vermis" was defined as the "Cerebellum" ROI. The hippocampus, parahippocampal and amygdala was grouped together with number 5 ROI of Yeo7 template, which we named it as "Limbic" network, including both cortical and subcortical structures. These 9 ROIs were used for HSI estimation. In addition, to compare our hub measures with the proposed functional clustering ratio (FCR) method to assess integration/segregations between networks (Boly et al., 2012; N. E. Cross et al., 2021), we also considered a baseline parcellation obtained using the Schaefer-100 atlas (Schaefer et al., 2018), The Schaefer-100 atlas, originally provided within the MNI ICBM 152 template at a 2x2x2 mm^3 resolution was resampled at a voxel resolution of $4 \times 4 \times 4$ mm^3 for our proposed analysis.

Estimation of Hubs of brain network using SPARK

For each preprocessed fMRI run on which we applied the gray matter mask previously described, we estimated the organization of functional connector hubs in individual brain networks at the voxel level using SPARK (Lee et al., 2016, 2018, 2022). Using SPARK, the whole-brain spatio-temporal activity in fMRI (Y) can be decomposed into n resting state networks, estimating n time-course characteristics (temporal features) and the corresponding n spatial maps. The collection of n temporal features is called a subject-specific dictionary. SPARK is based on a data-driven sparse general linear model (GLM), which represents the BOLD signal measured in each voxel as a weighted linear combination of k temporal features. As the main specificity of SPARK method, k is the level of sparsity specific to this voxel, indicating that only a small number of networks, among those estimated N networks, are actually involved in this voxel. Hubs are then defined as brain voxels that are involved in more than one functional network (i.e., $k>1$) that are overlapping in time and space. Importantly, SPARK is not only able to estimate a realistic/sparse number of network associated within one particular voxel, SPARK can also uniquely identify what are those connected/integrated networks. The implementation of SPARK is described as follows.

Step 1. In order to assess individual-level reproducibility of sparse GLM decomposition, SPARK actually consists in applying hub estimation several times on data sets exhibiting similar properties, using a bootstrap resampling-based strategy. To do so, we first applied the circular block bootstrap resampling to the preprocessed data ($\mathbf{Y}$) and generated $b=1, ..., 200$ resampled datasets with equal dimension. For the circular block bootstrap resampling, the length of each block was randomly selected between 10 and 30 continuous time samples to preserve the temporal structure in the BOLD signals (Bellec et al., 2010b). For each resampled data ($\mathbf{Y}_b$), the same sparse GLM considered for analyzing Y was applied. Sparse GLM was actually a variant of K-Singular value Decomposition (SVD) algorithm (Lee et al., 2011, 2018), a sparse dictionary learning method providing the estimation of resting state networks and their sparse representation in every voxel. The total number of networks N and voxel-specific level of sparsity k were estimated for each subject using the minimum description criteria, as proposed in (Lee et al., 2018).

Step 2. The parallel process of sparse dictionary learning for every resampled data (time by voxel) generated 200 sets of outputs - the sparse representation of N time-course characteristics (time by N) and the corresponding N spatial maps (N by voxel) of resting state networks.

Step 3. To find a spatially reproducible set of resting state networks across the 200 resampled datasets, we then applied nearest neighbor spatial clustering to the collection of all 200 x N spatial maps to identify N clusters. The maps were then spatially averaged within each cluster, therefore only retaining most reproducible results at the individual level.

Step 4. Statistically inconsistent elements with a low signal amplitude in these average maps were considered as Gaussian noise and removed by thresholding (p<0.05). Because we wanted to estimate only highly reproducible networks across the bootstrap resampled datasets in our analysis, several voxels then resulted in the estimation of *k*-hubness as zero. However, this does not necessarily mean that the voxel was never involved in any of the estimated networks, but rather that the corresponding signal for that voxel was noisy and results were not reproducible.

Step 5. An expert (KL) reviewed all those estimated spatial maps by visual inspection to manually classify and exclude the maps that were still contaminated by physiological noise, such as remaining cardiac, respiratory artifacts or subject motion, according to the manual classification criteria proposed in Griffanti et al (Griffanti et al., 2017; Lee et al., 2019). On average, about 14.41 atoms were estimated from SPARK among all subjects, from which about 4.35 noisy atoms were discarded.

Step 6. Voxel-level *k*-hubness (k^V) was finally estimated by counting the number of networks involved in each voxel (**Figure 3-1E**). Technically, this was done by counting the non-zero values in each column from the individual sparse coefficient matrix (the total number of networks-by-the number of whole brain voxels) using SPARK. For group-level analyses, a group average *k*-hubness map was obtained by averaging *k*-hubness in each voxel across subjects at each state.

Hierarchical Segregation Index (HSI)

Using SPARK, measuring *k*-hubness at the voxel level can identify connector hubs that are involved in more than one functional network. Given that we can also consider a set of voxels involved in a specific region of interest or consistent resting state network (e.g., Yeo parcellation), *k*-hubness at the region level can be also estimated by counting the number of resting state networks involved in a specific ROI. In this context, we propose the use of the measure of *k*-hubness over different levels or spatial scales, to estimate the hierarchical segregation of functional brain networks within a specific ROI, an approach that is actually similar to the one suggested for FCR estimation using Bayesian framework (see details below, **Figure 3-1E**) (Boly et al., 2012).

To estimate region-level *k*-hubness (k^R) (**Figure 3-1E**), voxels belonging to a region R were first identified and the corresponding columns in the individual sparse coefficient matrix were collected. This sub-matrix is therefore a *N*-by-n^R matrix, where n^R indicates the number of voxels belonging

to the region R. Then, we computed the volume proportion ($\%vol_j^R$) by counting the number of voxels belonging to this region R that were involved in each network *j* (n_j^R) with respect to the total number of voxels in the region R (n^R).

$\%vol_j^R = \frac{n_j^R}{n^R} \times 100\%$.

When estimating region-level *k*-hubness (k^R), we considered only the major networks involved within each region, by selecting the networks for which more than 10% of the within-region volume was involved, i.e., $\%vol_j^R > 10\%$. This 10% threshold was empirically chosen to find a tradeoff between the detection power and sensitivity.

To assess if a region R was functionally segregated or divided into sub-networks within this region, we defined the HSI_i for each voxel *i* as the ratio of region-level *k*-hubness for a region R to which the voxel *i* belongs to ($k_{i\in R}^R$), to the corresponding voxel-level *k*-hubness (k_i^V) as follows:

$HSI_i = \frac{k_{i\in R}^R}{k_i^V}$.

A high HSI value reflects that the number of networks involved in this region to which this voxel belongs to is larger than the number of networks involved in this voxel. This also reflects that this voxel may be involved in several networks (k_i^V), but it belongs to a large system (the pre-defined region R) that involves more subnetworks, whereas functional integration between those sub-networks is low. Therefore, a high HSI value suggests within-region inhomogeneity of the region R, in other words, the presence of sub-networks involved in other voxels in this system and therefore segregation between those sub-networks. On the other hand, a low HSI value reflects that this voxel belongs to a system R that involves a similar number of networks than the voxel level value k_i^V. Therefore, a low HSI rather suggests within-region homogeneity or integration between subnetworks, reflecting that the function of this voxel is associated with the function of the entire region. Our new proposed metric HSI can be considered as a measure of within-region functional integration/segregation, offering the unique property of providing estimations at the voxel level.

In this context, a priori definition of a region was important for the estimation of the HSI. First, we had to choose a network parcellation that was at lower spatial scale than the number of networks estimated by SPARK (N ranging from 9 to 21, mean = 14.41). We therefore considered the nine cortical parcellation scheme by integrating the modified Yeo-7 cortical networks and two anatomically defined subcortical networks using the AAL atlas (**Figure 3-2A**). For several voxels that were exhibiting k_i^V=0 at the voxel level, we did not estimate HSI and assigned HSI_i=0.

Voxel-wise between-state comparisons

To compare our hubness measures h (e.g., k_i^V or HSI_i for a specific voxel i) between different brain states (WR, NREM2, NREM3), we performed voxel-wise two sample permutation tests, therefore taking inter-subject variability through non parametric approaches. To do so, considering n individual hubness maps from two different brain states A and B (e.g., WR vs NREM2), group average hubness values $\langle h \rangle_A$ and $\langle h \rangle_B$ were calculated for states A and B, by averaging the h_i values in each voxel i across n subjects. A test statistic T was defined as the observed difference in each voxel as:

$$T = \langle h \rangle_A - \langle h \rangle_B$$

To test if the observed difference was statistically significant, we generated null data using 10,000 permutations. For each permutation, the n hubness maps from two states A and B were pooled and shuffled to classify them into two randomized states A' and B', each consisting of n randomly selected maps. The difference between two randomized states was calculated as:

$T_{null} = \langle h \rangle_{A'} - \langle h \rangle_{B'}$.

Finally, a p-value was estimated for T from each voxel with respect to 10,000 samples from the null distribution. The p-value was then null data and adjusted using the false discovery rate (FDR) correction. A separate t-score map was calculated between two stages using student t-statistics. The resulting t statistic maps were then thresholded using the p-value from the previous permutation test ($p_{FDR} < 0.05$).

Functional Clustering Ratio (FCR)

As originally proposed by Marrelec et al (Marrelec et al., 2008b), the Functional Clustering Ratio (FCR) is another metric developed within the Bayesian framework, allowing to quantify the segregation of a large network system into its sub-systems. Using mutual information derived metric to assess integration of information within a system (Marrelec et al., 2008b), FCR is defined as the ratio of the integration within subsystems (I_{WS}) to the integration between subsystems (I_{BW}). Therefore, an increase in FCR indicates that subsystems become functionally more independent to each other, quantifying the degree of functional segregation of a given system into subsystems. We refer the reader to Marrelec et al (Marrelec et al., 2008b) and Boly et al (Boly et al., 2012).

$$FCR = \frac{I_{WS}}{I_{BS}}$$

Estimating FCR requires *a priori* definition of hierarchical structure of the brain (Boly et al., 2012). In the present study, we considered a four-level cortical hierarchy. We first considered the whole

cerebral cortex as the system at the highest level (level 4). The whole cortex was then divided into seven non-overlapping functional networks using first the Yeo-7 atlas (level 3), and then into seventeen non-overlapping functional networks using the Yeo-17 atlas (level 2) (Thomas Yeo et al., 2011b). Finally, we considered the Schaefer-100 cortical atlas defined within the non-linear MNI ICBM 152 space, as our proposed baseline brain parcellation (level 1). Notably, we cannot estimate FCR for hierarchy lower than Schaefer-100, because FCR requires that one should avoid an ill-posed problem where the number of parcels (the Schaefer100 parcels) exceeds the number of timeframes (the maximum of 120 timeframes of our resting state fMRI data). Finally, at this lower spatial scale (level 1), parcel-level fMRI time-series were computed by averaging individual fMRI time series across voxels belonging to each of the 100 parcels. Note that we are using the same hierarchical strategy proposed in Cross et al (N. E. Cross et al., 2021) to estimate FCR on those data.

This four-level cortical hierarchy allowed us to compute FCR between two different sets of levels: (1) between levels 4 and 3: the segregation of whole cerebral cortex into seven large networks (FCR_w), and (2) between levels 3 vs 2: the segregation of the seven large networks into smaller 17 sub-networks (FCR_R). The computation of FCR requires defining the common spatial boundaries and an exact assignment of subsystems to its higher-level system. Notably, we are investigating functional segregation on similar scales using HSI (from 9 pre-defined ROIs to around 14.41 SPARK atoms) and FCR (from Yeo7 to Yeo17). In addition, because of the aforementioned reason that in FCR, the number of parcels should not exceed the number of timeframes, the NREM3 data of 3 subjects were excluded for this analysis specifically, due to their shorter time length.

Brain-behavior associations

To assess performance when performing cognitive tasks in different conditions (after a normal night, after the recovery nap), we measured the reaction time of participants, i.e., the time delay between stimuli presentation and the response (button-press), as well as the percentage of correct response. Since the main objective of the study was to investigate resting state functional connectivity patterns during wakefulness and sleep, therefore, we are not presenting here statistical analyses of task-evoked fMRI responses, previously reported in (N. E. Cross et al., 2021). In this study, we quantified the correlation between our proposed HSI measure and these behavioral scores measured from N-back, MCT and ANT tasks. First, the voxel-wise HSI values were averaged within each functional networks for each subject ($< HSI >_R$), which were defined using 9 ROIs (Yeo-7 networks + two anatomical regions including basal ganglia and cerebellum). As a result, nine region-average $< HSI >_R$ values were obtained per subject in each state. Between-state

difference in region-average $< HSI >_R$ values were then computed for each subject ($\Delta < HSI >_R$). Specifically, our goal was to study if there was any association between changes in $< HSI >_R$ values and changes scores of individual task performance (accuracy in % and latency in ms) across conditions.

Meanwhile, the average of HSI values within a region disregards other important information such as within-region inhomogeneity. To avoid such a bias, instead of directly associate these values to behavioral scores, we applied a bootstrap approach to acquire more robust statistics adjusted for HSI (Efron & Tibshirani, 1994). This included a resampling procedure to obtain 1,000 bootstrap replications of $< HSI >_R$ values for each region R. For example, assuming that there were m Schaefer100 parcels belonging to one of the Yeo-7 network R. Then, a bootstrap replication $< HSI >'_R$ was generated by resampling a new set of m Schaefer100 parcels with replacement and computing the average HSI. For each replication $< HSI >'_R$, the corresponding correlation coefficient and p-value between <HSI> and task performance were calculated. The resulting 1000 correlation coefficient and 1000 p-values were represented separately as histograms, to demonstrate the relation between the HSI values in one region R and task performance, offering more robustness than simply calculate the averaged HSI.

Comparison between HSI and FCR metric of network segregation

Finally, both HSI and FCR are providing measures of functional network segregation within a similar hierarchical model of brain networks architecture: larger HSI or FCR value represent more segregation between subsystems within a large system. Therefore, we first compared FCR_w estimates to the HSI values averaged across the voxels in the whole brain ($< HSI >_W$). At a lower level of the hierarchy, when then compared FCR_R values computed for a region R to the HSI values averaged across voxels belonging to the same network ($< HSI >_R$). Notably, using FCR, we have only investigated the cortical region within the extent of Yeo7 template, while in HSI, we have also investigated areas including hippocampus, amygdala, basal ganglia and cerebellum. Therefore, care was needed when interpretating the results.

In order to take into account of the variance of HSI in one region R, we also proposed the resampling procedure to obtain 1,000 bootstrap replications of $< HSI >_R$ values for each region R. To do so, we used the Schaefer100 atlas and the assignment from Schaefer100 to Yeo-7 networks as used for FCR computations, such that one of the Yeo-7 networks involves n parcels. Then, a bootstrap replication $< HSI >'_R$ of 1000 times was generated by resampling a new set of n parcels with replacement and computing the average. For each replication $< HSI >'_R$, the corresponding

correlation coefficient and p-value between $< HSI >'_R$ and FCR_R estimated from the same network R were calculated. The resulting 1000 correlation coefficient and 1000 p-values were represented separately as histograms, to demonstrate the relation between the HSI values in one region R and task performance, offering more robustness than simply calculate the averaged HSI.

3.7 Appendix: contribution of co-first authors

It is important to mention that this first study was completed in close collaboration with Dr. **Kangjoo Lee**, who is now a postdoctoral fellow at Yale University, New Haven, US. Dr. Lee was also supervised by Dr. Grova and graduated from the Ph.D. program in Integrated Program in Neuroscience from McGill University, Montreal, Canada, in June 2018. This study is a continuation of a previous study from Dr. Lee's Ph.D. dissertation: *Reorganization of Functional Brain Network Hubs during Non-Rapid Eye Movement (NREM) Sleep after Sleep Deprivation* (will be referred to as "*the original study*"). **In *the original study*,** Dr. Lee investigated the same topic as *in this new study*: connector hub reorganization during recovery nap after sleep deprivation. Dr. Lee initiated the development of a new method named Hierarchical Segregation Index (HSI) based on a Sparsity-based analysis of reliable k-hubness (SPARK), whereas SPARK method was also mainly developed and validated by Dr Lee during her PhD (Lee et al., 2016, 2018, 2019).

In this *original study* included (a) group comparison of k-hubness and HSI compared between wakefulness, NREM2, and NREM3; (b) the association between HSI and cognitive performance after recovery nap. Significantly, during the Ph.D. defense of Dr. Lee, it was suggested that the regional k-hubness used in HSI might be biased by the size of chosen regions of interest required for HIS estimation. Moreover, in the meantime, few more subjects have been acquired following the same protocol considered in the original study. Therefore, in *the new study*, with close collaboration with Dr. Lee, I further evaluated and validated the HSI methodology, reran and expanded the analysis, while including new dataset, and finally included new research objectives, and expanded the interpretation of results.

3.1.1 Similarity between *the original study* and *the new study*

(a) The same study design was applied, using EEG-fMRI acquisition on healthy subjects to investigate the fMRI characteristic during the recovery nap after total sleep deprivation and its relation to cognitive performance. (b) This fMRI dataset underwent the same fMRI preprocessing procedure by the NIAK toolbox with the same parameters and consequently underwent the same analysis of SPARK to calculate brain connector hubs. (c) Both studies investigated the group differences of k-hubness and HSI in wakefulness, NREM2, and NREM3, using permutation tests. (d) Both studies investigated the association between HSI and cognitive performance including the N-back task, attention network task, and psychomotor vigilance task.

3.1.2 The difference between two studies

(a) in *the new study*, one fMRI segment from the wakefulness category following whole night sleep

deprivation was further excluded, because the percentage of *noisy atoms / (noisy atoms + signal atoms)* was found to be larger than 50% after running SPARK (since participants were fighting not to fall asleep during this resting state acquisition. Therefore, we are now comparing wakeful resting state after normal night with sleep data recorded during the recovery nap following whole night sleep deprivation. We excluded this fMRI segment to ensure reliable data quanlity. (b) In the new study, I carefully investigated the association between ROI size required for HSI estimation and regional k-hubness, in *the new study*. Notably the threshold for calculating regional k was set to 6% in this new analysis instead of 10% as in *the original study*. (c) Additionally, in *the new study*, we now compared HSI measure of network segregation with another methodology called Functional Clustering Ratio (FCR) in the collaboration with Dr. **Nathan Cross** (Boly et al., 2012; N. E. Cross et al., 2021; Marrelec et al., 2007), which quantifies functional segregation by assessing the integration between sub-networks and within each sub-network. To provide more robust statistics, I also implemented resampling procedures to ensure a more robust comparison between HSI and FCR. (d) In *the new study*, when investigating the association between HSI and cognitive tasks, I also considered the same aforementioned resampling procedure to have a more robust summary of the HSI value in one ROI. (e) In *the new study*, we investigated the association between the difference of HSI in NREM and wakefulness and the differences in cognitive task scores after a recovery nap and after a normal night of sleep, therefore, using the fMRI during wakefulness as the baseline, and using the cognitive performance after a normal night of sleep as a baseline as well. However, in *the original study*, the association between HSI in NREM and cognitive performance after a recovery nap was directly investigated, therefore, without the baselines. (f) In *the new study*, I also proposed a detailed investigation the functional networks mainly involved in the visual area and the dorsal attention area in different arousal states (awake, NREM2, NREM3). (g) In *the new study,* the EEG denoising has been improved and therefore new sleep stage classification was considered, which allowed more reliable identification of NREM fMRI segments in *the new study.*

3.1.3 My detailed contribution

a) I studied the association between the size of ROI and regional k-hubness at the different thresholds. In our study, we have separated the whole brain into 9 brain regions (ROI), which consist of 7 ROIs from the Yeo7 template (Thomas Yeo et al., 2011a) and 2 subcortical ROIs adapted from the AAL template (Rolls et al., 2020). We have applied SPARK which counts how many resting-state networks (RSN) are involved in each brain voxel and identify the spatial maps of each network. The regional k-hubness instead is defined by the number of RSNs mainly involved in each brain ROI. If the spatial overlaps between an RSN and an ROI are larger than x% of the total number of voxels in the ROI, then this RSN will be identified as "involved" with this ROI and vice versa. (The details of the ROI template, SPARK, voxel k-hubness, and regional k-hubness

can be found in the "materials and methods" in the manuscript). Yet it still needs to be investigated if there was any correlation between the size of ROI and regional k value that could bias the results. For example, ROIs with larger spatial extents such as the DMN area tend to involve more RSNs. Although we applied a percentage threshold of x% to avoid this effect as much as possible, the effect still needs to be validated, while the threshold x% itself needs to be chosen with caution. To do so, I rerun the analysis of regional k for a series of the different thresholds between **0% to 50%.** One example violin plot of regional k from all fMRI segments (WR, N2, and N3 fMRI segments are concatenated) categorized and arranged by the size of ROI, at a threshold of 6%, can be found in **Figure A1**. The Pearson correlation coefficients between regional k and size of ROI as a functional to threshold x% can be found in **Figure A2**. As shown in **Figure A2**, x% should not be too small which would not effectively prevent this ROI-size bias. In the meantime, x% should also not be too large since it would not preserve enough hubness information. Therefore, considering the above factors, we have set the threshold at **6%** in *the new study*, to ensure that the bias of regional k caused by different ROI sizes is minimum.

b) I have individually investigated an issue of redundant networks from SPARK output and adapted the code of the SPARK toolbox (Lee et al., 2016). During Study 1, Dr. Lee discovered an issue that the current version of the SPARK toolbox could sometime generate around 1 or several pairs of redundant network atoms, where the spatial patterns of two atoms are almost identical. In brief, the pipeline of SPARK includes: First, it applies bootstrap resampling to an fMRI time series, then applies a sparse GLM on each bootstrap sample to estimate a series of spatial network maps by data-driven temporal dictionary learning. The maps are then **clustered** into several consistent spatial networks. Finally, **absolute values** of the clustered networks are taken (the sign of the clustered networks are not informational because of the sign ambiguity of the dictionary learning process) and are **thresholded** (to remove the estimated background noise). After investigation using 2 testing fMRI data, I have found that those redundant atoms are always sign-flipped before taking absolute values in the pipeline. Therefore, we suspected that during the spatial clustering step of the pipeline, the sign-flipped activities have been clustered into two different consistent networks though they pertain to the same desired spatial information, leading to the redundancy of final network outputs. To fix this issue, I have updated the pipeline of SPARK to take absolute values of spatial networks before spatial clustering instead of taking absolute values after spatial clustering. This instead will make sure the sign-flipped activities will be clustered into one consistent network. Test runs using the updated version of SPARK showed no redundant networks. **However,** we have also questioned the accuracy of the thresholding part of the updated SPARK pipeline. In SPARK, because the C-mean spatial clustering will amplify any signals that are consistent among different networks, the histogram of all clustered spatial networks will be dominated by background noise with the signal of interests (i.e., the desired RSNs) only on the tails

of the distribution. The thresholding of background noise was originally done by approximating the histogram of clustered spatial networks into inverse normal distribution whose **mean is at the peak of the histogram** (illustrated as **Figure A3**), after which, only the network coefficient of $p<0.05$ on the histogram will be kept while the dominant central peak of the histogram will be removed as background noise. Hence, we suspect that after we revise the code to take absolute values before spatial clustering, forcing the resulting non-negative histogram into normal distribution will not be statically accurate enough. Therefore, after investigating, I also added a step in the SPARK pipeline to manually mirror the histogram to the negative quadrant, in the meantime forcing the mean of the approximated normal distribution to be 0, to ensure the validity of the thresholding. The rest of the pipeline was then be applied as usual. Notably, although all investigation mentioned above were done during *Study 1*, unfortunately, we did not have enough time to rerun the large data cohort with the updated version of SPARK. Therefore, in *Study 1*, the redundant networks were finally manually removed by Dr. Lee. However, this updated version of SPARK was then applied to *Study 2*.

Aside from a) and b) that are less reflected during the manuscript, I have also conducted the majority of analyses of *Study 1*. A summary of the rest of my contribution is described below:

c) Using the SPARK output provided by Dr. Lee with redundant atoms manually removed, I rerun the analysis of regional k-hubness and HSI. I conducted group comparisons of voxel k, regional k, and HSI between WR, NREM2, and NREM3 stages by permutation test with FDR correction. I identified the coordinates and anatomical labels of all clusters of voxels with significant differences in voxel k or HSI between stages. I generated **Figure 3-1B, 1C, 1D, 1F, and 1G, Figure 3-2 and Figure 3-3.**

d) With the assistance of Dr. Nathan Cross, who provided the original code of FCR and helped with the code adaption, I calculated FCR for all fMRI segments at two different hierarchical levels: from the whole brain to Yeo7 levels, from Yeo7 levels to Yeo17 levels (Thomas Yeo et al., 2011a). While other hierarchical structures such as MIST (Urchs et al., 2019) have also been tested, the Yeo7-Yeo17 structure was chosen to facilitate the comparison of results with Cross et al and Boly et al (Boly et al., 2012; N. E. Cross et al., 2021). I then assessed the correlation between HSI and FCR results, with a self-developed bootstrap resampling technique to generate a more robust summary of HSI in each brain region. I generated **Figure 3-5**.

e) I assessed the association between HSI and cognitive performance after a normal night of sleep and after a recovery nap following total sleep deprivation. The same resampling technique mentioned in d) was also applied. I generated **Figure 3-4**.

f) I investigated the different patterns of networks involved in the dorsal attention area across different brain states, by applying robust k-mean clustering on all networks found in all subjects. I generated **Figure 3-6**.

g) I supported the writing of the manuscript in several parts of methodology: the bootstrap resampling technique mentioned in d) and e), and the k-mean clustering mentioned in f). I generate all the figures mentioned above.

3.1.4 Detailed contribution of Dr. Lee

a) During the collaboration, Dr. Lee, my supervisor Dr. Christophe Grova and I meet regularly to offer suggestions, guidance, and interpretation of the results of the analyses done by me.

b) fMRI preprocessing and running of SPARK were done by Dr. Lee assisted by Fatemeh Razavipour. The physiological noisy atoms and redundant atoms were manually removed by Dr. Lee because of her expertise, while I was getting trained for performing this task. However, after I was trained, I performed the fMRI preprocessing, SPARK and manual removal of physiological noisy atoms in *Study 2* of *Chapter 4*.

c) Dr. Lee provided the objectives of the whole study which are consistent with *the original study* from her Ph.D. dissertation, including a group comparison of HSI between states, and the association of HSI and cognitive performances.

d) Dr. Lee was the original author of SPARK. Dr. Lee also originally developed and supported the code of regional k-hubness and HSI. Dr. Lee generated **Figure 3-1A, 1E, and 1H**.

e) Dr. Lee and I both contributed in the manuscript writing.

f) Although the majority of the figures were generated by me, all figures have been visually improved by Dr. Lee.

g) Dr. Lee and I both contributed in interpretation of the results and literature research.

Chapter 4 – *Study 2: A preliminary investigation: connector hub reorganization in frontal lobe epilepsy and temporal lobe epilepsy*

4.1 Introduction

Epilepsy surgery may be considered for 30% of patients resistant to drug therapy. The standard surgical intervention consists of focal resection targeting the epilepsy focus (EF), the brain region from where the epileptic seizure starts. However, there is clear electrophysiological evidence that epilepsy is a network disease (Bartolomei et al., 2017). Epileptogenic networks (EN) are the brain regions producing and propagating epileptic activities (Bartolomei et al., 2017).

Therefore, in this chapter, we intend to apply the same method of HSI based on SPARK as described in **Chapter 3**, on the topic of functional connectivity in epilepsy. We applied HSI the same way and using the same hierarchical template as described in **Chapter 3**. Furthermore, we applied an additional methodology that quantifies the disruption and emergence of hubs in patient groups, when compared to a control group. These new metrics defined as hub disruption index (HDI) and hub emergence index (HEI), estimated using a linear regression model based on SPARK, was investigated by Lee and originally proposed by Achard et al., 2012 (Achard et al., 2012; Lee et al., 2018). Notably, a similar HDI metric was also considered to assess functional hub reorganization during two different levels of propofol-induced sedation (Vatansever et al., 2020), and also to investigate functional hub reorganization at different arousal states monitored by pupillometry (Lee et al., 2022). The aforementioned network segregation using HSI and hub reorganization using HDI/HEI will be compared between the two typical focal epilepsy types: TLE and FLE, to investigate if there is any characteristic pattern of network disruption/reorganization in these two types of epilepsy.

However, it is worth mentioning that this second study is only in a preliminary stage with exploratory results available. Other than Dr. Lee, this study was completed in close collaboration with the labs of Dr. Boris Bernhardt and Dr. Birgit Frauscher, who acquired the datasets of healthy control, TLE, and FLE used in this study and supported parts of fMRI preprocessing pipelines. The dataset of controls, TLE and FLE will keep growing, therefore we are expecting to further improve such analysis by including more participants and patients. We might also include post-surgical outcome results when they are available. Therefore, in the long term, our objectives also include searching for possible neuroimaging biomarkers based on hubness that could predict postsurgical outcomes. Consequently, our long-term hypotheses would be the following: Specific connector hub

reorganizations in epilepsy will predict the postsurgical outcome: a) For an EF located in a region that is not a hub in healthy subjects, hub disruption will tend to isolate the EN from the rest of the brain, resulting a local EN. Resection of a local EN is likely associated with a good surgical outcome. b) For an EF located in a region that is a connector hub in healthy subjects, hub disruption, and emergence will result in a widespread EN involving distant brain regions. Such epilepsy will be difficult to be treated by focal resection.

The aforementioned long-term hypotheses may be further studied after the completion of this thesis, in collaboration with other lab members. Nonetheless, the present **Chapter 4** described in this chapter preliminarily compares the functional network reorganization in TLE and FLE patients when compared to healthy controls.

4.2 Methodology

This study was completed in collaboration with **Dr. Boris Bernhardt, Jessica Royer, Dr. Raul Rodriguez-Cruces, and Dr. Birgit Frauscher**, who have acquired and provided the whole dataset of healthy controls, TLE patients, and FLE patients, and completed the majority of fMRI preprocessing with an fMRI toolbox called MICA, developed by their group (Cruces et al., 2022). The healthy control subjects included in this project are also part of an open-source MRI dataset recently published (Royer et al., 2021). **In our preliminary analysis, we proposed to apply SPARK methodology introduced in previous chapter (i.e. k-hubness, regional-k, and HSI) on this dataset.** More data will be available in near future and we will continue our collaboration after submitting this thesis, aiming at completing this study with a publication.

Participants

26 healthy controls, 14 TLE patients (11 left-lateralized, 1 right- lateralized, and 2 bilateral), and 11 FLE patients (5 left- lateralized and 6 left- lateralized) were included in this study. Controls and patients are sex and age matched. All healthy subjects denied any history of neurological and psychiatric illness. All subjects went through a single acquisition session. After fMRI preprocessing and running them through the SPARK pipeline (Lee et al., 2016), manual removal of physiological noise was done. Subjects exhibiting a ratio of the number of noisy atoms / total number of atoms > 50% were further excluded from the analysis (2 healthy controls, 2 TLE, and 1 FLE subjects), indicating their fMRI data were dominated by physiological noise such as vascular noise or movement noise. Therefore, 24 healthy controls, 12 TLE, and 10 FLE subjects were included in the final analysis.

Data acquisition

The data acquisition took place at the McConnell Brain Imaging Centre of the Montreal Neurological Institute and Hospital. Using a 3T Siemens MRI system with a 64-channel head coil, all participants undertook two T1-weighted structural scans, DWI, and rs-fMRI. The rs-fMRI data were acquired using multiband acceleration 2D-BOLD imaging, for a duration of 7 min, with 3mm isotropic voxels, TR=600ms, TE=30ms. All participants were instructed to keep their eyes opened, to look at a fixed cross and not to sleep. More details regarding scanning parameters including information on the T1-weighted and DWI scans can be found in (Royer et al., 2021).

fMRI data preprocessing

The motion correction and band-pass filtering steps were done using a recently published fMRI preprocessing pipeline called MICApipe (Cruces et al., 2022), developed in the lab of Dr Bernhardt.

The link to its open-source code is https://github.com/MICA-MNI/micapipe. MICApipe is a comprehensive multimodal MRI preprocessing toolkit that can not only preprocess T1-weighted MRI, rs-fMRI, and DWI, but also several output results, including functional connectome using fMRI data, structural connectome using DWI data, geodesic distance matrices and microstructural profile covariance matrices. In brief, the typical MICApipe of fMRI preprocessing includes motion correction, co-registration, normalization by registering all subjects to FreeSurfer space, spatial smoothing, and at the end, registration to FreeSurfer cortical surface and parcellation. To facilitate the analysis of SPARK, since we have more experience using fMRI data in volumetric MNI space, we considered output fMRI file of MICApipe after motion correction, but before interpolation on the cortical surface. To do so, we first co-registered all subjects to MNI 152 nonlinear asymmetric space in the resolution of 2*2*2 mm^3 and then completed the rest of the fMRI preprocessing. Notably, with some adaptions, SPARK could also be applied to fMRI data in other normalized spaces aside from MNI and notably along the cortical surface, but this was out of the scope of present study.

Therefore, the first part of fMRI preprocessing by MICApipe starts with removing the first 5 TRs. Notably, slice timing was skipped because some argued that slice timing is less necessary for multiband acquisition fMRI data because the short TR indicates little time gap between each slice and slice timing would show less difference (Functional Imaging Laboratory, 2016). Motion correction within scans was then applied using the "3dvolreg" function from AFNI (Cox, 1996) as well as distortion correction. A function called "fsl_motion_outliers" from FSL (Woolrich et al., 2009) was then applied, and the time frames exhibiting excessive motion were identified and saved as confounds (to be elaborated in the next section: **scrubbing vs despiking**). Next, a high-pass filter of >0.1Hz was applied to remove unwanted frequencies. ICA-FIX from FSL (Griffanti et al., 2014; Salimi-Khorshidi et al., 2014) was then applied to identify and remove nuisance variable signals, in replacement of conventional regression of white matter and cerebrospinal fluid signals.

We then manually added steps to complete the preprocessing and ensure compatibility with SPARK. The second part of fMRI preprocessing by MICApipe starts with brain extraction, applying the recon-all function from FreeSurfer (Reuter et al., 2012) on T1-weighted anatomical data and applying the BET toolbox on fMRI data (Smith, 2002). Secondly, all fMRI data (3mm isotropic voxels) were co-registered to the corresponding T1-weighted anatomical MRI (0.8 mm isotropic voxels), and subsequently registered and resampled at a 2mm resolution on the asymmetric nonlinear MNI152 template (Fonov et al., 2009, 2011), using FLIRT from FSL with 12 parameters affine transformation (Greve & Fischl, 2009; Jenkinson et al., 2002; Jenkinson & Smith, 2001). This 2mm MNI space was then downsampled to 4mm resolution, ending up at a similar resolution

when compared to our previous studies using SPARK. Afterwards, spatial smoothing with full width at half maximum (FWHM) = 6mm was applied, consistent with previous studies in our group (Lee et al., 2018). Importantly, the motion outlier confounds estimated using MICApipe (i.e. "fsl_motion_outliers") were regressed out from the fMRI data using FSL, to further decrease the influence of small "spiking" motions.

Comparison between scrubbing and despiking

It is worth mentioning that as a fully data-driven technique, SPARK is highly sensitive to motion components. In our previous studies (Lee et al., 2016, 2018) and also in Chapter 3, we considered an additional motion control process called scrubbing (Power et al., 2014) during fMRI preprocessing. Scrubbing consists in removing, from the fMRI time series, time points exhibiting frame displacement (FD) larger than a certain threshold, FD > 0.5 mm was considered in (Lee et al., 2016, 2018). However, in this study, instead of scrubbing, we applied another motion control technique where a confound of motion outliers was regressed out, which is the so-called "despiking" process. Using the function "fsl_motion_outliers" from FSL (Woolrich et al., 2009), motion outliers were identified as time points with frame displacement larger than 75th percentile + 1.5 times the Interquartile Range (IQR) among its distribution. Note that this is the standard definition of outliers used in boxplot representation. The time points that would have been be removed with scrubbing versus despiking are respectively shown in **Figure A4**, considering all healthy control subjects as an example. Our results are suggesting that on subjects exhibiting relatively small movements, despiking would be more aggressive, while on subjects exhibiting larger movements, scrubbing would be more aggressive. Nonetheless, while we separately applied scrubbing and despiking on one testing subject and did two trial runs of SPARK, the output k-hubness map showed no significant differences, and we also found similar RSNs involved and a similar ratio of noisy atom, when considering the two approaches. Therefore, we decided to applied the despiking procedure, which also aligns the convention in MICApipe.

Adaptation of SPARK for fMRI with shorter TR

After fMRI preprocessing, SPARK was applied to all subjects to generate a k-hubness map for each subject, where the k-hubness denotes the number of networks connected to each voxel (Lee et al., 2016, 2018, 2022). The details of SPARK can be found in the methodology part of *Chapter 3*. As introduced in *Contribution of Authors* in *Chapter 3*, and adapted version of SPARK was applied in this study to avoid generating redundant RSN atoms, by taking absolute values before C-mean clustering instead of after.

In addition, to adapt fMRI data analysis of shorter TR using SPARK, we had to implement two

adjustments:
(1) A parameter of SPARK called window block length *h* was adjusted, which is the length of a sliding time window that is used to generate bootstrap samples of fMRI time series. This length parameter of the block Bootstrap ensure independency between Bootstrap sample and also taking into account fMRI intrinsic autocorrelation for each Bootstrap sample, as originally proposed in Bellec et al (Bellec et al., 2010a). In SPARK, we chose the most optimal window block length *h* within the range of sqrt(T) < *h* <= 2*sqrt(T) (T=number of time points) to preserve temporal dependencies, as proposed in Bellec et al (Bellec et al., 2010a). This range was usually enlarged to a small extent to ensure robustness. Therefore, since the number of time points was T=695 for the multiband accelerated fMRI data of this study (TR=600ms, time length is around 7min), we therefore set the window block length to be 20 < *h* < 55, while it was 10 < *h* < 30 in *Study 1* of *Chapter 3* (TR=2500ms, where T ranged from 91 to 121 after scrubbing).

(2) The fMRI time series were downsampled temporally before estimating optimal k-hubness for sparse dictionary learning with K-SVD. In the sparse dictionary learning of SPARK, the scale of the number of outputs SPARK atoms (RSNs), e.g., the total number of networks estimated, is estimated from the data using a minimum description length (MDL) principle, as we introduced and evaluated in Lee et al 2018 (Lee et al., 2018; Saito, 1994), allowing to find the best trade-off between goodness-of-fit and model complexity. Nonetheless, the scale of networks is also subjective and depends on which scale the researcher is interested in. It is worth mentioning that downsampling or upsampling the time series before MDL estimation would result in significant changes in the resulting global scale of networks. Therefore, to investigate the functional networks on a similar scale to *Study 1* and to our previous studies (the global number of the network was ranging from 10 to 20 before manual removal of physiological noisy atoms), we downsampled the time series of the current study by a factor of 4 to end up with similar global scale values and therefore range of k-hubness values. It could have been of interest to investigate SPARK results at a more accurate temporal resolution, taking advantage of multiband acquisitions, but this was out of the scope of present study. Similar method has also been applied in Lee et al ((Lee et al., 2011).

Similar to *Study 1*, after applying SPARK on all subjects, atoms resulting from physiological noise were visually identified and manually removed, for example, atoms showing patterns of motion noise or noise from dominant veins or vessels (Lee et al., 2019). Subsequently, subjects exhibiting a ratio of the number of noisy atoms / total number of atoms > 50% were further excluded.

Functional segregation of TLE and FLE

The same methods proposed in *Study 1* to estimate regional k and HSI were applied to the current dataset. The same group comparison of voxel k-hubness and HSI using permutation test was also considered.

Hub disruption and hub emergence in TLE and FLE

To quantify the hub alterations in epilepsy groups when compared to healthy groups, we applied two algorithms: hub disruption index (HDI) and hub emergence index (HEI), following methodology originally proposed by (Achard et al., 2012) and further adapted and validated by Lee et al, (Lee et al., 2018, 2022).

Group-level HDI and HEI are estimating by comparing hubness distribution of each participant (control or patient) to the distribution of hubness found within the healthy control group, using the following linear regression model:

$$d^P = a\frac{\mu_k^C}{\sigma_k^C} + b$$

$$\text{While, } d^P = \frac{\mu_k^P - \mu_k^C}{\sigma_k^C}$$

$$a = HDI, b = HEI$$

μ_k^P denotes the average k-hubness in a specific patient group (TLE or FLE) for one voxel in a selected ROI (e.g., the hippocampus), μ_k^C denotes the average k-hubness in the control group for one voxel in the ROI, σ_k^C denotes the standard deviation (SD) of k-hubness in the control group for one voxel in the ROI. Representing d^P as y-coordinates and $\frac{\mu_k^C}{\sigma_k^C}$ as x-coordinates for *n* voxels in the ROI, we obtain a scatterplot with N data points. By fitting a straight line through the aforementioned scatter plot, the slope **a** will be defined as HDI, and the intercept **b** will be defined HEI. HDI and HEI can therefore quantify the k-hubness alterations/reorganization in the patient group when compared to the mean distribution of k-hubness values within the control group. Specifically, a negative HDI (slope) suggests the voxels that are hubs in controls are becoming non-hub in patients, or their hubness is decreasing in patients, indicating an overall hub disruption within the ROI. A positive HDI (slope) suggests the hub region in controls is having even higher k-hubness in patients, indicating more involvement of the ROI with other parts of the brain, i.e., "hyperconnectivity". A positive HEI (intercept) indicates the region that is non-hub in controls tends to become hub in patients. It is worth mentioning that HEI will not be negative because voxels will not involve any negative number of networks (Lee et al., 2018).

Individual-level HDI and HEI could also be computed using a similar linear regression model:

$$d_i^P = a\frac{\mu_k^C}{\sigma_k^C} + b$$

$$While, d_i^P = \frac{k_i^P - \mu_k^C}{\sigma_k^C}$$

$$a = HDI_i, b = HEI_i$$

Notably, k_i^P indicates the k-hubness of one voxel in the ROI for one single patient. The resulted individual-level HDI_i and HEI_i will instead indicate the extent of hub alterations of one subject specifically, when compared to the mean of the control group. Subsequently, the distribution of individual-level HDI_i and HEI_i will be compared across groups using violin plots. The individual-level HDI_i and HEI_i of each control subject were also calculated to facilitate the comparison.

4.3 Results

4.3.1 Network segregation for TLE and FLE patients

After applying fMRI preprocessing and SPARK to estimate k-hubness, we applied the same regional k and HSI method as *Chapter 3*, using the same atlas. The results of averaged voxel k-hubness map are shown in **Figure 4-1A**, the results of averaged and SD of regional k-hubness are shown in **Figure 4-1D**, and the results of averaged HSI map are shown in **Figure 4-1B**.

We applied the same group comparison method using non parametric permutation tests (see section 3.6 of this thesis). No significant difference was found between the three groups for voxel level k-hubness values. However, we found significant differences in regional k-hubness among groups, as illustrated in **Figure 4-1D**. The number of RSNs involved in ventral attention network, frontoparietal network, DMN and cerebellum was reduced in TLE comparing to HC. The number of RSNs involved in limbic network, frontoparietal, DMN and cerebellum was reduced in FLE comparing to HC. No significant difference was found in regional k-hubness when comparing TLE to FLE. We also found significant differences in HSI among groups as shown in **Figure 4-1C**. When compared to controls, TLE patients exhibited increased network segregation mostly in the caudate, thalamus, frontal orbital lobe, and both mesial temporal lobe (mTL) region, as well as decreased network segregation mainly in the dorsolateral frontal lobe, mesial prefrontal lobe and precuneus. On the other hand, when comparing FLE patients to controls, FLE data were associated with increased network segregation principally in the thalamus and mTL regions, together with reduced segregation in the cerebellum, mesial frontal lobe, dorsolateral frontal lobe, and PCC regions. When comparing directly TLE and FLE patients, we found that FLE data were characterized by significant increased functional network segregation mainly in subcortical regions including the thalamus, head caudate, pallidum, and putamen, near the midline of the frontal cortex, and also in mTL regions.

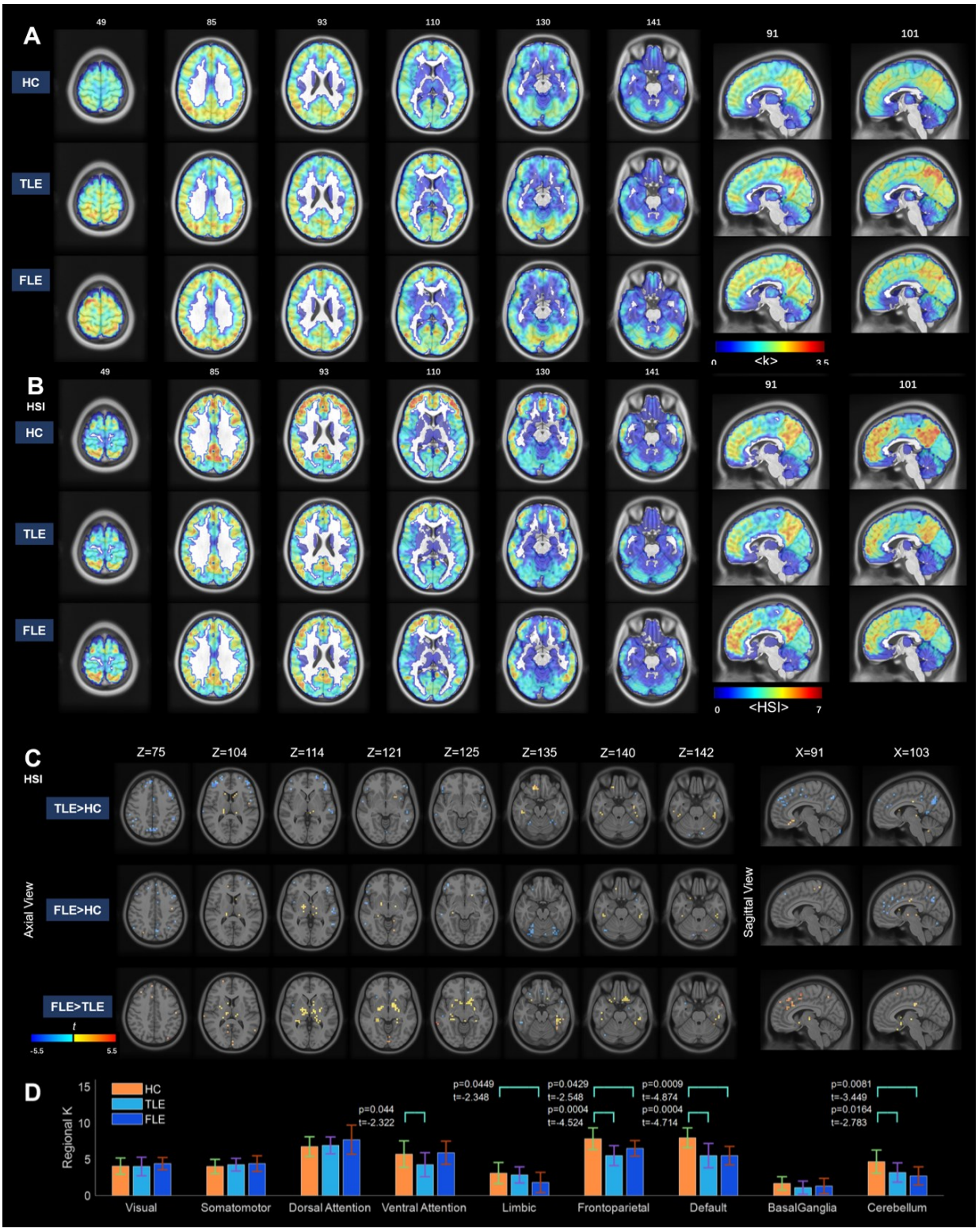

Figure 4-1 Altered functional network segregation and regional involvements of RSNs in epilepsy. (A) Group average voxel-level k-hubness map. Non-parametric permutation test was also applied, but no voxel was found with significant differences between group. Therefore, the result of between group comparison of voxel-level k-hubness is

not shown. (B) Group average HSI map. Non-parametric permutation test was also applied, the voxels with significant differences between groups were shown in Figure 4-1. (C) Group comparison of HSI between HC, TLE, and FLE groups showing in t-statistics map which is filtered by $p<0.05$ according to permutation test. Only the voxels with significant differences (non-parametric permutation test, $p<0.05$, FDR corrected) between the two groups are shown, according to the color bar. (D) The mean and standard deviation of region-level k-hubness in nine pre-defined networks. The pairs with significant differences are marked with red solid indicators (permutation test applied, $p<0.05$, FDR corrected).

4.3.2 Hub disruption and hub emergence of TLE and FLE

We applied group-level and individual-level HDI and HEI to both patient groups. HDI and HEI can be applied either to the whole brain or on any particular ROI. Notably, because this study is still in a preliminary stage, we are not presenting a systematic investigation of ROI, instead, we chose a few ROIs of interest. All ROIs mentioned below were defined according to the Automated Anatomical Labelling version 3 (AAL3) template (Rolls et al., 2020). The name of those ROIs was the same as the label name in AAL3. The definition of those ROIs is bilateral. For example, in **Figure 4-2**, ROI named "thalamus" indicates both the left and right thalamus.

(1) We first investigated HDI/HEI within 3 subcortical regions: **thalamus, caudate, and putamen**, as illustrated in **Figure 4-2**, since the thalamus has been suggested to be involve in seizure propagation at some degree (He et al., 2015; Martín-López et al., 2017), caudate and putamen have been reported with reduced grey matter volume in FLE (Klugah-Brown et al., 2019), and as we found significant clusters in subcortical regions in our HSI results. Group-level HDI of caudate and putamen indicates an overall hub disruption in both TLE and FLE, while TLE generally exhibited more hub emergence than FLE in caudate. In caudate nuclei, TLE shows significant differences with HC of both individual-level HDI (iHDI) and individual-level HEI (iHEI), suggesting hub disruption and emergence. In FLE, only hub disruption was found showing significant differences with HC of iHDI. In the putamen, we found significant differences between FLE and HC (iHDI and iHEI) but non for TLE. Surprisingly, the thalamus region, unlike the majority of ROIs we have investigated, shows mostly positive HDI. Notably, as shown in the iHDI graph (Column 2) of **Figure 4-2**, the distribution of the thalamus is not gaussian, unlike the generally Gaussian distribution of other ROIs, despite outliners. Therefore, the current result of the thalamus region should be interpreted with caution. We suspect several reasons that may explain those findings: lack of power because of our sample size, a lower signal-to-noise ratio fMRI signal in the thalamus, and the associated difficulty of SPARK in estimating hubs in this structure (several voxels associated with k=0 values) (see **Discussion**). If the aforementioned issues can be resolved in future studies and if suppose a similar positive HDI and HEI still occur, we might then conclude of a special hyperconnectivity of the thalamus region in TLE and FLE, but this is too early to propose

such a conclusion for the moment and our analysis deserves further investigations.

(2) Secondly, we investigated **the mTL and the DMN regions**, with the same ROIs considered in our previous study of Lee et al, who reported hub disruption and hub emergence in both mTL and DMN in mesial TLE patients (Lee et al., 2018). For the ROI definition, we followed the same definition of mTL ROI as in the paper of Lee et al., which includes the amygdala, hippocampus, and parahippocampal gyrus using AAL3. The results of mTL are shown in **Figure 4-3,** and the results of DMN are shown in Row 3 of **Figure A5**. We found both significant hub disruption and hub emergence in both TLE and FLE in the mTL region. Our TLE results in mTL regions are clearly in agreement with our previous findings reported in (Lee et al., 2018). Interestingly, we are reporting for the first-time hub disruption and hub emergence in mTL structure for FLE patients when compared to controls, suggesting remote network reorganizations. On the other hand, we did not find any significant differences in the DMN regions. As the insignificant trend shown in **Figure A5 (Row 3)**, if we were expecting more participating patients, we might be able to find the hub disruption and emergence in DMN regions in TLE groups, but not in FLE, which could be a distinction between TLE and FLE.

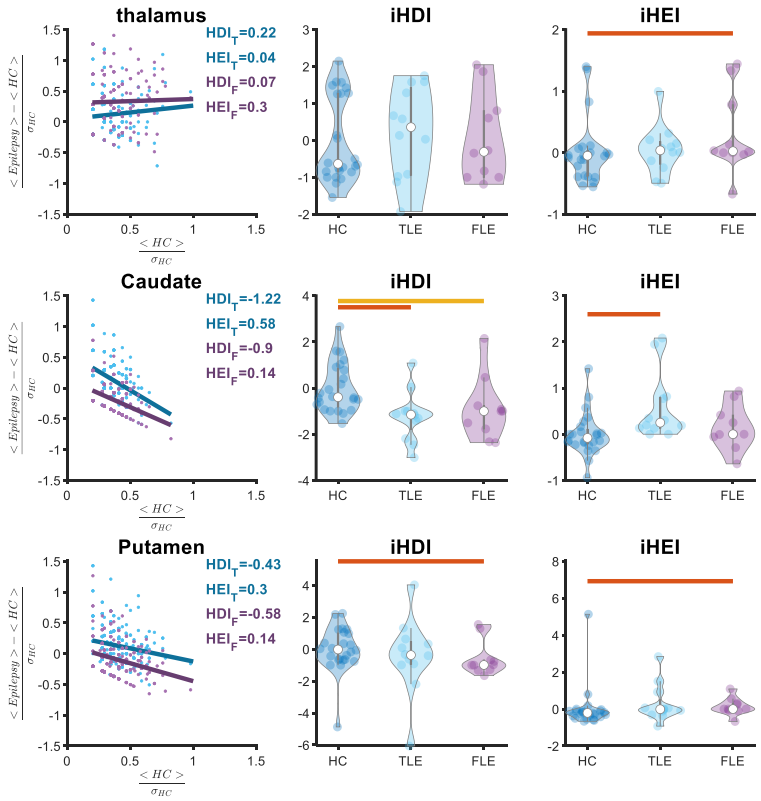

Figure 4-2 HDI and HEI of selected subcortical regions (thalamus, caudate, and putamen). Column 1 denotes the group-level HDI and HEI. <Epilepsy> indicates averaged k-hubness of one voxel across all patients (either FLE

or TLE). <HC> indicates the averaged k-hubness across healthy controls. σ_{HC} indicates the Standard Deviation (SD) of healthy controls. Statistics of TLE patients are shown in blue, and the statistics of FLE patients are shown in purple. The blue (TLE) and purple (FLE) solid lines are the best line of fit for the linear regression models. HDI is the slope of this line and HEI is the intercept of it. Each blue point or purple point represents one voxel in the corresponding ROI. Column 2 and Column 3 are presenting the distribution of individual HDI and HEI for all healthy controls (darker blue), TLE (blue), and FLE (purple) patients, denoted here as iHDI and iHEI respectively. The pairs of groups with significant differences of iHDI or iHEI values are marked as red, orange, or yellow horizontal lines ($p<0.05$, Kruskal Wallis test applied). It is worth mentioning that the y-axis was not on the same scale for different ROIs to facilitate showing the distribution shape better.

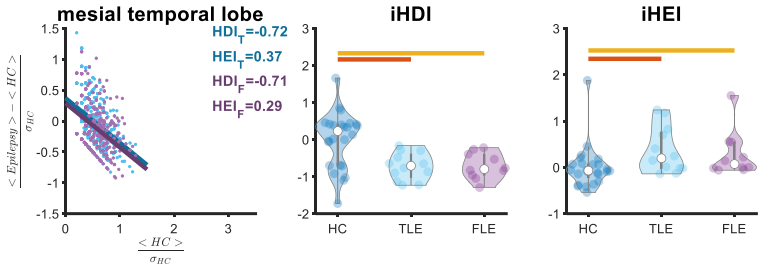

Figure 4-3 HDI and HEI of mTL regions. The mTL regions include the amygdala, hippocampus, and parahippocampal gyrus, as defined according to the AAL atlas. The color and notions are the same as **Figure 4-2.**

(3) Finally, we investigated the HDI and HEI in some frontal lobe regions, since we have found significant HSI differences between groups in the mesial frontal region. We are mainly reporting significant differences between groups of iHDI and iHEI in 4 ROIs: **superior frontal lobe, middle frontal lobe, superior mesial frontal lobe, and supplementary motor areas** (as shown in **Figure 4-4**), all frontal regions located close to the midline of the brain between two hemispheres, showing agreement with HSI our results with HSI. Notably, all ROIs defined are bilateral. We found mainly hub disruption and sometimes hub emergence, occurring more in TLE patients than in FLE patients. Only in the supplementary motor cortex, we found a significant increase in iHEI in FLE, but not in TLE. Nonetheless, **Figure 4-4** still indicates a general hub disruption in the frontal area in TLE, even whose lesions are not located in the frontal cortex, which might suggest a more severe global network disruption in TLE when compared to FLE. We have also investigated all other frontal lobe regions; however, we did not find significant differences in iHDI/iHEI.

(4) Aside from the aforementioned regions, we also found significant differences in iHDI or iHEI between the TLE and FLE in the **transverse temporal lobe and the superior occipital lobe**, as illustrated in **Figure A4 (Row 1 and Row 2).** Nonetheless, in these two regions, only TLE showed a trend to have hub disruption and emergence, whereas FLE was not showing significant hubness changes.

Generally, based on preliminary results, we generally found more alterations reported in HDI than in HEI, suggesting rather hub disruption, i.e., hubs in controls becoming non hubs in patients, suggesting regularization of the network and loss of distant connections. TLE patients generally exhibited more hub alterations when compared to FLE. In FLE, only the superior frontal mesial lobe, supplementary motor area, mTL, caudate and putamen were showing significant differences in hub alterations (thalamus was not counted). Among those, only **supplementary motor area** and **putamen** show different patterns when comparing TLE and FLE. The supplementary motor areas show significantly more hub emergence in FLE compared to TLE. In the putamen, our preliminary results are suggesting that hub alteration occurs in FLE but not in TLE. These findings indicate that those 2 ROIs might perhaps serve as biomarkers of distinction between FLE and TLE.

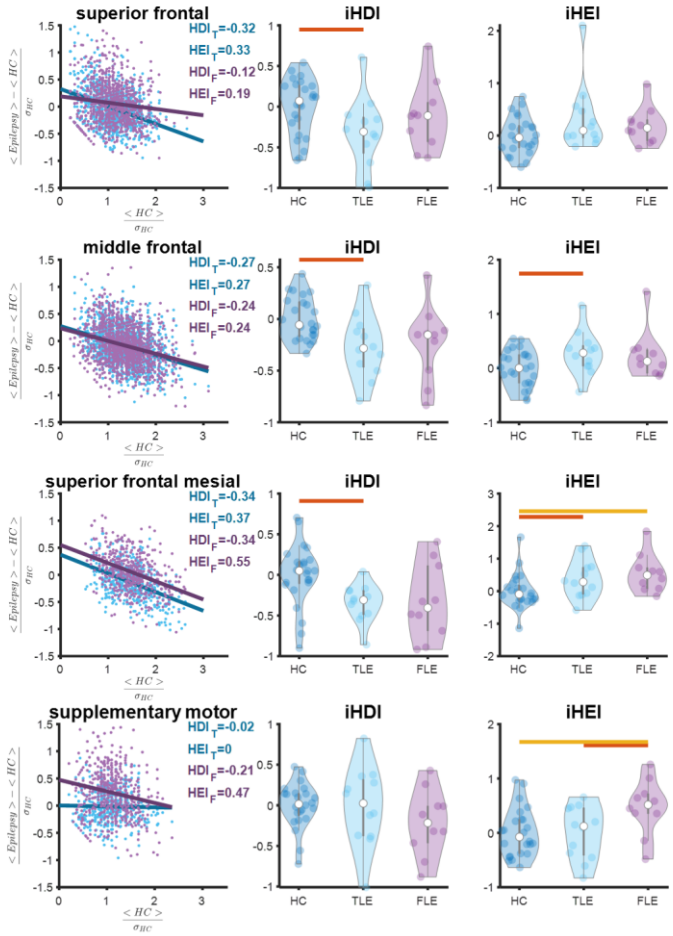

Figure 4-4 HDI and HEI of selected frontal regions near mesial frontal lobe. The color and notions are the same as Figure 4-2.

4.4 Discussion and conclusion

By applying the same method of HSI as described in chapter 3 on our dataset involving healthy

controls, TLE and FLE patients, we found significant alterations of functional segregation between groups revealed by HSI, predominantly in subcortical regions, mesial frontal lobe, and mTL regions. Additionally, we found a decreased number of networks connecting ventral attention network, limbic, frontoparietal, DMN and cerebellum regions in TLE or FLE when compared to healthy controls, revealed by regional k values (**Figure 4-1**). The results using regional k indicate the large-scale RSNs are generally less interconnected with each other in epilepsy, in other words, some connector hubs are disrupted in TLE and FLE, which is in agreement with our previous founding in mesial TLE (Lee et al., 2018). Since HSI = regional k / voxel k, and because we found significantly decreased regional k in epilepsy but no significant changes in voxel k, it might indicate that generally in TLE and FLE, there is no appearance of new RSN or complete disappearance of RSN, but instead, existing large-scale networks might have broken down into smaller networks and are less connected with each other. This is opposed to the patterns of segregation we found in **Chapter 3** using sleep data on all healthy subject cohorts, where we found changes both in voxel-level k and region-level k during sleep when compared to wakefulness. It suggests that although the "small-world" macrostructure varied due to the disruption of long-range connections, there is globally no reduced or hyper neural activity in TLE and FLE when compared to controls at rest.

In addition, using the HDI and HEI algorithm as in Lee et al (2018), we first found similar patterns of hub reorganization in TLE (**Figure 4-3**) (Lee et al., 2018), which are attached in **Figure A6**. Surprisingly, whereas hub disruption in TLE was expected because of the commonly found mTL sclerosis in TLE, we also found very similar HDI and HEI in FLE in the mTL regions, suggesting more attention is needed regarding the role of mTL in FLE. This hypothesis would deserve further investigation. In caudate nuclei, hub disruption was found for both TLE and FLE, while hub emergence was only found for TLE. In the putamen, FLE showed distinct hub disruption and emergence, which can serve as a potential biomarker for FLE (**Figure 4-2**). In mesial frontal area, hub disruption and emergence were found more in TLE and less in FLE (**Figure 4-4**), aligning with our results from HSI, whereas in mesial frontal area TLE showed segregation but not FLE (**Figure 4-1**). In addition, this result can explain the commonly found reduced cognitive ability in TLE, because the mesial frontal region supports (Stretton & Thompson, 2012).

Considering the definition of k-hubness, a voxel or region with higher k-hubness is more likely to be a connector hub participating to long-range connection while one with lower k-hubness is more likely a provincial hub participating in local communication. Considering the multi-level and complex hierarchical structure of the brain functional connectome, the connector hub and provincial hub are defined relatively instead of with a certain threshold. Thus, in our application of HDI and HEI, the results should also be interpreted relatively, a ROI with significantly positive

HEI and negative HDI would indicate that the voxels participating in longer-range communication are losing long-range connection, in the meantime, the voxels that are non-hub or participate in local communication are engaging more with other brain areas. Such patterns of reorganization appeared in the majority of results shown in Figure 4-2 to Figure 4-4. Such patterns also generally align with the inference we got from the results of regional k that large-scale RSNs are breaking down and less interconnected in TLE and FLE. Accordingly, we have verified the reorganization of functional connectivity in epilepsy on both network-level using HSI and voxel-level using HDI/HEI. Our results again addressed the importance of treating epilepsy as a network disease instead of focally and highlighted the importance of research that predicts post-surgical outcomes by examining whether the targeted lesion is a connector hub or not.

Additionally, we found unconventional positive HDI especially in TLE in the thalamus region, which might indicate hyperconnectivity where the regions that are connector hubs in controls are engaging with even more long-range connections in patients. However, our results on this question should be interpreted with caution, especially because of bimodal distribution of HDI and HEI results found in the thalamus (see **Figure 4-2**). In the future, aside from including more epilepsy patients and control subjects, we might consider tailoring SPARK to the need of investigating the role of the thalamus in epileptic functional connectivity, by sourcing the dictionary learning from the fMRI time-series from thalamic or subcortical structures only. Such an approach would likely compensate the issue of relatively lower signal-to-noise (SNR) ratio in thalamus region in fMRI acquisition, since the thalamus is one the most remote regions from the MR head coils. Nonetheless, if supposing the aforementioned measures can be taken in the future and similar HDI and HEI were to be found, we might speculate the thalamus has even more long-range communication to other RSNs, which can either compensate for decreased cognitive ability or more plausibly, form an underlying network that is responsible for seizure generation and propagation. The role of thalamus nuclei in the propagation of seizure, termination of seizure, and consciousness during seizures have been suggested in the literature (Evangelista et al., 2015; Feng et al., 2017; Velíšek, 2018), while further investigation from the perspective of functional networks would offer valuable information as well. Overall, although with only preliminary results, we have found significant functional connectivity alterations in TLE and FLE compared to controls. In the future, to complete this study, we expect to include more analysis: including more participants, tailoring the SPARK algorithm, as well as investigating the rate of appearance of different RSNs among groups, and investigating the role of different thalamus nuclei.

Chapter 5 Conclusion

In this thesis, we have introduced the background of functional connectivity studies in *Chapter 1*. In *Chapter 2*, we have introduced several types of state-of-the-art methodologies used in functional connectivity and addressed the specificity of SPARK. Subsequently, we have investigated functional networks using SPARK for two specific applications: sleep and epilepsy. In *Chapter 3*, we found that the visual cortex showed significantly more segregation in NREM2 compared to NREM3 (NREM2>NREM3≈WR) and the orbitofrontal cortex showed significantly more segregation in NREM3 compared to NREM2 and wakefulness (NREM3>WR>NREM2). We have also found that more functional segregation during the recovery nap can be associated with poorer working memory performance after the nap. In *Chapter 4*, we found altered patterns of network segregation predominantly in subcortical structures near the thalamus (FLE>TLE≈HC), mesial frontal lobe (HC>FLE>TLE), dorsolateral frontal regions (HC>TLE≈FLE), and mTL (FLE>TLE>HC). We have also found fewer networks interconnected to ventral attention, limbic, frontoparietal, DMN, and cerebellum networks. In addition, we found hub disruption and emergence in TLE in Caudate, mTL, and mesial frontal lobe, while in FLE other than general disruptions in several other ROIs we have also found distinct hub disruption and emergence in putamen and hub emergence in the supplementary motor area.

The main methodology used in this thesis, SPARK, is a novel method to quantify functional hubs, in the meantime handles the overlaps between functional networks. This thesis identified the difference in functional segregation between different NREM stages and offered a perspective on how recovery nap after sleep deprivation correlates with cognitive ability. Despite being in a preliminary state, this thesis also found specific functional network patterns associated with TLE or FLE.

However, this thesis involves several limitations. In *Study 1* of *Chapter 3*, firstly, the overall blood flow level might differ in sleep comparing to rest. Therefore, it needs to be validated that if HSI results will be biased by such effect. A validation analysis can be done, where this effect will be modeled and regressed out from the fMRI time-series, and then conducting the same analysis afterward and comparing the results to existing results. Secondly, our research question was restricted to a one-hour recovery nap after total sleep deprivation. By waking up a participant after one-hour nap, we interrupted the recovery of severely impaired cognitive function. Variables caused by the “interruption” might contribute to the cognitive performance variability, such as the length of time taken to wake up the participant, or which part of the sleep cycles (REM, NREM1,

or NREM4) was the participant in when woken up, we question if those variables affect the cognitive ability afterward. More investigation is required to reveal how sleep recovers cognitive ability systematically, considering the influence of sleep cycles. In *Study 2* of *Chapter 4*, as mentioned in the discussion section of Chapter 4, firstly we expect a greater number of participants to draw more reliable conclusions from group comparison, and secondly, a tailored version of SPARK with dictionary learning focusing on thalamus is required to compensate the low SNR of the thalamus and to further investigate its network association. Thirdly, currently simultaneous EEG is not involved during the fMRI acquisition, which should be considered because it identifies fMRI segment with epileptic spike discharge that can appear in some epilepsy patients even during rest, and such fMRI segments should be excluded from the following analysis to increase reliability. Lastly, in the current stage of analysis, the ROIs explored with HDI/HSI was defined according to AAL template, although the AAL template is not the optimal parcellations to study FC, given that the sulcation patterns do not completely align with functional boundaries and networks. Other templates can be considered in future investigation.

In the future, many possible directions can be further investigated related to our research topic. In study 1, as mentioned in the previous paragraph, a similar study design but with different lengths of sleep can offer more insights into exploring the whole scheme of cognitive restoration, which can potentially lead to professional advice on how to get more effective sleep with inadequate time, or even contribute to advancement in sleep disorder treatment. In study 2, the most essential future interest is to investigate if HSI, HDI, or HEI can serve as biomarkers to predict the post-surgical outcome. Combining with other modalities such as the structural biomarkers using DWI and the metabolic biomarkers using positron emission tomography (PET), we might be able to offer an anticipated rate of success for lobectomy, which can potentially lead to significant advancement in pre-surgical assessment.

Reference

AASM. (2007). *AASM Scoring Manual versión 2.5 - American Academy of Sleep Medicine*. https://aasm.org/clinical-resources/scoring-manual/

Achard, S., Delon-Martin, C., Vértes, P. E., Renard, F., Schenck, M., Schneider, F., Heinrich, C., Kremer, S., & Bullmore, E. T. (2012). Hubs of brain functional networks are radically reorganized in comatose patients. *Proceedings of the National Academy of Sciences of the United States of America*, *109*(50), 20608–20613. https://doi.org/10.1073/PNAS.1208933109/SUPPL_FILE/PNAS.201208933SI.PDF

Acharya, U. R., Bhat, S., Faust, O., Adeli, H., Chua, E. C. P., Lim, W. J. E., & Koh, J. E. W. (2015). Nonlinear dynamics measures for automated EEG-based sleep stage detection. *European Neurology*, *74*(5–6), 268–287. https://doi.org/10.1159/000441975

Ad-Dab'bagh, Y., Einarson, D., Lyttelton, O., Muehlboeck, J.-S., Mok, K., Ivanov, O., Vincent, R. D., Lepage, C., Lerch, J., Fombonne, E., & Evans, A. C. (1998). The CIVET Image-Processing Environment: A Fully Automated Comprehensive Pipeline for Anatomical Neuroimaging Research B-References for tools called upon by CIVET: Figure 2: Example screen shots of the CIVET GUI Figure 1: Diagrammatic Representation of The CIVET Pipeline Environment. *IEEE Trans Med Imaging*, *17*(6), 95.

Aertsen, A. M. H. J., Gerstein, G. L., Habib, M. K., & Palm, G. (1989). Dynamics of neuronal firing correlation: modulation of "effective connectivity." *Journal of Neurophysiology*, *61*(5). https://doi.org/10.1152/JN.1989.61.5.900

Alizadeh, M., Kozlowski, L., Muller, J., Ashraf, N., Shahrampour, S., Mohamed, F. B., Wu, C., & Sharan, A. (2019). Hemispheric Regional Based Analysis of Diffusion Tensor Imaging and Diffusion Tensor Tractography in Patients with Temporal Lobe Epilepsy and Correlation with Patient outcomes. *Scientific Reports 2019 9:1*, *9*(1), 1–8. https://doi.org/10.1038/s41598-018-36818-x

Allen, P. J., Josephs, O., & Turner, R. (2000). A method for removing imaging artifact from continuous EEG recorded during functional MRI. *NeuroImage*, *12*(2), 230–239. https://doi.org/10.1006/NIMG.2000.0599

Bartolomei, F., Lagarde, S., Wendling, F., McGonigal, A., Jirsa, V., Guye, M., & Bénar, C. (2017). Defining epileptogenic networks: Contribution of SEEG and signal analysis. *Epilepsia*, *58*(7), 1131–1147. https://doi.org/10.1111/EPI.13791

Beckmann, C. F., DeLuca, M., Devlin, J. T., & Smith, S. M. (2005). Investigations into resting-state connectivity using independent component analysis. *Philosophical Transactions of the Royal Society B: Biological Sciences*, *360*(1457), 1001–1013. https://doi.org/10.1098/rstb.2005.1634

Bellec, P., Rosa-Neto, P., Lyttelton, O. C., Benali, H., & Evans, A. C. (2010a). Multi-level bootstrap analysis of stable clusters in resting-state fMRI. *NeuroImage*, *51*(3), 1126–1139. https://doi.org/10.1016/J.NEUROIMAGE.2010.02.082

Bellec, P., Rosa-Neto, P., Lyttelton, O. C., Benali, H., & Evans, A. C. (2010b). Multi-level bootstrap analysis of stable clusters in resting-state fMRI. *NeuroImage*, *51*(3), 1126–1139. https://doi.org/10.1016/J.NEUROIMAGE.2010.02.082

Berry, R. B., Gamaldo, C. E., Harding, S. M., Brooks, R., Lloyd, R. M., Vaughn, B. v., & Marcus, C. L. (2015). AASM Scoring Manual Version 2.2 Updates: New Chapters for Scoring Infant Sleep Staging and Home Sleep Apnea Testing. *Journal of Clinical Sleep Medicine : JCSM : Official Publication of the American*

Academy of Sleep Medicine, *11*(11), 1253. https://doi.org/10.5664/JCSM.5176

Bethlehem, R. A. I., Paquola, C., Seidlitz, J., Ronan, L., Bernhardt, B., Consortium, C. C. A. N., & Tsvetanov, K. A. (2020). Dispersion of functional gradients across the adult lifespan. *NeuroImage*, *222*. https://doi.org/10.1016/J.NEUROIMAGE.2020.117299

Bettus, G., Guedj, E., Joyeux, F., Confort-Gouny, S., Soulier, E., Laguitton, V., Cozzone, P. J., Chauvel, P., Ranjeva, J. P., Bartolomei, F., & Guye, M. (2009). Decreased basal fMRI functional connectivity in epileptogenic networks and contralateral compensatory mechanisms. *Human Brain Mapping*, *30*(5), 1580–1591. https://doi.org/10.1002/HBM.20625

Birn, R. M., Diamond, J. B., Smith, M. A., & Bandettini, P. A. (2006). Separating respiratory-variation-related fluctuations from neuronal-activity-related fluctuations in fMRI. *NeuroImage*, *31*(4), 1536–1548. https://doi.org/10.1016/J.NEUROIMAGE.2006.02.048

Birn, R. M., Smith, M. A., Jones, T. B., & Bandettini, P. A. (2008). The Respiration Response Function: The temporal dynamics of fMRI signal fluctuations related to changes in respiration. *NeuroImage*, *40*(2), 644. https://doi.org/10.1016/J.NEUROIMAGE.2007.11.059

Biswal, B. B., Mennes, M., Zuo, X. N., Gohel, S., Kelly, C., Smith, S. M., Beckmann, C. F., Adelstein, J. S., Buckner, R. L., Colcombe, S., Dogonowski, A. M., Ernst, M., Fair, D., Hampson, M., Hoptman, M. J., Hyde, J. S., Kiviniemi, V. J., Kötter, R., Li, S. J., … Milham, M. P. (2010). Toward discovery science of human brain function. *Proceedings of the National Academy of Sciences of the United States of America*, *107*(10), 4734–4739. https://doi.org/10.1073/pnas.0911855107

Biswal, B. B., van Kylen, J., & Hyde, J. S. (1997). Simultaneous assessment of flow and BOLD signals in resting-state functional connectivity maps. *NMR in Biomedicine*, *10*(4–5), 165–170. https://doi.org/10.1002/(sici)1099-1492(199706/08)10:4/5<165::aid-nbm454>3.0.co;2-7

Biswal, B., Zerrin Yetkin, F., Haughton, V. M., & Hyde, J. S. (1995). Functional connectivity in the motor cortex of resting human brain using echo-planar MRI. *Magnetic Resonance in Medicine*, *34*(4), 537–541. https://doi.org/10.1002/MRM.1910340409

Boly, M., Perlbarg, V., Marrelec, G., Schabus, M., Laureys, S., Doyon, J., Pélégrini-Issac, M., Maquet, P., & Benali, H. (2012). Hierarchical clustering of brain activity during human nonrapid eye movement sleep. *Proceedings of the National Academy of Sciences of the United States of America*, *109*(15), 5856–5861. https://doi.org/10.1073/PNAS.1111133109/SUPPL_FILE/PNAS.201111133SI.PDF

Bordier, C., Nicolini, C., & Bifone, A. (2017). Graph analysis and modularity of brain functional connectivity networks: Searching for the optimal threshold. *Frontiers in Neuroscience*, *11*(AUG), 441. https://doi.org/10.3389/FNINS.2017.00441/BIBTEX

Buckner, R. L., & Vincent, J. L. (2007). Unrest at rest: default activity and spontaneous network correlations. *NeuroImage*, *37*(4), 1091–1096. https://doi.org/10.1016/J.NEUROIMAGE.2007.01.010

Bullmore, E., & Sporns, O. (2009). Complex brain networks: graph theoretical analysis of structural and functional systems. *Nature Reviews Neuroscience 2009 10:3*, *10*(3), 186–198. https://doi.org/10.1038/nrn2575

Calhoun, V. D., Adali, T., Pearlson, G. D., & Pekar, J. J. (2001). A method for making group inferences from functional MRI data using independent component analysis. *Human Brain Mapping*, *14*(3), 140–151. https://doi.org/10.1002/HBM.1048

Campos, B. M., Coan, A. C., Beltramini, G. C., Liu, M., Yassuda, C. L., Ghizoni, E., Beaulieu, C., Gross, D. W.,

& Cendes, F. (2015). White matter abnormalities associate with type and localization of focal epileptogenic lesions. *Epilepsia*, *56*(1), 125–132. https://doi.org/10.1111/epi.12871

Chee, M. W. L., & Choo, W. C. (2004). Functional Imaging of Working Memory after 24 Hr of Total Sleep Deprivation. *Journal of Neuroscience*, *24*(19), 4560–4567. https://doi.org/10.1523/JNEUROSCI.0007-04.2004

Collingnon, A., Maes, F., Delaere, D., Vandermeulen, D., Suetens, P., & Marchal, G. (1995). Automated multi-modality image registration based on information theory. *IPMI*, 263–274.

Constable, R. T., Scheinost, D., Finn, E. S., Shen, X., Hampson, M., Winstanley, F. S., Spencer, D. D., & Papademetris, X. (2013). Potential Use and Challenges of Functional Connectivity Mapping in Intractable Epilepsy. *Frontiers in Neurology*, *0*, 39. https://doi.org/10.3389/FNEUR.2013.00039

Cordes, D., Haughton, V. M., Arfanakis, K., Carew, J. D., Turski, P. A., Moritz, C. H., Quigley, M. A., & Meyerand, M. E. (2001). Frequencies contributing to functional connectivity in the cerebral cortex in "resting-state" data. *AJNR. American Journal of Neuroradiology*, *22*(7), 1326–1333.

Cordes, D., Haughton, V. M., Arfanakis, K., Wendt, G. J., Turski, P. A., Moritz, C. H., Quigley, M. A., & Meyerand, M. E. (2000). Mapping functionally related regions of brain with functional connectivity MR imaging. *AJNR. American Journal of Neuroradiology*, *21*(9), 1636–1644.

Cox, R. W. (1996). AFNI: Software for analysis and visualization of functional magnetic resonance neuroimages. *Computers and Biomedical Research*, *29*(3), 162–173. https://doi.org/10.1006/cbmr.1996.0014

Cross, N. E., Pomares, F. B., Nguyen, A., Perrault, A. A., Jegou, A., Uji, M., Lee, K., Razavipour, F., Ka'b Ali, O. bin, Aydin, U., Benali, H., Grova, C., & Dang-Vu, T. T. (2021). An altered balance of integrated and segregated brain activity is a marker of cognitive deficits following sleep deprivation. *PLOS Biology*, *19*(11), e3001232. https://doi.org/10.1371/JOURNAL.PBIO.3001232

Cross, N., Paquola, C., Pomares, F. B., Perrault, A. A., Jegou, A., Nguyen, A., Aydin, U., Bernhardt, B. C., Grova, C., & Dang-Vu, T. T. (2021a). Cortical gradients of functional connectivity are robust to state-dependent changes following sleep deprivation. *NeuroImage*, *226*, 117547. https://doi.org/10.1016/J.NEUROIMAGE.2020.117547

Cross, N., Paquola, C., Pomares, F. B., Perrault, A. A., Jegou, A., Nguyen, A., Aydin, U., Bernhardt, B. C., Grova, C., & Dang-Vu, T. T. (2021b). Cortical gradients of functional connectivity are robust to state-dependent changes following sleep deprivation. *NeuroImage*, *226*, 117547. https://doi.org/10.1016/J.NEUROIMAGE.2020.117547

Cruces, R. R., Royer, J., Herholz, P., Larivière, S., Wael, R. V. de, Paquola, C., Benkarim, O., Park, B., Degré-Pelletier, J., Nelson, M., DeKraker, J., Tardif, C., Poline, J.-B., Concha, L., & Bernhardt, B. C. (2022). Micapipe: A Pipeline for Multimodal Neuroimaging and Connectome Analysis. *BioRxiv*, 2022.01.31.478189. https://doi.org/10.1101/2022.01.31.478189

Culhane-Shelburne, K., Chapieski, L., Hiscock, M., & Glaze, D. (2002). Executive functions in children with frontal and temporal lobe epilepsy. *Journal of the International Neuropsychological Society*, *8*(5), 623–632. https://doi.org/10.1017/S1355617702801308

Damoiseaux, J. S., Rombouts, S. A. R. B., Barkhof, F., Scheltens, P., Stam, C. J., Smith, S. M., & Beckmann, C. F. (2006a). Consistent resting-state networks across healthy subjects. *Proceedings of the National Academy of Sciences of the United States of America*, *103*(37), 13848–13853. https://doi.org/10.1073/PNAS.0601417103

Damoiseaux, J. S., Rombouts, S. A. R. B., Barkhof, F., Scheltens, P., Stam, C. J., Smith, S. M., & Beckmann, C. F. (2006b). Consistent resting-state networks across healthy subjects. *Proceedings of the National Academy of Sciences of the United States of America*, *103*(37), 13848–13853. https://doi.org/10.1073/PNAS.0601417103

Dang-Vu, T. T., Cartwright, R. D., Mograss, M. A., Ellenbogen, J. M., & Foulkes, D. (2022, July 28). *sleep*. Encyclopedia Britannica. Https://Www.Britannica.Com/Science/Sleep.

Dang-Vu, T. T., Schabus, M., Desseilles, M., Albouy, G., Boly, M., Darsaud, A., Gais, S., Rauchs, G., Sterpenich, V., Vandewalle, G., Carrier, J., Moonen, G., Balteau, E., Degueldre, C., Luxen, A., Phillips, C., & Maquet, P. (2008). Spontaneous neural activity during human slow wave sleep. *Proceedings of the National Academy of Sciences of the United States of America*, *105*(39), 15160–15165. https://doi.org/10.1073/PNAS.0801819105/SUPPL_FILE/0801819105SI.PDF

de Gennaro, L., & Ferrara, M. (2003). Sleep spindles: An overview. *Sleep Medicine Reviews*, *7*(5), 423–440. https://doi.org/10.1053/smrv.2002.0252

de Havas, J. A., Parimal, S., Soon, C. S., & Chee, M. W. L. (2012). Sleep deprivation reduces default mode network connectivity and anti-correlation during rest and task performance. *NeuroImage*, *59*(2), 1745–1751. https://doi.org/10.1016/J.NEUROIMAGE.2011.08.026

de Luca, C. J., Adam, A., Wotiz, R., Gilmore, L. D., & Nawab, S. H. (2006). Decomposition of surface EMG signals. *Journal of Neurophysiology*, *96*(3), 1646–1657. https://doi.org/10.1152/JN.00009.2006/ASSET/IMAGES/LARGE/Z9K0090676200010.JPEG

Efron, B., & Tibshirani, R. J. (1994). *An introduction to the bootstrap*. CRC press.

Evangelista, E., Bénar, C., Bonini, F., Carron, R., Colombet, B., Régis, J., & Bartolomei, F. (2015). Does the thalamo-cortical synchrony play a role in seizure termination? *Frontiers in Neurology*, *6*(SEP), 192. https://doi.org/10.3389/FNEUR.2015.00192/BIBTEX

Fan, J., McCandliss, B. D., Fossella, J., Flombaum, J. I., & Posner, M. I. (2005). The activation of attentional networks. *NeuroImage*, *26*(2), 471–479. https://doi.org/10.1016/J.NEUROIMAGE.2005.02.004

Feng, L., Motelow, J. E., Ma, C., Biche, W., McCafferty, C., Smith, N., Liu, M., Zhan, Q., Jia, R., Xiao, B., Duque, A., & Blumenfeld, H. (2017). Seizures and Sleep in the Thalamus: Focal Limbic Seizures Show Divergent Activity Patterns in Different Thalamic Nuclei. *The Journal of Neuroscience*, *37*(47), 11441. https://doi.org/10.1523/JNEUROSCI.1011-17.2017

Ferri, R., Manconi, M., Plazzi, G., Bruni, O., Vandi, S., Montagna, P., Ferini-Strambi, L., & Zucconi, M. (2008). A quantitative statistical analysis of the submentalis muscle EMG amplitude during sleep in normal controls and patients with REM sleep behavior disorder. *Journal of Sleep Research*, *17*(1), 89–100. https://doi.org/10.1111/J.1365-2869.2008.00631.X

Finn, E. S., Shen, X., Scheinost, D., Rosenberg, M. D., Huang, J., Chun, M. M., Papademetris, X., & Constable, R. T. (2015). Functional connectome fingerprinting: identifying individuals using patterns of brain connectivity. *Nature Neuroscience 2015 18:11*, *18*(11), 1664–1671. https://doi.org/10.1038/nn.4135

Fonov, V., Evans, A. C., Botteron, K., Almli, C. R., McKinstry, R. C., & Collins, D. L. (2011). Unbiased average age-appropriate atlases for pediatric studies. *NeuroImage*, *54*(1), 313–327. https://doi.org/10.1016/j.neuroimage.2010.07.033

Fonov, V., Evans, A., McKinstry, R., Almli, C., & Collins, D. (2009). Unbiased nonlinear average age-appropriate brain templates from birth to adulthood. *NeuroImage*, *47*, S102. https://doi.org/10.1016/S1053-

8119(09)70884-5

Fox, M. D., & Raichle, M. E. (2007). Spontaneous fluctuations in brain activity observed with functional magnetic resonance imaging. *Nature Reviews Neuroscience 2007 8:9*, *8*(9), 700–711. https://doi.org/10.1038/nrn2201

Fox, M. D., Snyder, A. Z., Vincent, J. L., Corbetta, M., van Essen, D. C., & Raichle, M. E. (2005). The human brain is intrinsically organized into dynamic, anticorrelated functional networks. *Proceedings of the National Academy of Sciences of the United States of America*, *102*(27), 9673–9678. https://doi.org/10.1073/PNAS.0504136102

Fransson, P. (2005). Spontaneous low-frequency BOLD signal fluctuations: An fMRI investigation of the resting-state default mode of brain function hypothesis. *Human Brain Mapping*, *26*(1), 15. https://doi.org/10.1002/HBM.20113

Friston, K. J., Frith, C. D., Liddle, P. F., & Frackowiak, R. S. J. (1993). Functional connectivity: the principal-component analysis of large (PET) data sets. *Journal of Cerebral Blood Flow and Metabolism : Official Journal of the International Society of Cerebral Blood Flow and Metabolism*, *13*(1), 5–14. https://doi.org/10.1038/JCBFM.1993.4

Friston, K., Kilner, J., & Harrison, L. (2006). A free energy principle for the brain. *Journal of Physiology, Paris*, *100*(1–3), 70–87. https://doi.org/10.1016/J.JPHYSPARIS.2006.10.001

Functional Imaging Laboratory. (2016). *SPM12 Manual*. https://web.archive.org/web/20170711224110/http://www.fil.ion.ucl.ac.uk/spm/doc/manual.pdf

Grabner, G., Janke, A. L., Budge, M. M., Smith, D., Pruessner, J., & Collins, D. L. (2006). Symmetric atlasing and model based segmentation: an application to the hippocampus in older adults. *Medical Image Computing and Computer-Assisted Intervention : MICCAI ... International Conference on Medical Image Computing and Computer-Assisted Intervention*, *9*(Pt 2), 58–66. https://doi.org/10.1007/11866763_8

Gramfort, A., Luessi, M., Larson, E., Engemann, D. A., Strohmeier, D., Brodbeck, C., Goj, R., Jas, M., Brooks, T., Parkkonen, L., & Hämäläinen, M. (2013). MEG and EEG data analysis with MNE-Python. *Frontiers in Neuroscience*, *0*(7 DEC), 267. https://doi.org/10.3389/FNINS.2013.00267/XML/NLM

Greve, D. N., & Fischl, B. (2009). Accurate and robust brain image alignment using boundary-based registration. *NeuroImage*, *48*(1), 63–72. https://doi.org/10.1016/J.NEUROIMAGE.2009.06.060

Griffanti, L., Douaud, G., Bijsterbosch, J., Evangelisti, S., Alfaro-Almagro, F., Glasser, M. F., Duff, E. P., Fitzgibbon, S., Westphal, R., Carone, D., Beckmann, C. F., & Smith, S. M. (2017). Hand classification of fMRI ICA noise components. *NeuroImage*, *154*, 188–205. https://doi.org/10.1016/J.NEUROIMAGE.2016.12.036

Griffanti, L., Salimi-Khorshidi, G., Beckmann, C. F., Auerbach, E. J., Douaud, G., Sexton, C. E., Zsoldos, E., Ebmeier, K. P., Filippini, N., Mackay, C. E., Moeller, S., Xu, J., Yacoub, E., Baselli, G., Ugurbil, K., Miller, K. L., & Smith, S. M. (2014). ICA-based artefact removal and accelerated fMRI acquisition for improved resting state network imaging. *NeuroImage*, *95*, 232–247. https://doi.org/10.1016/J.NEUROIMAGE.2014.03.034

He, X., Doucet, G. E., Sperling, M., Sharan, A., & Tracy, J. I. (2015). Reduced thalamocortical functional connectivity in temporal lobe epilepsy. *Epilepsia*, *56*(10), 1571–1579. https://doi.org/10.1111/epi.13085

Heuvel, M. P. van den, & Sporns, O. (2011). Rich-Club Organization of the Human Connectome. *Journal of Neuroscience*, *31*(44), 15775–15786. https://doi.org/10.1523/JNEUROSCI.3539-11.2011

Honey, C. J., Sporns, O., Cammoun, L., Gigandet, X., Thiran, J. P., Meuli, R., & Hagmann, P. (2009). Predicting human resting-state functional connectivity from structural connectivity. *Proceedings of the National Academy of Sciences of the United States of America*, *106*(6), 2035–2040. https://doi.org/10.1073/PNAS.0811168106

Horovitz, S. G., Braun, A. R., Carr, W. S., Picchioni, D., Balkin, T. J., Fukunaga, M., & Duyn, J. H. (2009). Decoupling of the brain's default mode network during deep sleep. *Proceedings of the National Academy of Sciences of the United States of America*, *106*(27), 11376–11381. https://doi.org/10.1073/PNAS.0901435106

Huettel, S. A. (2004). Linking Hemodynamic and Electrophysiological Measures of Brain Activity: Evidence from Functional MRI and Intracranial Field Potentials. *Cerebral Cortex*, *14*(2), 165–173. https://doi.org/10.1093/cercor/bhg115

Jenkinson, M., Bannister, P., Brady, M., & Smith, S. (2002). Improved optimization for the robust and accurate linear registration and motion correction of brain images. *NeuroImage*, *17*(2), 825–841. https://doi.org/10.1016/S1053-8119(02)91132-8

Jenkinson, M., & Smith, S. (2001). A global optimisation method for robust affine registration of brain images. *Medical Image Analysis*, *5*(2), 143–156. https://doi.org/10.1016/S1361-8415(01)00036-6

Jovicich, J., Czanner, S., Greve, D., Haley, E., van der Kouwe, A., Gollub, R., Kennedy, D., Schmitt, F., Brown, G., MacFall, J., Fischl, B., & Dale, A. (2006). Reliability in multi-site structural MRI studies: effects of gradient non-linearity correction on phantom and human data. *NeuroImage*, *30*(2), 436–443. https://doi.org/10.1016/J.NEUROIMAGE.2005.09.046

Klugah-Brown, B., Luo, C., Peng, R., He, H., Li, J., Dong, L., & Yao, D. (2019). Altered structural and causal connectivity in frontal lobe epilepsy. *BMC Neurology*, *19*(1), 1–9. https://doi.org/10.1186/S12883-019-1300-Z/FIGURES/3

Knoop, M. S., de Groot, E. R., & Dudink, J. (2021). Current ideas about the roles of rapid eye movement and non–rapid eye movement sleep in brain development. *Acta Paediatrica (Oslo, Norway : 1992)*, *110*(1), 36. https://doi.org/10.1111/APA.15485

Le, N. H., Nguyen, K. N., & Nguyen, H. M. (2018). Comparison analysis of ICA versus MCA-KSVD blind source separation on task-related fMRI data. *Proceedings - 9th Asia-Pacific Signal and Information Processing Association Annual Summit and Conference, APSIPA ASC 2017*, *2018-February*, 1129–1135. https://doi.org/10.1109/APSIPA.2017.8282196

Lee, K., Horien, C., O'Connor, D., Garand-Sheridan, B., Tokoglu, F., Scheinost, D., Lake, E. M. R., & Constable, R. T. (2022). Arousal impacts distributed hubs modulating the integration of brain functional connectivity. *NeuroImage*, *258*, 119364. https://doi.org/10.1016/J.NEUROIMAGE.2022.119364

Lee, K., Khoo, H. M., Fourcade, C., Gotman, J., & Grova, C. (2019). Automatic classification and removal of structured physiological noise for resting state functional connectivity MRI analysis. *Magnetic Resonance Imaging*, *58*, 97–107. https://doi.org/10.1016/J.MRI.2019.01.019

Lee, K., Khoo, H. M., Lina, J. M., Dubeau, F., Gotman, J., & Grova, C. (2018). Disruption, emergence and lateralization of brain network hubs in mesial temporal lobe epilepsy. *NeuroImage : Clinical*, *20*, 71. https://doi.org/10.1016/J.NICL.2018.06.029

Lee, K., Lina, J. M., Gotman, J., & Grova, C. (2016). SPARK: Sparsity-based analysis of reliable k-hubness and overlapping network structure in brain functional connectivity. *NeuroImage*, *134*, 434–449.

https://doi.org/10.1016/J.NEUROIMAGE.2016.03.049

Lee, K., Tak, S., & Ye, J. C. (2011). A data-driven sparse GLM for fMRI analysis using sparse dictionary learning with MDL criterion. *IEEE Transactions on Medical Imaging*, *30*(5), 1076–1089. https://doi.org/10.1109/TMI.2010.2097275

Leergaard, T. B., Hilgetag, C. C., & Sporns, O. (2012). Mapping the connectome: Multi-level analysis of brain connectivity. *Frontiers in Neuroinformatics*, *6*(APRIL 2012), 14. https://doi.org/10.3389/FNINF.2012.00014/XML/NLM

Lichstein, K. L., Riedel, B. W., & Richman, S. L. (2000). The Mackworth Clock Test: a computerized version. *The Journal of Psychology*, *134*(2), 153–161. https://doi.org/10.1080/00223980009600858

Liu, T. T., & Falahpour, M. (2020). Vigilance Effects in Resting-State fMRI. *Frontiers in Neuroscience*, *14*, 321. https://doi.org/10.3389/FNINS.2020.00321/BIBTEX

Liu, W., Yue, Q., Tian, Y., Gong, Q., Zhou, D., & Wu, X. (2021). Neural functional connectivity in patients with periventricular nodular heterotopia-mediated epilepsy. *Epilepsy Research*, *170*. https://doi.org/10.1016/J.EPLEPSYRES.2021.106548

Lund, T. E., Madsen, K. H., Sidaros, K., Luo, W. L., & Nichols, T. E. (2006). Non-white noise in fMRI: does modelling have an impact? *NeuroImage*, *29*(1), 54–66. https://doi.org/10.1016/J.NEUROIMAGE.2005.07.005

Marrelec, G., Bellec, P., Krainik, A., Duffau, H., Pélégrini-Issac, M., Lehéricy, S., Benali, H., & Doyon, J. (2008a). Regions, systems, and the brain: hierarchical measures of functional integration in fMRI. *Medical Image Analysis*, *12*(4), 484–496. https://doi.org/10.1016/J.MEDIA.2008.02.002

Marrelec, G., Bellec, P., Krainik, A., Duffau, H., Pélégrini-Issac, M., Lehéricy, S., Benali, H., & Doyon, J. (2008b). Regions, systems, and the brain: hierarchical measures of functional integration in fMRI. *Medical Image Analysis*, *12*(4), 484–496. https://doi.org/10.1016/J.MEDIA.2008.02.002

Marrelec, G., Horwitz, B., Kim, J., Pélégrini-Issac, M., Benali, H., & Doyon, J. (2007). Using partial correlation to enhance structural equation modeling of functional MRI data. *Magnetic Resonance Imaging*, *25*(8), 1181–1189. https://doi.org/10.1016/J.MRI.2007.02.012

Marrelec, G., Krainik, A., Duffau, H., Pélégrini-Issac, M., Lehéricy, S., Doyon, J., & Benali, H. (2006a). Partial correlation for functional brain interactivity investigation in functional MRI. *NeuroImage*, *32*(1), 228–237. https://doi.org/10.1016/J.NEUROIMAGE.2005.12.057

Marrelec, G., Krainik, A., Duffau, H., Pélégrini-Issac, M., Lehéricy, S., Doyon, J., & Benali, H. (2006b). Partial correlation for functional brain interactivity investigation in functional MRI. *NeuroImage*, *32*(1), 228–237. https://doi.org/10.1016/J.NEUROIMAGE.2005.12.057

Marshall, L., Helgadóttir, H., Mölle, M., & Born, J. (2006). Boosting slow oscillations during sleep potentiates memory. *Nature*, *444*(7119), 610–613. https://doi.org/10.1038/NATURE05278

Martín-López, D., Jiménez-Jiménez, D., Cabañés-Martínez, L., Selway, R. P., Valentín, A., & Alarcón, G. (2017). The Role of Thalamus Versus Cortex in Epilepsy: Evidence from Human Ictal Centromedian Recordings in Patients Assessed for Deep Brain Stimulation. *International Journal of Neural Systems*, *27*(7). https://doi.org/10.1142/S0129065717500101

Massimini, M., Ferrarelli, F., Huber, R., Esser, S. K., Singh, H., & Tononi, G. (2005). Breakdown of cortical effective connectivity during sleep. *Science (New York, N.Y.)*, *309*(5744), 2228–2232. https://doi.org/10.1126/SCIENCE.1117256

Minoshima, S., Berger, K., Lee, K., & Mintun, M. (1992). An automated method for rotation correction and centering of 3D functional brain images. *Journal of Nuclear Medicine*, *33*(8), 1579–1585.

Moussa, M. N., Steen, M. R., Laurienti, P. J., & Hayasaka, S. (2012). Consistency of Network Modules in Resting-State fMRI Connectome Data. *PLoS ONE*, *7*(8), 44428. https://doi.org/10.1371/JOURNAL.PONE.0044428

Ngo, H. V. v., Martinetz, T., Born, J., & Mölle, M. (2013). Auditory closed-loop stimulation of the sleep slow oscillation enhances memory. *Neuron*, *78*(3), 545–553. https://doi.org/10.1016/J.NEURON.2013.03.006

Nguyen, H. M., Chen, J., & Glover, G. (2022). Morphological Component Analysis of functional MRI Brain Networks. *IEEE Transactions on Bio-Medical Engineering*, *PP*. https://doi.org/10.1109/TBME.2022.3162606

Nir, Y., Mukamel, R., Dinstein, I., Privman, E., Harel, M., Fisch, L., Gelbard-Sagiv, H., Kipervasser, S., Andelman, F., Neufeld, M. Y., Kramer, U., Arieli, A., Fried, I., & Malach, R. (2008). Interhemispheric correlations of slow spontaneous neuronal fluctuations revealed in human sensory cortex. *Nature Neuroscience*, *11*(9), 1100–1108. https://doi.org/10.1038/NN.2177

Ogawa, S., Lee, T. M., Kay, A. R., & Tank, D. W. (1990). Brain magnetic resonance imaging with contrast dependent on blood oxygenation. *Proceedings of the National Academy of Sciences*, *87*(24), 9868–9872. https://doi.org/10.1073/PNAS.87.24.9868

Orżanowski, T. (2016). Nonuniformity correction algorithm with efficient pixel offset estimation for infrared focal plane arrays. *SpringerPlus*, *5*(1). https://doi.org/10.1186/S40064-016-3534-1

Perez, C., & Germon, R. (2016). Graph Creation and Analysis for Linking Actors: Application to Social Data. *Automating Open Source Intelligence: Algorithms for OSINT*, 103–129. https://doi.org/10.1016/B978-0-12-802916-9.00007-5

Perlbarg, V., Bellec, P., Anton, J. L., Pélégrini-Issac, M., Doyon, J., & Benali, H. (2007). CORSICA: correction of structured noise in fMRI by automatic identification of ICA components. *Magnetic Resonance Imaging*, *25*(1), 35–46. https://doi.org/10.1016/J.MRI.2006.09.042

Pittau, F., Grova, C., Moeller, F., Dubeau, F., & Gotman, J. (2012). Patterns of altered functional connectivity in mesial temporal lobe epilepsy. *Epilepsia*, *53*(6), 1013. https://doi.org/10.1111/J.1528-1167.2012.03464.X

Power, J. D., Mitra, A., Laumann, T. O., Snyder, A. Z., Schlaggar, B. L., & Petersen, S. E. (2014). Methods to detect, characterize, and remove motion artifact in resting state fMRI. *NeuroImage*, *84*, 320–341. https://doi.org/10.1016/J.NEUROIMAGE.2013.08.048

Power, J. D., Schlaggar, B. L., Lessov-Schlaggar, C. N., & Petersen, S. E. (2013). Evidence for hubs in human functional brain networks. *Neuron*, *79*(4), 798–813. https://doi.org/10.1016/J.NEURON.2013.07.035

Raichle, M. E., & Mintun, M. A. (2006). Brain work and brain imaging. *Annual Review of Neuroscience*, *29*, 449–476. https://doi.org/10.1146/ANNUREV.NEURO.29.051605.112819

Reuter, M., Schmansky, N. J., Rosas, H. D., & Fischl, B. (2012). Within-subject template estimation for unbiased longitudinal image analysis. *NeuroImage*, *61*(4), 1402–1418. https://doi.org/10.1016/J.NEUROIMAGE.2012.02.084

Rolls, E. T., Huang, C. C., Lin, C. P., Feng, J., & Joliot, M. (2020). Automated anatomical labelling atlas 3. *NeuroImage*, *206*, 116189. https://doi.org/10.1016/J.NEUROIMAGE.2019.116189

Royer, J., Bernhardt, B. C., Larivière, S., Gleichgerrcht, E., Vorderwülbecke, B. J., Vulliémoz, S., & Bonilha, L. (2022). Epilepsy and brain network hubs. In *Epilepsia* (Vol. 63, Issue 3, pp. 537–550). John Wiley and Sons

Inc. https://doi.org/10.1111/epi.17171

Royer, J., Rodríguez-Cruces, R., Tavakol, S., Larivière, S., Li, Q., Vos De Wael, R., Paquola, C., Benkarim, O., Park, B.-Y., Lowe, A. J., Margulies, D., Smallwood, J., Bernasconi, A., Bernasconi, N., Frauscher, B., Bernhardt, B. C., & Royer, J. D. (2021). An Open MRI Dataset for Multiscale Neuroscience. *BioRxiv*, 2021.08.04.454795. https://doi.org/10.1101/2021.08.04.454795

Rubinov, M., & Sporns, O. (2010). Complex network measures of brain connectivity: uses and interpretations. *NeuroImage*, *52*(3), 1059–1069. https://doi.org/10.1016/J.NEUROIMAGE.2009.10.003

Sahoo, D., Satterthwaite, T. D., & Davatzikos, C. (2019). *Extraction of hierarchical functional connectivity components in human brain using resting-state fMRI*. https://doi.org/10.1109/TMI.2020.3042873

Saito, N. (1994). Simultaneous Noise Suppression and Signal Compression Using a Library of Orthonormal Bases and the Minimum Description Length Criterion. *Wavelet Analysis and Its Applications*, *4*(C), 299–324. https://doi.org/10.1016/B978-0-08-052087-2.50017-7

Salimi-Khorshidi, G., Douaud, G., Beckmann, C. F., Glasser, M. F., Griffanti, L., & Smith, S. M. (2014). Automatic denoising of functional MRI data: combining independent component analysis and hierarchical fusion of classifiers. *NeuroImage*, *90*, 449–468. https://doi.org/10.1016/J.NEUROIMAGE.2013.11.046

Salvador, R., Suckling, J., Schwarzbauer, C., & Bullmore, E. (2005). Undirected graphs of frequency-dependent functional connectivity in whole brain networks. *Philosophical Transactions of the Royal Society B: Biological Sciences*, *360*(1457), 937. https://doi.org/10.1098/RSTB.2005.1645

Sämann, P. G., Wehrle, R., Hoehn, D., Spoormaker, V. I., Peters, H., Tully, C., Holsboer, F., & Czisch, M. (2011). Development of the brain's default mode network from wakefulness to slow wave sleep. *Cerebral Cortex (New York, N.Y. : 1991)*, *21*(9), 2082–2093. https://doi.org/10.1093/CERCOR/BHQ295

Schaefer, A., Kong, R., Gordon, E. M., Laumann, T. O., Zuo, X.-N., Holmes, A. J., Eickhoff, S. B., & Yeo, B. T. T. (2018). Local-Global Parcellation of the Human Cerebral Cortex from Intrinsic Functional Connectivity MRI. *Cerebral Cortex (New York, N.Y. : 1991)*, *28*(9), 3095–3114. https://doi.org/10.1093/CERCOR/BHX179

Seghouane, A. K., & Iqbal, A. (2017). Sequential dictionary learning from correlated data: Application to fMRI data analysis. *IEEE Transactions on Image Processing*, *26*(6), 3002–3015. https://doi.org/10.1109/TIP.2017.2686014

Smith, S. M. (2002). Fast robust automated brain extraction. *Human Brain Mapping*, *17*(3), 143–155. https://doi.org/10.1002/HBM.10062

Smith, S. M., Fox, P. T., Miller, K. L., Glahn, D. C., Fox, P. M., Mackay, C. E., Filippini, N., Watkins, K. E., Toro, R., Laird, A. R., & Beckmann, C. F. (2009). Correspondence of the brain's functional architecture during activation and rest. *Proceedings of the National Academy of Sciences of the United States of America*, *106*(31), 13040–13045. https://doi.org/10.1073/PNAS.0905267106/SUPPL_FILE/0905267106SI.PDF

Smitha, K. A., Arun, K. M., Rajesh, P. G., Joel, S. E., Venkatesan, R., Thomas, B., & Kesavadas, C. (2018). Multiband fMRI as a plausible, time-saving technique for resting-state data acquisition: Study on functional connectivity mapping using graph theoretical measures. *Magnetic Resonance Imaging*, *53*, 1–6. https://doi.org/10.1016/J.MRI.2018.06.013

Spoormaker, V. I., Czisch, M., Maquet, P., & Jäncke, L. (2011). Large-scale functional brain networks in human non-rapid eye movement sleep: Insights from combined electroencephalographic/functional magnetic resonance imaging studies. *Philosophical Transactions of the Royal Society A: Mathematical, Physical and*

Engineering Sciences, *369*(1952), 3708–3729. https://doi.org/10.1098/RSTA.2011.0078

Spoormaker, V. I., Schröter, M. S., Gleiser, P. M., Andrade, K. C., Dresler, M., Wehrle, R., Sämann, P. G., & Czisch, M. (2010). Development of a Large-Scale Functional Brain Network during Human Non-Rapid Eye Movement Sleep. *Journal of Neuroscience*, *30*(34), 11379–11387. https://doi.org/10.1523/JNEUROSCI.2015-10.2010

Steriade, M., McCormick, D. A., & Sejnowski, T. J. (1993). Thalamocortical oscillations in the sleeping and aroused brain. *Science (New York, N.Y.)*, *262*(5134), 679–685. https://doi.org/10.1126/SCIENCE.8235588

Stretton, J., & Thompson, P. J. (2012). Frontal lobe function in temporal lobe epilepsy. *Epilepsy Research*, *98*(1), 1. https://doi.org/10.1016/J.EPLEPSYRES.2011.10.009

Tagliazucchi, E., von Wegner, F., Morzelewski, A., Brodbeck, V., Jahnke, K., & Laufs, H. (2013). Breakdown of long-range temporal dependence in default mode and attention networks during deep sleep. *Proceedings of the National Academy of Sciences of the United States of America*, *110*(38), 15419–15424. https://doi.org/10.1073/PNAS.1312848110/SUPPL_FILE/SAPP.PDF

Taillard, J., Sagaspe, P., Berthomier, C., Brandewinder, M., Amieva, H., Dartigues, J. F., Rainfray, M., Harston, S., Micoulaud-Franchi, J. A., & Philip, P. (2019). Non-REM Sleep Characteristics Predict Early Cognitive Impairment in an Aging Population. *Frontiers in Neurology*, *10*. https://doi.org/10.3389/FNEUR.2019.00197

Thomas Yeo, B. T., Krienen, F. M., Sepulcre, J., Sabuncu, M. R., Lashkari, D., Hollinshead, M., Roffman, J. L., Smoller, J. W., Zöllei, L., Polimeni, J. R., Fisch, B., Liu, H., & Buckner, R. L. (2011a). The organization of the human cerebral cortex estimated by intrinsic functional connectivity. *Journal of Neurophysiology*, *106*(3), 1125–1165. https://doi.org/10.1152/JN.00338.2011

Thomas Yeo, B. T., Krienen, F. M., Sepulcre, J., Sabuncu, M. R., Lashkari, D., Hollinshead, M., Roffman, J. L., Smoller, J. W., Zöllei, L., Polimeni, J. R., Fisch, B., Liu, H., & Buckner, R. L. (2011b). The organization of the human cerebral cortex estimated by intrinsic functional connectivity. *Journal of Neurophysiology*, *106*(3), 1125–1165. https://doi.org/10.1152/JN.00338.2011

Tononi, G., Sporns, O., & Edelman, G. M. (1994). A measure for brain complexity: relating functional segregation and integration in the nervous system. *Proceedings of the National Academy of Sciences of the United States of America*, *91*(11), 5033. https://doi.org/10.1073/PNAS.91.11.5033

Tzourio-Mazoyer, N., Landeau, B., Papathanassiou, D., Crivello, F., Etard, O., Delcroix, N., Mazoyer, B., & Joliot, M. (2002). Automated anatomical labeling of activations in SPM using a macroscopic anatomical parcellation of the MNI MRI single-subject brain. *NeuroImage*, *15*(1), 273–289. https://doi.org/10.1006/nimg.2001.0978

Uji, M., Cross, N., Pomares, F. B., Perrault, A. A., Jegou, A., Nguyen, A., Aydin, U., Lina, J. M., Dang-Vu, T. T., & Grova, C. (2021). Data-driven beamforming technique to attenuate ballistocardiogram artefacts in electroencephalography-functional magnetic resonance imaging without detecting cardiac pulses in electrocardiography recordings. *Human Brain Mapping*, *42*(12), 3993–4021. https://doi.org/10.1002/HBM.25535

Urchs, S., Armoza, J., Moreau, C., Benhajali, Y., St-Aubin, J., Orban, P., & Bellec, P. (2019). MIST: A multi-resolution parcellation of functional brain networks. *MNI Open Research*, *1*, 3. https://doi.org/10.12688/mniopenres.12767.2

van den Heuvel, M. P., & Hulshoff Pol, H. E. (2010a). Exploring the brain network: A review on resting-state

fMRI functional connectivity. *European Neuropsychopharmacology*, *20*, 519–534. https://doi.org/10.1016/j.euroneuro.2010.03.008

van den Heuvel, M. P., & Hulshoff Pol, H. E. (2010b). Exploring the brain network: A review on resting-state fMRI functional connectivity. In *European Neuropsychopharmacology* (Vol. 20, Issue 8, pp. 519–534). https://doi.org/10.1016/j.euroneuro.2010.03.008

Vatansever, D., Schröter, M., Adapa, R. M., Bullmore, E. T., Menon, D. K., & Stamatakis, E. A. (2020). Reorganisation of Brain Hubs across Altered States of Consciousness. *Scientific Reports 2020 10:1*, *10*(1), 1–11. https://doi.org/10.1038/s41598-020-60258-1

Velíšek, L. (2018). "Can You Hear Me Now?" AMPA Receptor-Mediated Tonotopy Disruption by Early Life Seizures. *Epilepsy Currents*, *18*(6), 391–393. https://doi.org/10.5698/1535-7597.18.6.391

Vincent, J. L., Snyder, A. Z., Fox, M. D., Shannon, B. J., Andrews, J. R., Raichle, M. E., & Buckner, R. L. (2006). Coherent spontaneous activity identifies a hippocampal-parietal memory network. *Journal of Neurophysiology*, *96*(6), 3517–3531. https://doi.org/10.1152/JN.00048.2006

Viviani, R., Grön, G., & Spitzer, M. (2005). Functional principal component analysis of fMRI data. *Human Brain Mapping*, *24*(2), 109. https://doi.org/10.1002/HBM.20074

Výtvarová, E., Mareček, R., Fousek, J., Strýček, O., & Rektor, I. (2017). Large-scale cortico-subcortical functional networks in focal epilepsies: The role of the basal ganglia. *NeuroImage : Clinical*, *14*, 28. https://doi.org/10.1016/J.NICL.2016.12.014

Waites, A. B., Briellmann, R. S., Saling, M. M., Abbott, D. F., & Jackson, G. D. (2006). Functional connectivity networks are disrupted in left temporal lobe epilepsy. *Annals of Neurology*, *59*(2), 335–343. https://doi.org/10.1002/ANA.20733

Watts, D. J., & Strogatz, S. H. (1998). Collective dynamics of 'small-world' networks. *Nature 1998 393:6684*, *393*(6684), 440–442. https://doi.org/10.1038/30918

Woods, R. P., Mazziotta, J. C., & Cherry, S. R. (1993). MRI-PET Registration with Automated Algorithm. *Journal of Computer Assisted Tomography*, *17*, 536–546.

Woolrich, M. W., Jbabdi, S., Patenaude, B., Chappell, M., Makni, S., Behrens, T., Beckmann, C., Jenkinson, M., & Smith, S. M. (2009). Bayesian analysis of neuroimaging data in FSL. *NeuroImage*, *45*(1 Suppl). https://doi.org/10.1016/J.NEUROIMAGE.2008.10.055

Worsley, K. J., Chen, J. I., Lerch, J., & Evans, A. C. (2005). Comparing functional connectivity via thresholding correlations and singular value decomposition. *Philosophical Transactions of the Royal Society B: Biological Sciences*, *360*(1457), 913–920. https://doi.org/10.1098/RSTB.2005.1637

Xie, J., Douglas, P. K., Wu, Y. N., Brody, A. L., & Anderson, A. E. (2017). Decoding the encoding of functional brain networks: An fMRI classification comparison of non-negative matrix factorization (NMF), independent component analysis (ICA), and sparse coding algorithms. *Journal of Neuroscience Methods*, *282*, 81–94. https://doi.org/10.1016/j.jneumeth.2017.03.008

Yeo, B. T. T., Krienen, F. M., Chee, M. W. L., & Buckner, R. L. (2014). Estimates of Segregation and Overlap of Functional Connectivity Networks in the Human Cerebral Cortex. *NeuroImage*, *88*, 212. https://doi.org/10.1016/J.NEUROIMAGE.2013.10.046

Zhang, D., & Raichle, M. E. (2010). Disease and the brain's dark energy. *Nature Reviews. Neurology*, *6*(1), 15–28. https://doi.org/10.1038/NRNEUROL.2009.198

Zhou, Y., Milham, M. P., Lui, Y. W., Miles, L., Reaume, J., Sodickson, D. K., Grossman, R. I., & Ge, Y. (2012).

Default-Mode Network Disruption in Mild Traumatic Brain Injury. *Radiology*, *265*(3), 882. https://doi.org/10.1148/RADIOL.12120748

Zijdenbos, A. P., Forghani, R., & Evans, A. C. (2002). Automatic "pipeline" analysis of 3-D MRI data for clinical trials: application to multiple sclerosis. *IEEE Transactions on Medical Imaging*, *21*(10), 1280–1291. https://doi.org/10.1109/TMI.2002.806283

Zuo, X. N., & Xing, X. X. (2014). Test-retest reliabilities of resting-state FMRI measurements in human brain functional connectomics: a systems neuroscience perspective. *Neuroscience and Biobehavioral Reviews*, *45*, 100–118. https://doi.org/10.1016/J.NEUBIOREV.2014.05.009

Appendix

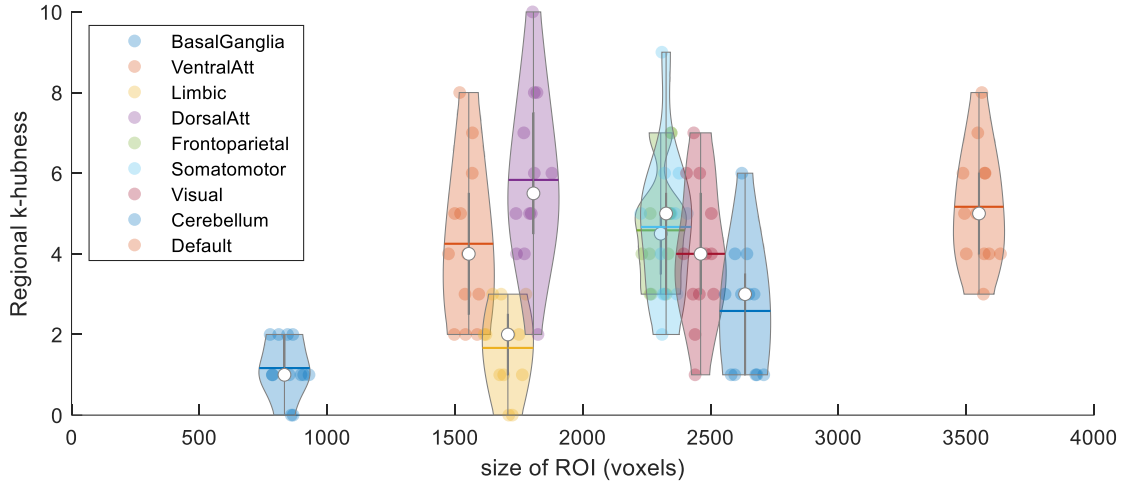

Figure A 1. Relationship between distribution of regional k-hubness and the size of ROIs with a 6% threshold applied on the regional k-hubness methods. Each violin indicates one ROI. The x-coordinates of the violins are the area of each ROI counted by voxels. In each violin, each point represents one subjects, whose y-coordinates indicate the regional k-hubness of this subject in this ROI.

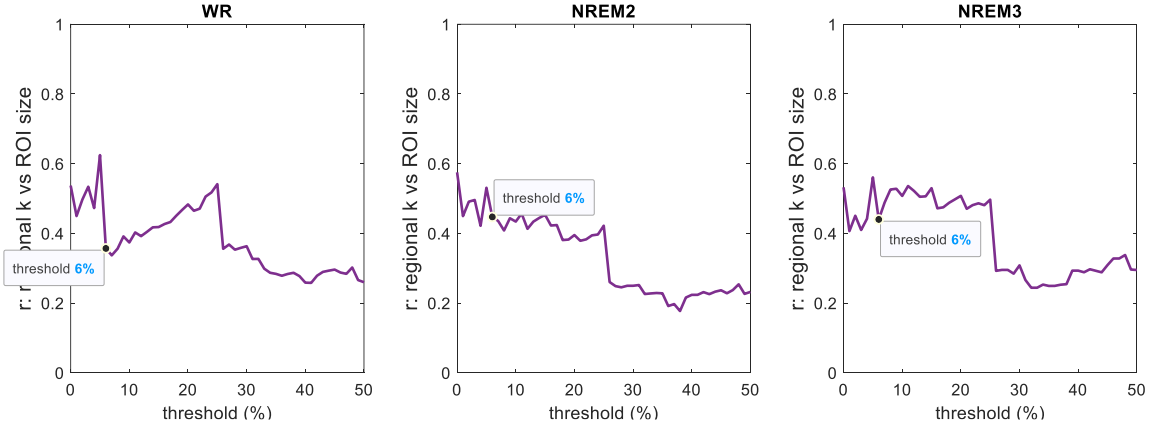

Figure A 2. Correlation coefficient between regional k-hubness and ROI size and its relevance with different threshold, in resting wakefulness (left), NREM2 (middle) and NREM3 (left).

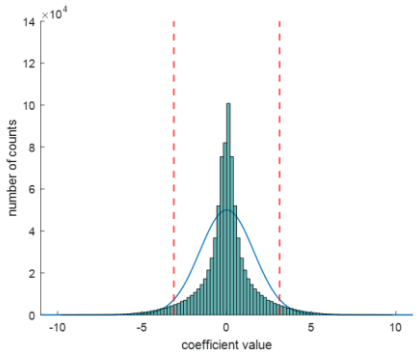

Figure A 3. An illustration of the thresholding procedure in SPARK pipeline. It shows the thresholding procedure before revising the pipeline. The blue solid curve indicates the probability density function a standard normal distribution, although the curve was enlarged in the direction of y-axis for better visualization. The green histogram indicates the distribution of the sparse spatial network atoms after clustering, which was fitted to a inverse normal distribution with the mean equal to the x-coordinates of the bin with largest number of counts. The red dash lines indicate p = 0.05. After the thresholding procedure, the spatial atom data inside the two red dash lines will be removed, but one outside the two red dash lines will be kept (p<0.05).

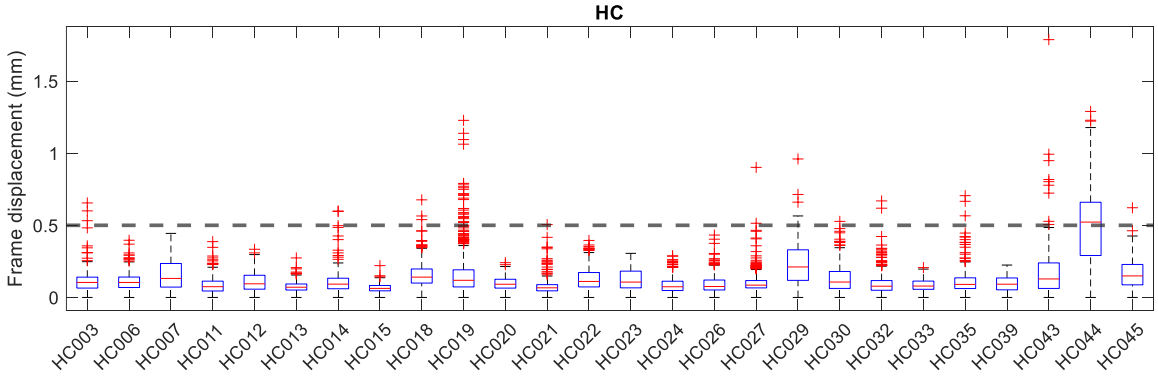

Figure A 4. The distribution of frame displacements of all time points of all healthy control subjects. The grey dash line indicates Frame Displacement = 0.5 mm, above which are the time points that would be removed using scrubbing. The red crosses are outliners identified with boxplot (>75% + 1.5 IQR), which are the time points that would be removed using despiking.

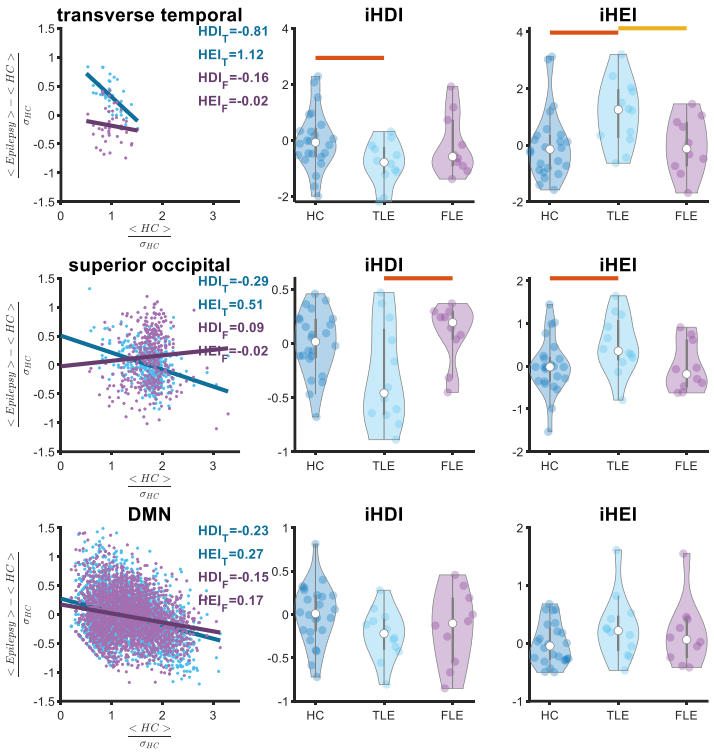

Figure A 5. HDI and HEI of the transverse temporal region (row 1), superior occipital lobe (row 2), and DMN (row 3). The color and notions are the same as Figure 4-2.

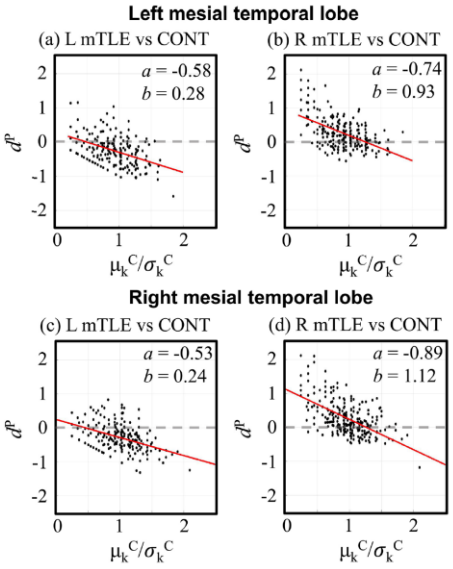

Figure A 6. HDI and HEI of right and left-lateralized mesial TLE of the ROI of left and right mTL. Adapted from Figure 2 of Lee et al., Neuroimaging: Clinical, 2018, for comparison purposes. a indicates HDI as the slope and b indicates HEI as the intercept.